ANKARA YILDIRIM BEYAZIT UNIVERSITY

GRADUATE SCHOOL OF NATURAL AND APPLIED SCIENCES

EFFECTS OF SOIL IMPROVEMENT TECHNIQUES ON THE SITE RESPONSE ANALYSIS (CASE STUDY)

M.Sc. Thesis by

Furkan YÖRÜBULUT

Department of Civil Engineering

January, 2025

ANKARA

EFFECTS OF SOIL IMPROVEMENT TECHNIQUES ON THE SITE RESPONSE ANALYSIS (CASE STUDY)

A Thesis Submitted to

The Graduate School of Natural and Applied Sciences of

Ankara Yıldırım Beyazıt University

In Partial Fulfillment of the Requirements for the Degree of Master of Science in Civil Engineering, Department of Civil Engineering

by

Furkan YÖRÜBULUT

January, 2025

ANKARA

M.Sc. THESIS EXAMINATION RESULT FORM

We have read the thesis entitled **"EFFECTS OF SOIL IMPROVEMENT TECHNIQUES ON THE SITE RESPONSE ANALYSIS (CASE STUDY)"** completed by **Furkan YÖRÜBULUT** under the supervision of **Prof. Dr. Taha TAŞKIRAN** and we certify that in our opinion it is fully adequate, in scope and in quality, as a thesis for the degree of Master of Science.

Prof. Dr. Taha TAŞKIRAN

Supervisor

Prof. Dr. Yüksel YILMAZ

Jury Member

Dr. Öğr. Üyesi Okan İLHAN

Jury Member

Prof. Dr. Sadettin ORHAN

Director

Graduate School of Natural and Applied Sciences

ETHICAL DECLARATION

I hereby declare that, in this thesis which has been prepared in accordance with the Thesis Writing Manual of Graduate School of Natural and Applied Sciences,

- All data, information and documents are obtained in the framework of academic and ethical rules,
- All information, documents and assessments are presented in accordance with scientific ethics and morals,
- All the materials that have been utilized are fully cited and referenced,
- No change has been made on the utilized materials,
- All the works presented are original,

and in any contrary case of above statements, I accept to renounce all my legal rights.

Date: 2025, 3 January **Furkan YÖRÜBULUT**

Signature:

ACKNOWLEDGMENTS

Firstly, I would like to express my sincere gratitude to my supervisor, Prof. Dr. Taha TAŞKIRAN for his tremendous support and motivation during my study. His immense knowledge and precious recommendations constituted the milestones of this study. His guidance assisted me all the time of my research and while writing this thesis.

I would also like to express my sincere gratitude to my family and NETSU A.Ş. for their valuable contribution to achieving the desired work in this thesis.

Finally, I would like to express my deep gratitude to my family, who provided me with emotional support, loving care, and constant encouragement throughout my years of study and the period during which this thesis was written.

2024, 3 January **Furkan YÖRÜBULUT**

EFFECTS OF SOIL IMPROVEMENT TECHNIQUES ON THE SITE RESPONSE ANALYSIS (CASE STUDY)

ABSTRACT

An earthquake-resistant structure constructed on soft soil will depend on the characteristics of the soil and the kind of foundation, such as shallow or deep foundation. The TBEC 2018 design recommendations offer an initiative-taking way to calculate seismic loads for spectral analysis approaches that assume a fixed base structure. This thesis tries to assess how jet grouts affect a site's response to acceleration and soil layers shear strains. Using the finite element program Plaxis 2D, the shear force produced at the shallow base is calculated, and the results are compared to the calculation based on TBEC 2018. The purpose is to ascertain if the numerical analysis in Plaxis 2D and the condensed analysis approach used by TBEC 2018 coincide.

A realistic soil model is created for dynamic analysis in Plaxis 2D, tested using a simplified material model and harmonic motion. The model's unimproved field site response analysis is used to determine earthquake behavior, showing reasonable agreement with two-dimensional liquefaction evaluation and site response analysis.

The structures are simulated using a soil model to assess jet impact, and vibration assessments are conducted to determine inherent frequencies and periods of vibration.

Comprehensive dynamic analyses have shown that the type of foundation significantly influences a structure's seismic response. As the inertial force moves upward through the soil layers, it amplifies or attenuates in a specific manner. Additionally, the impact of ground improvement techniques on this acceleration value has been clearly modeled. Due to jet grouting systems beneath the foundation, the calculated inertial force on the rigid base has been reduced. This highlights the need for a special design foundation shear analysis to guarantee the earthquake safety of jet grout-supported structures.

Keywords: Foundation, Liquefaction Evaluation, Earthquake, TBEC 2018, Soil Improvement, Jet Grout, Two-Dimensional Site Response Analysis, Plaxis 2D.

ZEMİN İYİLEŞTİRME TEKNİKLERİNİN SAHA TEPKİ ANALİZİ ÜZERİNDEKİ ETKİLERİNİN ARAŞTIRILMASI

ÖZ

Yumuşak zeminler üzerine inşa edilen yapıların deprem performansı hem zeminin özelliklerine hem de kullanılan temel türüne (sığ veya derin) doğrudan bağlıdır. Türkiye Bina Deprem Yönetmeliği 2018 (TBDY 2018), özellikle sabit temelli yapılar için spektral analiz yöntemiyle sismik yük hesaplamalarında önemli bir çerçeve sunmaktadır. Bu çalışmada, jet enjeksiyonlu kolonların yumuşak zeminlerin ivme ve kesme gerilmelerine karşı davranışı, sonlu elemanlar programı PLAXIS 2D kullanılarak sayısal olarak modellenmiştir. Elde edilen sonuçlar, TBDY 2018'deki basitleştirilmiş yöntemlerle karşılaştırılarak, sayısal analizlerin yönetmelik hükümleriyle ne derece örtüştüğü incelenmiştir. Amaç, jet enjeksiyonlu kolonların deprem performansına olan etkisini daha iyi anlamak ve yönetmeliklerin sunduğu basitleştirilmiş yöntemlerin yeterliğini değerlendirmektir.

Yapılar, jet kolonların zemin üzerindeki etkisini daha iyi anlayabilmek için toprak modelinde simüle edilmiştir. Belirlenen zemin koşullarını temsil etmek üzere, üst üste dizilmiş dört farklı yapı modeli oluşturulmuştur. Bu modeller üzerinde yapılan serbest titreşim analizleri ile yapıların doğal frekansları (veya titreşim periyotları) belirlenmiştir. Elde edilen sonuçlar, TBDY 2018 ve logaritmik bozulma teorisi ile karşılaştırılmıştır. Bu karşılaştırma sayesinde, jet kolonların yapıların dinamik davranışına olan etkisi ve yönetmelikle katsayıların uygunluğu değerlendirilmiştir.

İvme kuvveti zemindeki katmanlardan yukarı doğru hareket ederken belirli şekilde büyür ya da küçülür. Ayrıca, zemin iyileştirme yöntemlerinin bu ivme değerine nasıl etki ettiği açık şekilde modellenmiştir. Temelin altında bulunan jet enjeksiyonu nedeniyle, rijit tabanın üzerindeki hesaplanan ivme kuvvetini azalttigi gozlemlenmistir. Bu durum, jet grout destekli yapıların depreme karşı güvenliğini garanti altına almak için özel tasarım temel kesme analizine duyulan ihtiyacı vurgulamaktadır.

Anahtar Kelimeler: Temel, Sıvılaşma Değerlendirmesi, Deprem, TBDY 2018, Zemin İyileştirme, Jet grout kolon, İki Boyutlu Saha Tepki Analizi.

CONTENTS

NOMENCLATURE

Symbols

G_0^{ref} Small strain shear modulus

c cohession

$\gamma_{0.7}$ Small strain shear modulus becomes about 70% of its initial value

E Modulus of elasticity

ν_{ur} Poisson ratio

E_{ur} Unloading-reloading modulus

PI Plasticity index

σ_{v0} Total vertical stress

σ'_{v0} Initial effective stress

P_w Pore water pressure

k_B^{*e} Bulk modulus factor

k_G^{*e} Shear modulus factor

P_{ref} Reference pressure

me & ne Rate of stress dependecy of stifness

C_N Overburden correction factor

C_E $ER_m/60$

ER_m The energy supplied is measured and expressed as a percentage (%) of the hammer energy that would theoretically fall unimproved.

C_R Correction factor to account for different rod lengths.

C_B Correction factor for nonstandard borehole diameters.

C_S Correction factor that depends on the sampler.

F_c Yield functions for compression

N_{SPT} Computed as N2 + N3, taking into account that N1, N2, and N3 are the number of blows required for each 15 cm penetration by the tube.

f_t Uniaxial tensile yield stress

f_{cy} Uniaxial compressive yield stress

H_{cu} Strain hardening/softening

H_{cf} Ultimate plastic strain

ε_{cf^p} Failure plastic strain

$f_c f_n$ Normalized compressive failure strength

P	Pressure, Pa
t	Time, s
Δt	Dynamic time, s
$\alpha \; and \; \beta$	Rayleight coefficient
N	SPT-N value
S_{ae}	Spectral acceleration
y^+	Dimensionless wall distance

Subscripts

φ	Friction angle

Acronyms

TBEC	Turkish Building Earthquake Code
PSA	Psedo Spectral Acceleration
SPT	Standart Penetration Test
CPT	Cone Penetration Test

LIST OF TABLES

LIST OF FIGURES

CHAPTER 1

INTRODUCTION

In many different building projects, jet grouting systems are used to support structures and transfer loads to the ground. However, the characteristics of the soil at the site significantly influence the performance of jet grouting systems. For the purpose of developing secure and dependable jet grout structures, the site response analysis is a critical factor to take into account. It entails researching the dynamic soil characteristics and how they respond under seismic loads.

The Turkish Building Earthquake Code (TBEC), which governs seismic design in Turkey, is a crucial regulation. Updated guidelines for seismic design of pile foundations and site response analysis are included in the most recent version of TBEC, referred to as TBEC 2018 in Turkey. These regulations, which improve the seismic performance of pile foundations in Turkey, are based on cutting-edge analytical and experimental methodologies.

So, the purpose of this thesis is to examine how site response analysis affects the seismic design of pile foundations in accordance with TBEC 2018 by using Plaxis 2D. The study will concentrate on the dynamic soil characteristics, the consequences of the interaction between the soil and the structure, and the effectiveness of pile foundations under various seismic hazard levels. The findings of this study will aid in the creation of pile foundations for seismic zones in Turkey that are safer and more dependable.

1.1 Structure of the Thesis

The seismic affect and energy distribution models in soil and foundation elements are examined in this thesis. The TBEC 2018 standard specifies certain points surrounding the dynamic analysis, and anaylsis results from the Plaxis 2D have been used to compare the AFAD Database results. Optimization study was carried out with the revised model. The thesis's flow chart is as follows,

At the introduction of the first chapter, general information was provided, and literature reviews on site response analysis were looked at.

The second chapter provides an introduction to the theoretical framework that was utilized to analyze the numerical model.

The third chapter looks at the thesis study's numerical model development. How to set up material model and analysis condition settings is explained in depth.

The numerical model was validated using test outcomes, and findings of site response analyses were described in the fourth chapter. The consequences of the optimization study were interpreted.

The thesis's conclusions have been assessed in the fifth chapter.

1.2 Aim of the Thesis

The impacts of sesimic affect in soil layers and structures have been studied. This method requires the usage of a finite element model. It is also vital that the factors utilized as analysis inputs, such as the convergence criteria and solution methodologies, be appropriately provided. The intention of thesis is to develop a site response analysis with finite element method. The resulting method is performed in revised cases. For next research, additional parameters and different soil improvement techniques will be added to the proven analysis model.

The specific resource objectives are:

1. To create a 2D finite element model based on the TBEC 2018 design specifications of a typical pile foundation system, which includes the jet grout column, soil, and foundation.
2. Using Plaxis 2D, conduct a site response study and identify the dynamic soil properties—such as soil stiffness and damping—that influence the behavior of the jet grout columns system.
3. To offer suggestions based on the study's findings for the design of jet grouting for soil improvement under the foundations in Kayseri & Turkey's seismic areas.

The finite element method by using Plaxis 2D software for geotechnical engineering dynamic analysis. The software helps to create a precise numerical model of the jet grout system, analyze the consequences of soil-structure interactions, and determine how well jet grout columns operate when subjected to seismic loads. To confirm the accuracy and dependability of the findings, the numerical simulations will be checked against existing experimental data and analytical solutions.

Overall, by offering insightful information on the implementation of the TBEC 2018 standards for site response analysis and seismic design of jet grout foundation by using Plaxis 2D. This study can help Turkey construct safer and more dependable jet grout columns under the foundation for seismic zones.

1.3 Literature Research

1.3.1 Overview

Along with computers, finite element method in site response analysis are also developing. Site response analysis is crucial in earthquake engineering as it evaluates how local soil conditions affect ground motion during seismic events. When the literature researches are examined, studies on this subject can be seen. This analysis typically involves the propagation of seismic waves from the bedrock through soil layers to the ground surface, which can amplify or attenuate ground shaking. Dynamic analysis numerical flow calculations for different kind of soil layers sites may be found in the literature. This section includes an overview of the important studies of thesis.

1.3.2 Literature Review

The Equivalent Linear method assumes linear elastic behavior for small strains, while the NL approach accounts for the nonlinear behavior of soil, especially at larger strains. Studies have shown that these methods yield different results based on input motions and soil properties. For instance, Tsai and Chen (2021) discuss how these approaches can significantly impact engineering practices and outcomes in site response analysis [1].

Most site response analyses are conducted in one dimension (1D), focusing on vertical propagation of seismic waves. This method simplifies the complex interaction between

soil layers but can still provide valuable insights into potential surface accelerations and spectral amplification factors [2].

Recent advancements emphasize a performance-based approach that incorporates probabilistic elements to account for variability in soil stratification and properties. This methodology enhances the reliability of predictions regarding site-specific responses to seismic loading [3].

Research focusing on specific regions, such as Istanbul, has demonstrated how local soil characteristics influence seismic wave propagation. Studies like Yildiz (2021) utilized both EQL and NL analyses to compare results across different soil profiles during significant earthquakes, revealing critical insights into local amplification effects. Yıldız (2021) utilized both EQL and NL analyses to compare results across different Istanbul soil profiles during major earthquakes. The study revealed critical insights into local amplification effects and the influence of soil properties on seismic wave propagation [4].

Seed et al. (1994) and Toro and Silva (2001) identified several key parameters that significantly impact site response analysis results, including soil stiffness, depth of soil column, and bedrock depth. Variations in these factors can lead to substantial differences in predicted ground motions [5].

Romero and Rix (2001) found that the types of sand and clay in a soil profile tremendously affect earthquake ground motions. Correct soil stratification is crucial for reliable site response analysis [6].

Hashash et al. (2015) evaluated the performance of 1D site response models using centrifuge experiments. They found the secant shear modulus is the most significant parameter, emphasizing the need for accurate soil stiffness characterization [7].

Ansal et al. (2024) discussed incorporating probabilistic elements into site response analysis to account for uncertainties in soil properties. This performance-based approach enhances reliability compared to deterministic analyses [8].

Silva (2005) highlighted the importance of considering a range of site and seismic parameters when performing site response analyses to bracket potential outcomes and account for uncertainties [9].

Akin, Mutluhan, et al. investigated the impact of jet grouting on the seismic response of structures founded on soft soils through numerical simulations and experimental testing. The effects of varying jet grouting parameters on structural periods and damping ratios are evaluated [10].

The study of Sedighi and other (2017) shows that jet grouting columns can significantly affect the seismic behavior of soils. However, the effectiveness of soil improvement methods depends on many factors such as soil properties, earthquake characteristics, and structural requirements. Therefore, a detailed analysis should be carried out for each project according to the site conditions [11].

The study of El-Emam, Magdi, et al. investigates how local soil conditions affect the intensity of ground shaking in major cities of the United Arab Emirates, such as Abu Dhabi, Dubai, and Sharjah. The research found that the surface soil layers in these areas can significantly amplify seismic waves, particularly within a specific frequency range. This amplification can pose significant risks to the safety of structures. The findings emphasize the importance of considering local soil conditions in earthquake engineering practices to ensure the safety of buildings and infrastructure [12].

1.4 Motivation and Objectives

Ground improvement techniques have become increasingly popular in recent years to enhance the geotechnical properties of soils, particularly in regions prone to seismic activity. The devastating effects of earthquakes on structures have highlighted the need for effective ground improvement methods to mitigate seismic hazards. This study is motivated by the growing concern over the safety of structures located in seismic regions and the potential of ground improvement techniques, such as jet grouting, to enhance the seismic performance of these structures.

The selection of appropriate ground improvement techniques is crucial for the design of safe and resilient structures. Jet grouting, a well-established ground improvement method, has been widely used to enhance the bearing capacity, reduce settlement, and improve the seismic resistance of soils. However, the effectiveness of jet grouting in mitigating seismic hazards and its influence on the dynamic response of structures under seismic loading conditions remain subjects of ongoing research.

The primary objective of this study is to quantitatively assess the influence of jet grouting on the seismic response of structures founded on soft soils. Specifically, this research aims to evaluate the effectiveness of jet grouting in mitigating seismic hazards such as liquefaction and excessive deformations, and to compare the results of numerical simulations using PLAXIS 2D with the predictions of the Turkish Building Earthquake Code (TBEC 2018). By achieving these objectives, this study aims to highlight the significance of ground improvement techniques in earthquake engineering applications.

CHAPTER 2

THEORY

2.1 Overview

This chapter provides a summary of the methodologies used in doing the thesis. The foundations and theory on which the methodologies are based are mentioned. In the analysis part of the study, the finite element model was implemented as the solver setting. The infrastructure of the soil model and the relevant governing equations are explained. The assumptions taken for the Plaxis 2D software, where seismic analyses are performed, are also explained with equations.

2.2 FEM Model Analysis in PLAXIS

An approximate numerical approach for tackling engineering and mathematics issues is the finite element method (FEM). A major issue element (a building or soil volume) is split into smaller portions using this technique. These discrete components, also known as "finite elements," might have borders with triangles, squares, or curves and consist of an approximation of the behavior of the larger component. Numerical integration is used to connect the elements, simulating the behavior of the entire element. Deformations in a collection of nodal points serve to characterize the deformation of the components (Nordal, 2016).

"Plaxis 2D is a two-dimensional finite element program, developed for the analysis of deformation, stability, and groundwater flow in geotechnical engineering" (Brinkgreve et al., 2016). Plane strain or axisymmetric 2D models may be built with Plaxis. It describes deformation using triangular components with 6 or 15 nodal points. To specify the soil property, there are various material models available. Plates, anchors, embedded beams, and geogrid are examples of structural elements that may be built ("Plaxis 2D Reference Manual," 2023.2).

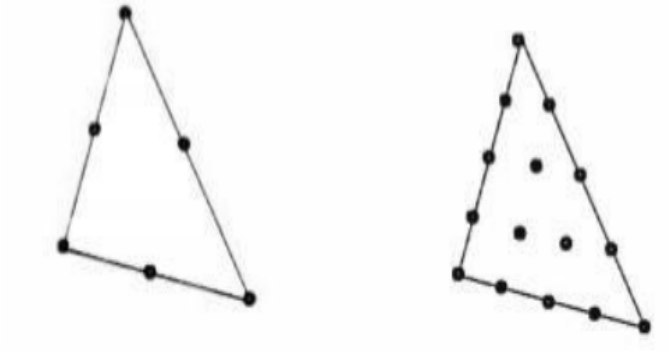

Figure 2.1 Triangular element with 6 and 15 nodes (Nordal, 2016)

2.3 Material Model

Different material models can represent the mechanical behavior of soil in PLAXIS with varying degrees of precision. The simplest model is the linear elastic model, which uses only the Young's modulus (E) and Poisson's ratio (v) to describe soil behavior. It is based on Hooke's law of elasticity. As a result, using the LE model to soil is inappropriate; concrete or unbroken rock should be used instead. The linear elastic completely plastic Mohr-Coulomb model (MC), which also includes the plasticity parameter c and dilatancy angle and it can represent soil behavior more accurately ("Plaxis 2D Material Models Manual," 2023.2).

Advanced models, such as the Hardening Soil Small-Strain Model (HSsmall) or the UBC3D-PLM Model can represent soil behavior more accurately. The HSsmall model and UBC3D-PLM models are used in this thesis to specify the behavior of the soil for dynamic analysis. As a result, this section describes the fundamental ideas behind the HSsmall and UBC3D-PLM models.

2.3.1 Hardening Soil Model with Small Strain Stiffness (HSsmall Model)

The beginning of the Hardening Soil model assumed elastic material behavior occurs when unloading and reloading. However, there is a very narrow strain range where soils may be said to be very elastic when they nearly fully recover from applied straining. Soil stiffness decreases nonlinearly with increasing strain amplitude. The classic S-shaped stiffness decrease curves are produced when soil stiffness is plotted

versus log(strain). In Figure 2.2 provides an illustration of one of these stiffness decrease curves. It also describes the appropriate strain ranges for laboratory experiments and the typical shear stresses that may be recorded in the surrounding area of geotechnical designs.

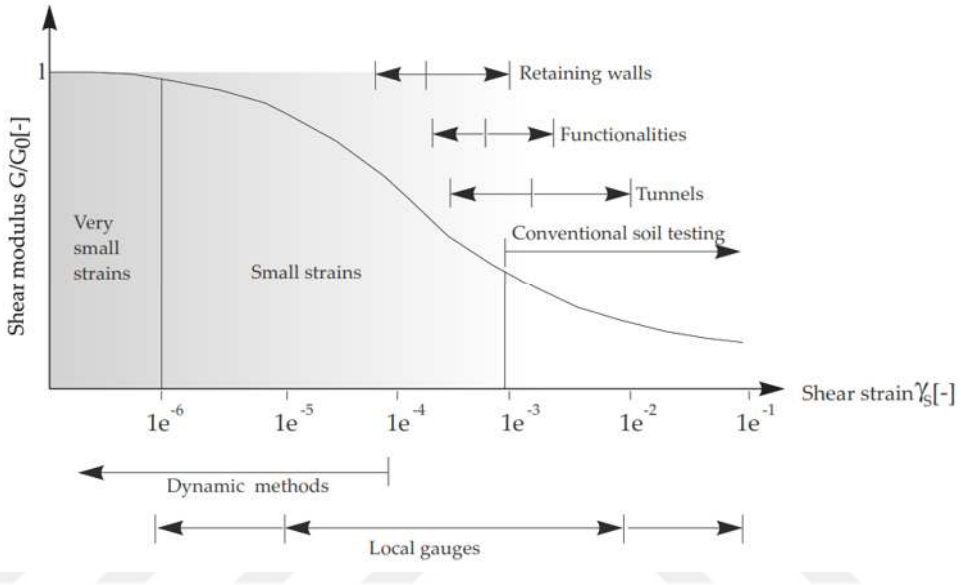

Figure 2.2 Characteristic stiffness-strain behaviour of soil with typical strain ranges for laboratory tests and structures (after Atkinson & Sallfors,1991)

The HSsmall model is a variant of the HS model that features improved soil stiffness for low strain. Compared to engineering stiffness, soil stiffness rises dramatically with extremely low stiffness. In this situation, the strain-stiffness connection is no longer linear. In addition to the other input parameters in the HS model, the HSsmall model adds two more parameters to address this phenomenon.

- small strain shear modulus (strain in the range of 1. 10^{-6}), G_0^{ref}
- strain level at which small-strain shear modulus becomes about 70% of its initial value, $\gamma_{0.7}$

The stress dependency of small strain stiffness is given by:

$$G_0 = G_0^{ref}\left(\frac{c.cos\phi - \sigma_3' sin\phi}{c.cos\phi + P_{ref} sin\phi}\right)^m \quad (2.1)$$

Stress-strain curve for small strain can be described with a hyperbolic low proposed by Hardin and Drnevich (1972):

$$\frac{G_s}{G_0} = \frac{1}{1 + |\frac{\gamma}{\gamma 0.7}|} \quad (2.2)$$

$$\frac{G_s}{G_0} = \frac{1}{1 + 0.385\frac{\gamma}{\gamma 0.7}} \quad (2.3)$$

This relation is used in Plaxis to describe stress-strain curve.

Again, according to Vucetic and Dobry (1991) G_s/G_0 vs γ curves depends on plasticity index, PI (usually taken for 50%).

The lower cut-off of tangent shear modulus is given by, $G_t \geq G_{ur}$

Here, unloading-reloading stiffness, $G_{ur} = E_{ur}/ 2(1+ \nu_{ur})$; E_{ur} is the unloading-reloading modulus and ν_{ur} is the poisson's ratio for loading/unloading. HSsmall model demonstrates more reliable displacements than HS model and more suitable for dynamic analysis since it captures cyclic behavior ("Plaxis 2D Material Models Manual," 2023.2).

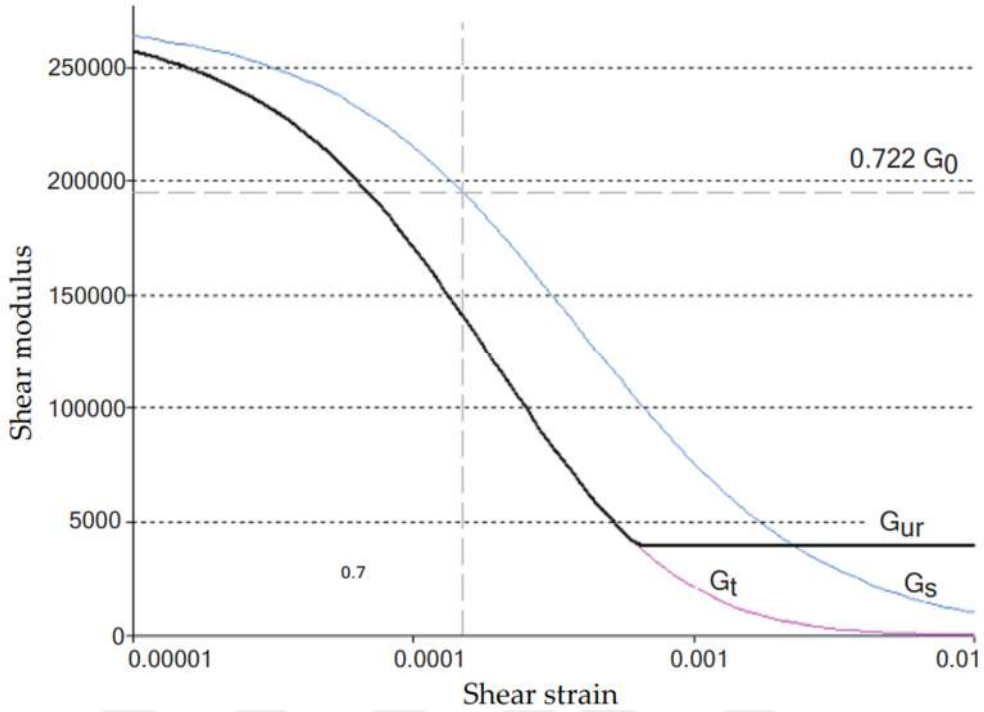

Figure 2.3 Secant and tangent shear modulus reduction curve ("Plaxis 2D Material Model Manual," 2023.2)

2.3.2 UBC3D-PLM Model

Soil shaking occurs when seismic waves travel from the source to the surface of the earth. At whatever depth in the soil deposit, the amplitude, length, and frequency content of the seismic waves vary due to the filtering effect of the soil deposit. An earthquake can cause a variety of effects, including landslides, soil liquefaction, and structural damage.

A wide range of phenomena that take place in saturated, cohesive-less soils when they are left undrained are referred to as liquefaction. Dry cohesionless soils tend to solidify under both static and periodic loads. The tendency to densify increases excess pore pressures that cannot quickly dissipate, which leads to a decrease in the effective stresses if these soils are saturated and the applied load acts quickly, as in the affect of the earthquake. The earth moves like a fluid when this situation occurs.

Coulomb's formula describes the shear resistance τ for cohesionless soils, which might explain this phenomenon.

$$\tau = \sigma'_{vo} tan(\varphi) \quad (2.4)$$

where;

σ'_{vo}: The initial effective stress

φ: The friction angle

The effective stress formula according to Terzaghi's formula by:

$$\sigma'_{vo} = \sigma_{vo} - P_w \quad (2.5)$$

Where;

σ_{vo}: The total vertical stress

P_w: The pore water pressure

The equation for excess pore pressures (ΔPw) during an earthquake is as follows:

$$\sigma'_{vo} = \sigma_{vo} - (P_w + \Delta P_w) \quad (2.6)$$

This indicates that the effective stress state tends to drop until it approaches zero, at which point the shear resistance is negative.

Identifying the liquefaction's predisposing and triggering elements is essential to assessing a site's potential liquefaction risk. The predisposing variables include the features of the soil deposit, including the gradation, plasticity, and size and shape of the particles. The magnitude, duration, and peak ground acceleration of the earthquake determine the triggering factors. In order to determine if liquefaction can happen at a particular location when a certain earthquake occurs, semi-empirical techniques or nonlinear dynamic studies may be employed.

According to Tsegaye (2010) and Petalas & Galavi (2012), the UBC3D-PLM model is an efficient stress elasto-plastic model that can simulate the liquefaction behavior of sands and silty sands under seismic loading. The initial UBCSAND (University of British Columbia Sand) model, which was presented by Puebla, Byrne & Phillips

(1997) and Beaty & Byrne (1988), served as the foundation for the UBC3D-PLM model formulation. Based on the original Duncan-Chang model, the original UBCSAND is a 2D model developed in classical plasticity theory with a hyperbolic strain hardening algorithm. The plastic shear strain at a given stress is related to the mobilized friction angle by the hardening rule.

The generalized 3D formulation of the UBC3D-PLM model is the primary distinction between it and the UBCSAND model. For main loading, the UBC3D-PLM model includes the Mohr-Coulomb yield condition in a three-dimensional principal stress space; for secondary loading, it utilizes a yield surface with a streamlined kinematic hardening rule. Additionally, for a stress path starting from the isotropic line Tsegaye (2010), a modified non-associated plastic potential function based on Drucker-Prager's criteria is utilized for the primary yield surface to uphold the assumption of stress-strain coaxially in the deviatoric plane.

A dynamic site response study can be used to determine a soil deposit's propensity for liquefaction. To conduct such an analysis, the following procedures are often required (Laera & Brinkgreve, 2015).

- Creation of the geotechnical model for the soil deposit, including layer distribution, water table depth, dynamic boundary conditions, and soil mechanical characteristics, to explain its behavior under static and cyclic loads.
- Definition of seismic input motion based on the individual site and the probabilistic research as described in the existing rules.
- Define the numerical model for the analysis, including dynamic boundary conditions.

In order to determine the distribution of soil layers, hydraulic conditions, and mechanical characteristics of the soil, a thorough and prolonged examination of the soil deposit is necessary for a site response study. The inquiry should be carried out as deep as a rock or formation that resembles a rock whenever feasible. To assess the index properties, stiffness, and strength of the soil layers in relation to their behavior under cyclic loading, both in situ and laboratory studies should be carried out. However, data from in situ tests such as SPT or CPT, or from drained triaxial testing,

are often the only ones accessible. Because of this, a particular formulation with input parameters based on these tests is implemented by the UBC3D-PLM model.

The following lists the primary attributes of the UBC3D-PLM model along with the appropriate input parameters:

Stress dependent stiffness according to a power law $k^*_B{}^e$, $k^*_G{}^e$, *me*, *ne, np*.

- Plastic straining due to primary deviatoric loading k^*G^p.
- Densification due to the number of cycles during secondary loading fdens.
- Post-liquefaction stiffness degradation fEpost
- Failure according to the Mohr-Coulomb failure criterion φcv, φp and c.

The non-linear, isotropic rule for the elastic behavior that is specified in terms of the elastic bulk modulus K and the elastic shear modulus G which are determined by the following equations is incorporated into the UBC3D-PLM model.

$$K = k^*_B{}^e P_{ref} \left(\frac{P'}{Pref}\right)^{me} \tag{2.7}$$

$$G = k^*_G{}^e P_{ref} \left(\frac{P'}{Pref}\right)^{ne} \tag{2.8}$$

$k^*_B{}^e$: Bulk modulus factor

$k^*_G{}^e$: Shear modulus factor

P_{ref} : Reference pressure

me & ne : Rate of stress dependecy of stifness

The model predicts pure elastic behavior with Gmax during the unloading procedure. Plastic behavior is considered once the stress state reaches the yield surface, provided that the stress point does not instantly return to the elastic zone.

An initial yield surface is established using a collection of Mohr-Coulomb functions. The hardening law defines the location and dimensions of the yield surface. More precisely, the model (which is akin to the Hardening Soil model) uses plastic hardening based on the theory of strain hardening. The amount of plastic strain resulting from the

mobilization of the shear strength (sin φ_{mob}) is governed by the hardening rule. The Mohr-Coulomb yield criteria yield the mobilized friction angle, which is as follows:

$$sin(\varphi_{mob}) = \frac{\sigma'_1 - \sigma'_3}{\sigma'_1 + \sigma'_3 - 2ccot(\varphi_p)} \tag{2.9}$$

In order to provide a seamless transition into the liquefied condition of the soil and to distinguish between main and secondary loading, the UBC3D-PLM model makes use of two yield surfaces. To increase the accuracy of the development of the excess pore pressure, the UBC3D-PLM model integrates a densification law through a secondary yield surface with a kinematic hardening rule. Lower plastic deformations are produced by this surface in comparison to the primary yield surface.

In earthquake engineering, a cyclic triaxial or cyclic direct simple shear test is often the appropriate method to extract all the parameters for the UBC3D-PLM model when the modeling aim is the beginning of liquefaction. However, in many instances, the only accessible data come from either in situ testing (SPT) or drained triaxial tests (CD TxC). Because of this, a particular formulation with input parameters based on these tests is implemented by the UBC3D-PLM model. When calibrating the UBC3D-PLM model, however, some of the equations based on SPT values that Beaty & Byrne (2011) suggested for the generic calibration of the UBCSAND model should be utilized with caution.

Beaty and Byrne (2011) presented a series of formulas for the first generic calibration of the UBCSAND model, which are based on the normalized N_{SPT} value, $(N_1)_{60}$. Makra (2013) updated the suggested formulas and emphasized the distinctions between the Plaxis implementation of the UBC3D-PLM model and the first UBCSAND 2D formulation. The following are the suggested formula for the general initial calibration:

$$k^*_G{}^e = 21.7 \text{ x } 20 \text{ x } (N_1)_{60}{}^{0.3333} \tag{2.10}$$

$$k^*_B{}^e = 0.7 \text{ x } k^*_G{}^e \tag{2.11}$$

$$k^*_B{}^p = \quad k^*_G{}^e \times (N_1)_{60}{}^2 \times 0.003 + 100 \tag{2.12}$$

Curve fitting is the recommended method of calibrating the index parameters me, ne, and np. These values have a range of 0 to 1. The default values that are proposed are me = ne = 0.5 and np = 0.4. As recommended by Souliotis & Gerolymos (2016), an alternative method for calibrating the parameters is to use the relative density correlations.

One can easily determine the strength parameters of the principal yield surface, φcv, φ_p, and c, using CD TxC or DSS testing. The cohesion c default value is 0, as is typically the case with granular soils devoid of a significant fine component. Using the SPT test, the peak friction angle φ_p may be computed as follows:

$$\varphi_p = \varphi_{cv} + 0.1 \times (N_1)_{60} + \max(0; ((N_1)_{60}-15)/5) \tag{2.13}$$

It is possible to obtain the constant volume friction angle, or φcv, straight from the SPT test by utilizing one of the correlations found in the literature (Bolton, 1986, p. 242; Mayne, 2001).

During secondary loading, the scaling of the plastic shear modulus factor is managed by a multiplier called the densification factor. A number below 1 indicates that the k *Gp is smaller, and the behavior is softer; otherwise, the range of values is 0 to 1. According to Petalas and Galavi (2012), fdens = 1.0 is advised since liquefaction triggering is not greatly impacted by variations in densification.

The parameter to modify the behavior of post-liquefaction is called f_{Epost}. f_{Epost} can have a value between 0.1 and 1, however a value between 0.2 and 1 is advised. In extremely thick sands, resistance is overestimated; this can be compensated for by raising the fEpost parameter. Although it may also be computed from the SPT test using the original UBCSAND (Beaty & Byrne, 2011), the failure ratio Rf has a default value of 0.9.

$$R_f = 1.1((N_1)_{60})-0.15 < 0.99 \tag{2.14}$$

Many procedural aspects, which are considered using correction factors, have an impact on the SPT blow count N_{SPT}. These details include rod lengths, hammer energy, sampler details, and borehole size. Furthermore, the corrected penetration resistance $(N_1)_{60}$, which may be stated as follows, can be obtained by correcting the N_{SPT} using the overburden stress effects.

$(N_1)_{60} = C_N C_E C_R C_B C_S N_{SPT}$

C_N : The overburden correction factor.

C_E : $ER_m/60$

ER_m : The energy supplied is measured and expressed as a percentage (%) of the hammer energy that would theoretically fall unimproved.
C_R : Correction factor to account for different rod lengths.
C_B : Correction factor for nonstandard borehole diameters.
C_S : Correction factor that depends on the sampler.

N_{SPT} : computed as N2 + N3, taking into account that N1, N2, and N3 are the number of blows required for each 15 cm penetration by the tube.

The excess pore pressure ratio $r_{u,\sigma'v}$, which is provided by: may be utilized to represent the liquefaction potential in terms of vertical effective stress.

$$r_u,\sigma'_v = \frac{\sigma'_{v0} - \sigma'_v}{\sigma'_{v0}} \quad (2.15)$$

where σ'_{v0} is the initial effective vertical stress before the seismic motion, and σ'_v represents the vertical effective stress as of right now during the dynamic's computation. A fully liquefied state is present in the relevant layer when ru, σ'_v equals 1. Zones having a maximum r_u, σ'_v of more than 0.7 are deemed to be liquefied according to Beaty and Perlea (2011).

2.3.3 Concrete Model

Due to concrete is stronger than soil, a linear elastic material model is typically used for its structural parts. However, in some geotechnical issues, an accurate design and

a dependable redistribution of stress-strain in the continuum need an inspection of the intricate non-linear behavior of the concrete structures. It is possible to distinguish between the following primary characteristics of the complicated behavior of concrete: strain hardening/softening, creep and shrinkage, time-dependent strength and stiffness, and restricted strength in compression and tension.

The Concrete model was initially developed to simulate shotcrete behavior in concrete buildings, soil enhancements, and soil reinforcing. It accounts for non-linear material behavior, resulting in more realistic stress distributions. The current engineering technique assumes a linear elastic material with unrealistically low Young's modulus, resulting in excessive lining stresses. The Concrete model accounts for this non-linearity, ensuring accurate lining deformations (Plaxis Material Model Manual)

The Concrete Model can model both time-dependent and time-independent behaviors, taking into account the loss in stiffness behavior following the breaking of brittle cemented materials. Time-dependent characteristics of concrete material under strain hardening-softening conditions under compression and tension include time-dependent strength, stiffness, creep, and shrinkage. The normalized strength and stiffness of cured concrete at a specific hydration time are examples of time-independent qualities. As such, the overall strain in the Concrete Model may be broken down into stresses related to elastic, plastic, creep, and shrinkage. (Schadlich & Schweiger ,2014)

$$\varepsilon = \varepsilon^{e} + \varepsilon^{p} + \varepsilon^{cr} + \varepsilon^{shr} \tag{2.16}$$

In soil model simulations, the yield surfaces show how stress states vary as stresses change. Two distinct yield surfaces, one based on the Rankine failure surface for tension and the Mohr-Coulomb failure criterion for compression, were used in the construction of the Concrete Model.

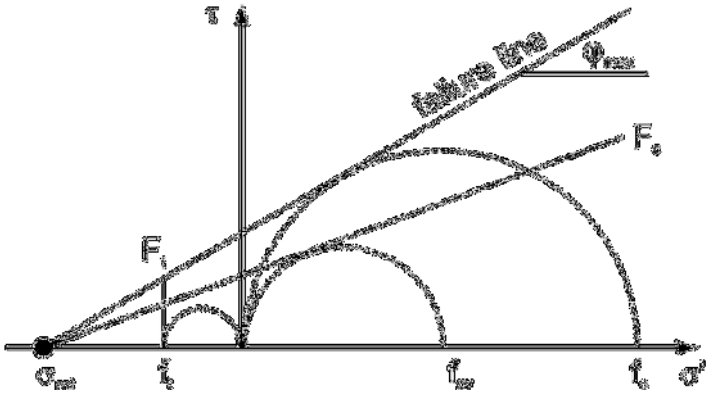

Figure 2.4 Yield surfaces and failure envelope for concrete model

Getting the strength parameters, the yield functions for compression (F_c) and tension (F_t) can be expressed in terms of primary stresses associated with the uniaxial compressive yield stress (f_{cy}) and the uniaxial tensile yield stress (f_t).

$$Fc = \frac{\sigma 1 - \sigma 3}{2} + \frac{\sigma 1 - \sigma 3 - 2\sigma rot}{2} \frac{fcy}{2\sigma rot + fcy} \tag{2.17}$$

$$Ft = \sigma 1\text{-}f1 \tag{2.18}$$

where σ_{rot} is the point where the isotropic axis and the Mohr-Coulomb failure envelope cross, and σ_1 and σ_3 are the main and minor principal stresses. σrot may be expressed as follows for a particular maximum friction angle (φ_{max}) of the failure envelope:

$$\sigma_{rot} = \frac{fc}{2}\left(\frac{1}{sin(\varphi max)} - 1\right) \tag{2.19}$$

The stress-strain curve is into four sections to represent how concrete behaves under compression. The behavior of hardened concrete is shown by the curve in Part I of below Figure 2.5, which reaches its peak compressive strength. Thereafter, it exhibits a linear softening behavior until it reaches Part II, the failure compressive strength, and Part III, the final compressive strength. The final portion (Part IV) is then decreased and stays constant at the concrete's residual strength. As a result of considering the

time-dependent behavior, the normalized parameters in the Concrete Model's tension and compression stress-strain curves control the material parameters.

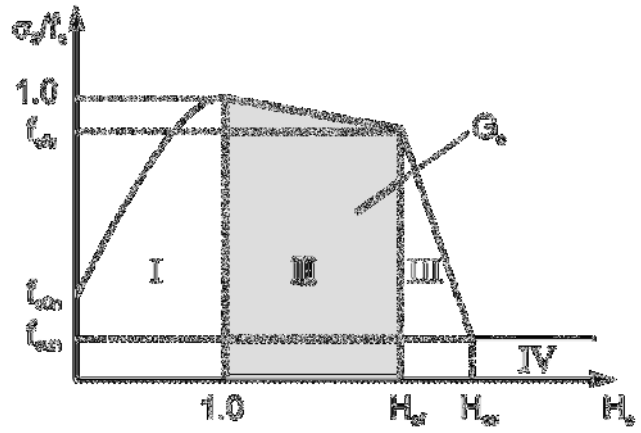

Figure 2.5 Concrete Model Stress/Strain Graph

The normalized values are used in the compression stress-strain curve for both the horizontal and vertical axes, as was previously described. As seen in Figure 2.5 above, the strain hardening/softening parameter ($H_c = \varepsilon_3^p / \varepsilon_{cp}^p$) is used on the horizontal axis to plot against the ratio of minor principal stress (σ_3) by the compressive concrete strength (f_c) on the vertical axis, normalized with the minor plastic strain (ε_{cp}^p) and plastic peak strain in uniaxial compression (σ_3). The parameters H_{cu} and H_{cf} represent the strain hardening/softening and ultimate plastic strain, respectively, normalized with the ultimate plastic strain (ε_{cf}^p) and the normalized compressive ultimate strength (f_{cun}), respectively, and the failure plastic strain (ε_{cu}^p) that corresponds to the normalized compressive failure strength ($f_c f_n$). The full mobilized compressive strength, $f_c = 1$, is correlated with $H_c = 1$.

The stress-strain curve (Figure 2.6) for the tension behavior of concrete is primarily divided into two sections. First, until the concrete material reaches its maximal tensile strength (f_t), linear elastic hardening action takes place under tension. Then, until the ultimate tensile strength (f_{tu}), it is decreased with the linear tension softening characteristic. When the residual strength is attained, there is no more softening and everything keeps the same (f_{tun}).

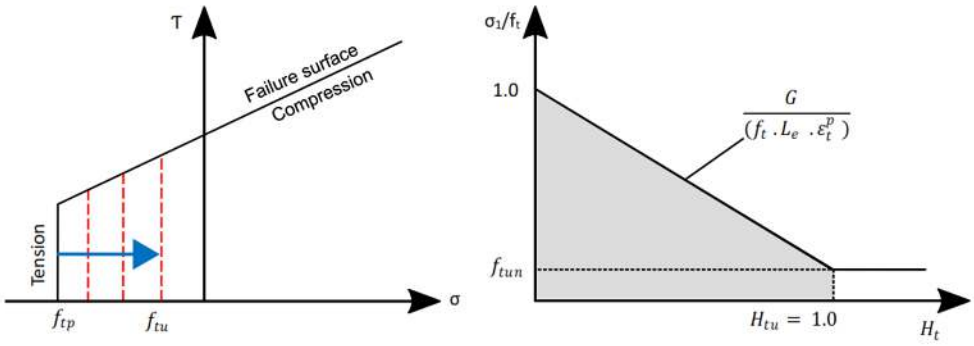

Figure 2.6 Tension softening

As demonstrated in Figure 2.6, the strain hardening/softening parameter ($H_t = \varepsilon_1^p / \varepsilon_{tu}^p$) is used on the horizontal axis to plot against the ratio of major principal stress (σ1) by the tensile concrete strength (f_t) on the vertical axis, normalized with the major plastic strain (ε_1^p) and plastic ultimate strain in uniaxial tension (ε_{tu}^p). The normalized tensile ultimate strength (f_{tun}) is equivalent to the ultimate plastic strain (ε_{tu}^p), where Htu is the strain softening parameter in tension normalized with it. The full mobilized tensile strength, $f_t = 1$, is correlated with $H_{tu} = 1$.

In compression, the plastic failure strain is related to the plastic peak strain in such a way that the ratio εcfp / εcpp stays constant. GC decreases with time as εcfp and εcpp decrease. Conversely, as time passes, the compressive strength fc rises, leading to greater Gc values. These opposing tendencies result in high fracture energy values early in life, a steep decline at about 12 hours, and a subsequent linear increase in Gc with fc. The intended ductile behavior at this stage is the reason for the high fracture energy at a relatively young age. Since extremely young concrete practically never fails under stress, theoretically there should be an unlimited fracture energy.

Creep and shrinkage control the time-dependency behavior of concrete or cement-admixed materials. Creep strain is caused by the concrete specimen's progressive distortion over time as a result of prolonged tension. In the meanwhile, shrinkage strain is unaffected by the stress state, which manifests itself over time as volume loss. The Concrete Model allows for the consideration of the time-dependent stresses associated with the previously mentioned creep factor and shrinkage factor.

The three main behaviors of concrete or soil treated with cement are shrinkage, creep, and strain hardening/softening. The ability to replicate the aforementioned properties is the primary benefit of the Concrete Model in Plaxis. However, as the main goal of this work is to suggest directions for applying the Concrete Model in Plaxis to cement-treated Bangkok clay that preserves the post-failure behavior, the time-dependency is turned off for this study. This study primarily focuses on the material model parameters associated with the time-independent behavior.

2.4 Dynamic Analysis

For both single source vibration and earthquake situations, Plaxis offers dynamic analysis. Typically, earthquake stresses are placed at the bottom boundary, and the shear waves that arise go upward. The simulation of the soil uses a simple strain model without geometric damping. Rayleigh damping is therefore advised in order to obtain a realistic outcome (Plaxis 2D Dynamic Manual).

Despite the fact that the analytical process for a dynamic load is virtually identical to that for a static situation, there are a few considerations to be made, such as:

2.4.1 Boundary Condition

Although soil grows indefinitely in actuality, in finite element analysis soil volumes are represented as a volumetric element that is laterally confined by limits. Static analysis works well with this type of simulation, because smaller volumes require less time and computation. However, in a dynamic study, the wave's propagation encounters the vertical limits and reflects back into the system, trapping energy (Stensløkken, 2016). A unique dynamic boundary condition can be used to overcome this issue. From the alternatives listed below, select the appropriate boundary condition ("Plaxis Bv," 2014)

I. Viscus boundary, has a viscus damper, which is often used when the vibration source is inside the mesh, and it absorbs the incoming energy.
II. Compliant base boundary, combination of a line prescribed displacement and a viscous barrier, only available on the mesh base, is typically used for earthquake situations.

III. Unimproved field boundary, only accessible for lateral boundaries, a viscous boundary like compliant base combined with a line prescribed displacement is ideal for earthquakes.

IV. Tied degree of unimproveddom, available only for PLAXIS 2D and the lateral limits (not in 3D). The left and right boundary nodes are connected in such a way that they experience the same displacement. applied most frequently to earthquake issues.

2.4.2 Element Size and Time Stepping

In Plaxis, mesh is automatically created based on a reliable triangulation process. By choosing the proper element distribution, it is possible to regulate the dimension of triangular elements (Laera & Brinkgreve, 2015). According to the "Plaxis 2D Reference Manual," published in 2016, there are five distinct types of element distributions that result in five different relative element size factors (r_e) and related average element sizes or target element sizes.

Target element dimension can be approximated based on the equation suggested by (Kuhlemeyer & Lysmer, 1973)

$$\text{Average element size} \leq V_{s,min}/ (8*f_{max}) \tag{2.20}$$

Here, Vs,min is the lowest shear wave velocity of the layer and fmax is the maximum frequency content of the input wave.

Every time a time step is taken, Plaxis automatically makes sure the wave passes one element. Critical time step is determined for this based on the element size and material stiffness. Next, the time step is modified in accordance with the input data points (Laera and Brinkgreve, 2015).

$$\delta_t = \frac{\Delta t}{m.n} \tag{2.21}$$

Here, Δt is the time step calculated from dynamic time interval Δt, maximum number of steps, m and number of sub steps, n.

2.4.3 Rayleigh Dmaping Parameter

The hysteretic damping of the soil model can effectively capture damping at strains exceeding $\%10^{-4}$ to $\%10^{-2}$, contingent upon the specific material properties. Specially, even at low deformation levels, the soil exhibits irreversible behavior. It is advisable to define Rayleigh damping coefficients corresponding to a modest damping ratio. According to the Rayleigh damping formulation, the damping matrix C is expressed as a combination of the mass matrix M and the stiffness matrix K, influenced by the Rayleigh coefficients α and β.

$$[C] = \alpha[M] + \beta[K] \tag{2.22}$$

2.4.4 Other Factors

In Plaxis analysis, Newmark time integration damping under dynamic conditions is typically provided a default value:

- αN= 0.25 and βN=0.5, for average acceleration
- αN= 0.3025 and βN=0.6 for damped Newmark scheme

To enhance the quality of the absorption at the borders, the relaxation coefficients C_1 and C_2 are used. When the soil is just exposed to a normal pressure wave, it is not essential and may be left at default (C_1=C_2=1). According to the Plaxis 2D Dynamic Manual, there are often shear waves in earthquake cases, in which case C_2= 0.25 and C_1=1 can be used.

2.5 Soil Improvement by Jet Grout Column

Soil improvement by jet grouting is a method to increase the mechanical strength value of the soil and helps to increasing bearing capacity of the soil. In this method, high-pressure cement grout is injected into the ground and creates cylindrical columns are formed from the soil material and cement mixture. Jet grouting method is used to increase the mechanical strength of the soil, reduce the risk of liquefaction, reduce permeability and reduce settlements.

2.5.1 Advantages of Jet Grout Column

- Faster: Jet grouting offers a faster solution than other remediation methods.
- Permanent: Jet grouting offers a permanent solution to increase the mechanical strength of the soil and improve its bearing capacity.
- Economical: Jet grouting is a more economical solution than other methods.
- Reliable: Jet grouting offers a reliable solution to increase the mechanical strength and bearing capacity of the soil.

2.5.2 Jet Grout Columns Application Method

I) Drilling: The ground is drilled and a drilling machine is used to inject the high-pressure cement grout into the ground.

II) Injection: High-pressure cement grout is injected into the ground and cylindrical columns are formed from the mixture of soil material and cement.

III) Column Formation: The formed columns are used to increase the mechanical strength of the soil and improve its bearing capacity.

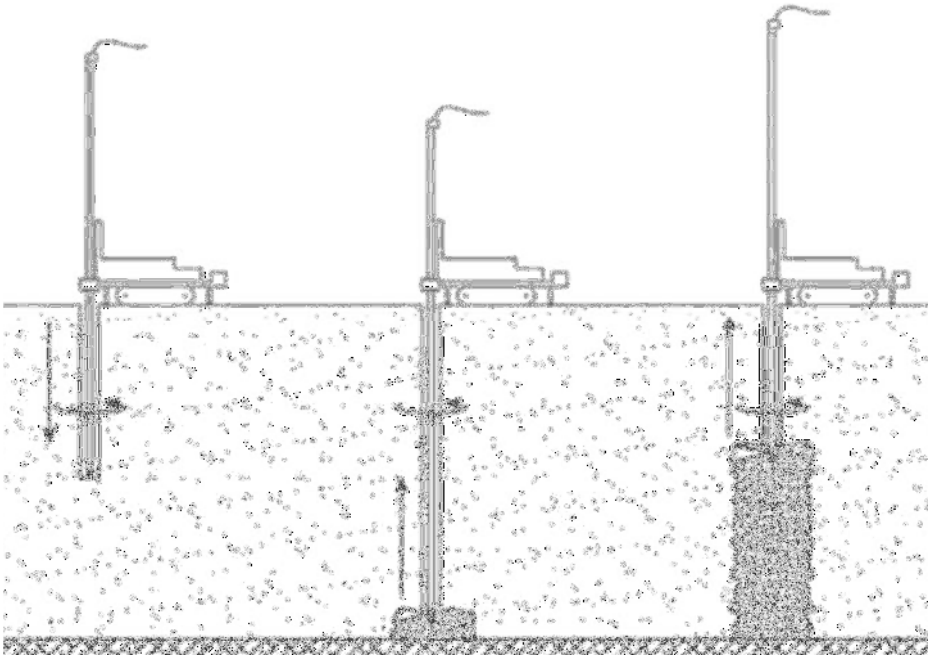

Figure 2.7 Jet Grout column manufacturing in the site

Jet grout columns are a versatile ground improvement technique that involves injecting a high-pressure jet of grout into the ground to create reinforced columns. These columns can be used in various applications to improve the ground's strength, stiffness, and permeability. Common application areas for jet grout columns include:

- Foundation support: Strengthening weak or unstable ground for building foundations, bridges, and other structures.
- Slope stabilization: Preventing landslides and erosion by improving the slope's stability.
- Seismic retrofitting: Enhancing the earthquake resistance of existing structures by strengthening the underlying ground.
- Dam construction: Providing a stable base for dams and retaining walls.
- Tunneling: Improving ground conditions for tunneling operations to prevent ground collapse and water inflow.
- Contaminant remediation: Containing and isolating contaminated groundwater by creating impermeable barriers.

The design and construction of jet grout columns involve several parameters, including:

- Grout type: The choice of grout material (e.g., cement-based, bentonite-based) depends on the specific requirements of the application.
- Grout pressure: The pressure at which the grout is injected affects the penetration depth and the diameter of the columns.
- Water-to-cement ratio: The ratio of water to cement in the grout mixture influences its strength and workability.
- Column spacing: The distance between the columns determines the degree of ground improvement achieved.
- Column depth: The desired depth of the columns depends on the project's requirements and the ground conditions.
- Column diameter: The diameter of the columns can be adjusted to meet specific load-bearing requirements.

2.5.3 Specification About the Jet Grout Columns

Jet grouting offers several advantages over traditional ground improvement techniques. Its rapid application and economical nature make it a desirable choice for many projects. Due to its wide range of applicability and the ability to inject grout in various geometries, jet grouting is suitable for diverse ground conditions and project requirements. Its non-destructive nature ensures minimal damage to existing structures, while its environmentally friendly approach using water and cement eliminates concerns about harmful chemicals. The flexibility of the equipment allows for easy operation in confined spaces, and the ability to start and end injection at specific depths provides precise control over the improved ground zone. Finally, jet grouting's vibration-unimproved and noise-unimproved operation minimizes disturbances to the surrounding area.

In liquefiable soils, bored piles are not used as ground improvement methods, instead jet grouting is suitable. The main reasons for using jet grouting instead of bored piles in soils with liquefaction potential are as follows:

Jet grouting is a highly effective method for preventing soil liquefaction, a phenomenon where saturated soil loses its strength and stiffness due to seismic shaking. By injecting pressurized cement into the ground, jet grouting fills voids and water veins, creating impermeable columns that significantly enhance the soil's resistance to liquefaction.

Compared to bored piles, jet grout columns offer several advantages. While bored piles may suffer from a loss of bearing capacity during liquefaction, jet grout columns are more resistant to this phenomenon. Additionally, jet grouting increases soil strength, reducing the likelihood of excessive settlements that can occur in liquefiable soils.

The wider coverage area of jet grout columns compared to bored piles allows for more effective liquefaction prevention. By strengthening a larger volume of soil, jet grouting reduces the risk of localized liquefaction.

In earthquake-prone regions, jet grouting is a popular choice for improving the seismic safety of structures. By mitigating the risk of liquefaction, jet grouting helps to prevent structural damage and protect lives.

As a result, the use of jet grouting in soils with liquefaction potential offers a more effective solution than bored piles. By increasing soil strength, it reduces the risk of liquefaction and ensures the safety of structures.

Figure 2.8 Jet Grout columns in the site view

2.6 Turkish Building Code (2018)

2.6.1 Identification of the Soil Type

There are 6 (six) different types of soil (A, B, C, D, E, F), and according to TBEC 2018, it is important to conduct a thorough examination to identify the soil type of the site. The national appendix lists these soil types and the criteria that relate to them for identification. If the data is available, it is additionally recommended that the classification be carried out using the average shear wave velocity over the top 30 m of the layer. The following equation (TBEC,2018) is used to get the average shear wave velocity at minor strain level ($V_{s,30}$) for the top 30 meters of soil.

$$V_{s30} = \frac{30}{\sum \frac{hi}{vi}} \tag{2.23}$$

Each layer's thickness, h_i, and the accompanying shear wave velocity, v_i, are used in this equation. For each nation, the national government divides the land into a number of seismic zones based on the level of national danger. According to the reference return period (TNCR) of the seismic activity or the reference probability of exceeding it in 50 years (PNCR), the reference peak ground acceleration varies depending on the area. This reference return time is given a significance value of 1,0. The design ground acceleration on type A ground ag for return periods other than the reference is equal to a_{gR} times the significance factor I (TBEC, 2018).

Depending on how a structure is used, many factors affect its relevance. The following table lists the significance classes and their related I values. For the return period, will be 1.

Table 2.1 Seismic importance classes

Seismic Importance Class	I value
I (Buildings that need to be used after an earthquake, long-term and intense buildings where valuables are stored buildings and buildings containing hazardous materials)	1.5
II (Buildings where people are concentrated for a short time)	1.2
III (Other types of buildings)	1.0

2.6.2 Basic Representation of Seismic Action

The elastic response spectrum (Figure 2.9) illustrates how the motion of an earthquake at a specific location on the surface is represented. For two levels of earthquake magnitude, the general version of TBEC-2018 offers elastic response spectra with identical shapes. While just one elastic response spectrum exists in Turkish Annex to represent seismic motion at various soil types. If the location is subject to earthquakes from many sources, it is advisable to take more than one form of spectra into account while designing seismic activity. Each type of spectrum and earthquake will have a distinct value for the input seismic action (a_g).

There are total two types of elastic response spectrum described in TBEC-2018.

2.6.2.1 Horizontal Elastic Response Spectrum

For each considering earthquake ground motion level, horizontal elastic design According to the vibration period, Eq. (2.23) defines the horizontal elastic design spectral accelerations ae S_{ae}(T) and natural gravity acceleration in g unit.

$$S_{ae}(T) = \begin{cases} \left(0.4 + 0.6\frac{T}{T_A}\right) S_{DS} & (0 \le T \le T_A) \\ S_{DS} & (T_A \le T \le T_B) \\ \frac{S_{D1}}{T} & (T_B \le T \le T_L) \\ \frac{S_{D1} T_L}{T^2} & (T_L \le T) \end{cases} \quad (2.23)$$

Here, T is the natural number that denotes the vibration period, and S_{DS} and S_{D1} are the design spectral acceleration coefficients. Corners of the horizontal design spectrum (TA and TB) Eq. (2.24), dependent on S_{DS} and S_{D1}, defines.

$$T_A = 0.2\frac{S_{D1}}{S_{DS}} \quad ; \quad T_B = \frac{S_{D1}}{S_{DS}} \quad (2.24)$$

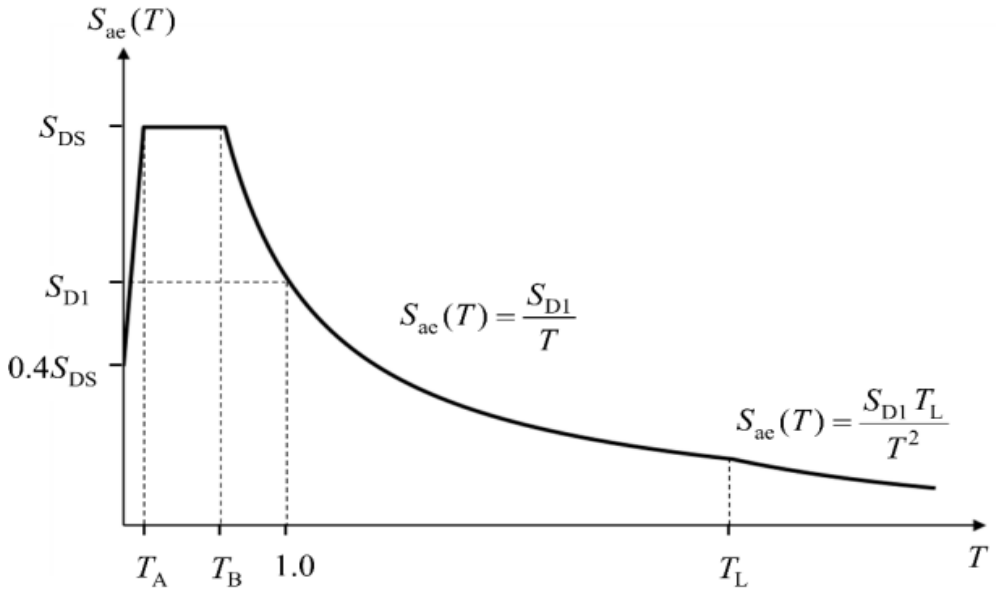

Figure 2.9 Horizontal elastic response spectrum graph

2.6.2.2 Vertical Elastic Response Spectrum

The vertical elastic design acceleration is evaluated for any earthquake ground motion level. Spectral accelerations of vertical elastic designs for ground motion and natural vibration, the horizontal earthquake short period design spectral acceleration coefficient, or $S_{aeD}(T)$, is defined. Equation (2.25) defines it in terms of the gravitational acceleration g unit is based on the period (Figure 2.9).

$$S_{aeD}(T) = \begin{cases} \left(0.32 + 0.48\dfrac{T}{T_{AD}}\right) S_{DS} & (0 \le T \le T_{AD}) \\ 0.8\ x\ S_{DS} & (T_{AD} \le T \le T_{BD}) \\ 0.8\ x\ S_{DS}\dfrac{T_{BD}}{T} & (T_{BD} \le T \le T_{LD}) \end{cases} \quad (2.25)$$

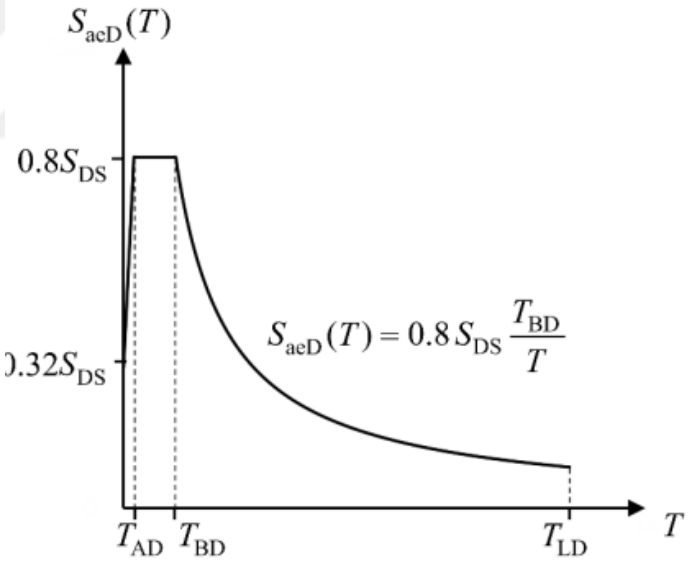

Figure 2.10 Vertical elastic response spectrum graph

CHAPTER 3

NUMERICAL MODELLING

3.1 Overview

The technique of this work is divided into two sections. The model creation procedure has been detailed first, followed by model validation and outcomes. Much work has been expended in learning how to utilize the Plaxis 2D software and refining the numerical technique.

In this section, important details in the process of creating a model to be input into FEM analysis and site area's introduction are mentioned. The numerical model development procedure is divided into 3 parts.

- First of all, the geometry of the model was created.
- Secondly, the model was prepared for FEM analyses and the boundary conditions required for the analyses were specified.
- Finally, the unimproved and improved model contitions used are described.

3.2 Introduction of Site

In this thesis, Kocasinan District of Kayseri Province, which is in Turkey and has a great earthquake risk, has been selected as the study area. The following information about the natural disaster hazard, geology of the region and the study area, tectonic situation, earthquake situation, hydrogeological situation studies and methods of geophysical studies are given in Figure 3.1.

Figure 3.1 Location of the site on the map of Turkey

The total surface area of the Kayseri is 16,969 km². Kayseri is in the Middle Kızılırmak section where the southern part of Central Anatolia and the Taurus Mountains converge. It is surrounded by Sivas to the east and northeast, Yozgat to the north, Nevşehir to the west, Niğde to the southwest, Adana and Kahramanmaraş to the south.

Figure 3.2 Location of the site on the map of satelitte view

This thesis was prepared to reveal the structure-soil interaction under dynamic loads by performing a site-specific soil behavior analysis since the basic soil group of the building located in Kocasinan District of Kayseri Province. In this context, a total of 11 scaled earthquake records were used and spectral acceleration coefficients were

generated to be used in the static project. The methodology applied in the report and the results obtained are presented below. Using the SPT pulse table, the number of $(N_{60})_{30}$ pulses was calculated as 12.63 (pulse/30 cm) in general. Also, as a result of Geophysical Measurements $(Vs)_{30}$ value was calculated as 187.00 m/sec. Due to the liquefaction risk of the soil, the Soil Class was determined as "ZF" as a result of the data obtained.

The study area is very close to one of the important faults in Turkey in terms of geologic location. The fracture line named as Erciyes Fault (Figure 1) in the Direct Fault Map of Turkey (Şaroğlu et al., 1992) is a continuation of the Ecemiş Fault and was named as Erciyes-Ecemiş Fault by some researchers (Kayabalı and Akın 2002), and later this line was extended to the North Anatolian Fault Zone and named as Central Anatolian Fault Zone (Koçyigit and Beyhan, 1998). In 1940, 35 people died in the Develi Earthquake (ML = 5.3) that occurred on the Erciyes Fault.

Erciyes Fault was formed as a result of Quaternary tectonism. The complete end of Erciyes volcanism was caused by vertical block movements. Erciyes Fault is also a strike slip fault line.

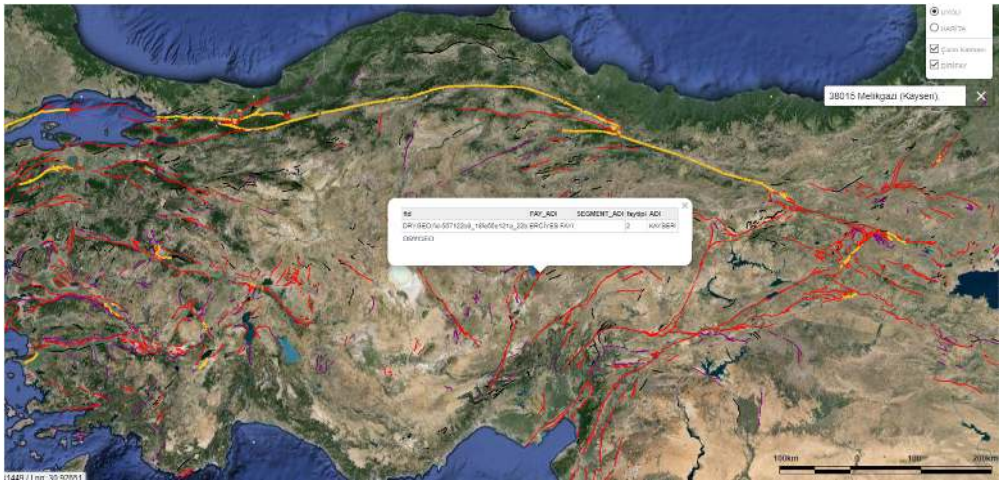

Figure 3.3 Turkey active fault map

The subject of this thesis is the 15th most populous city in Turkey and the city has serious fault zones surrounding the city. For this reason, when the drilling (SPT) results obtained from the region are examined, it is understood that it has a multi-layered soil layer and the sandy soil profile, which is the most critical for liquefaction, is used. The parameters of the described sandy soil were correlated with the NovoSPT program

according to the SPT-N values and the soil parameters were defined in the Plaxis 2D program according to the correlation results.

3.3 Introduction of FEM Model

The drilling works carried out in Kayseri have a depth of approximately 20.00 m. While modeling the mentioned site, it has a depth of 44.50 m and a width of 60 m. A 20.00 m long and 1 m depth concrete foundation was placed on this site.

A sandy soil with 12 different parameters was used to create the soil model in Plaxis2D program. 11 different seismic forces were applied at the bottom of the soil and the response of the soil was observed. Then, a foundation was constructed on this soil and circular jet grout columns with a diameter of 1 m, a length of 15.00 m and a spacing of 2.80 m were added to the model and the final response of the soil to the 11 different seismic forces were analyzed.

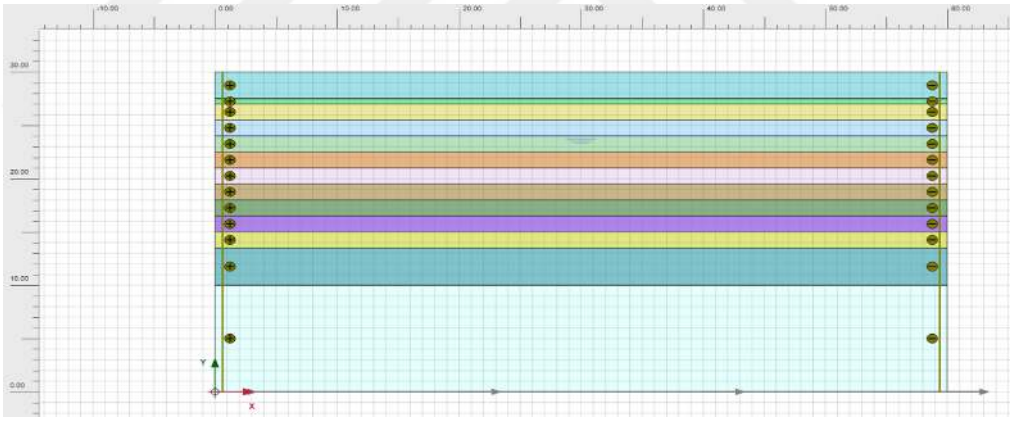

Figure 3.4 Unimproved model schematic view

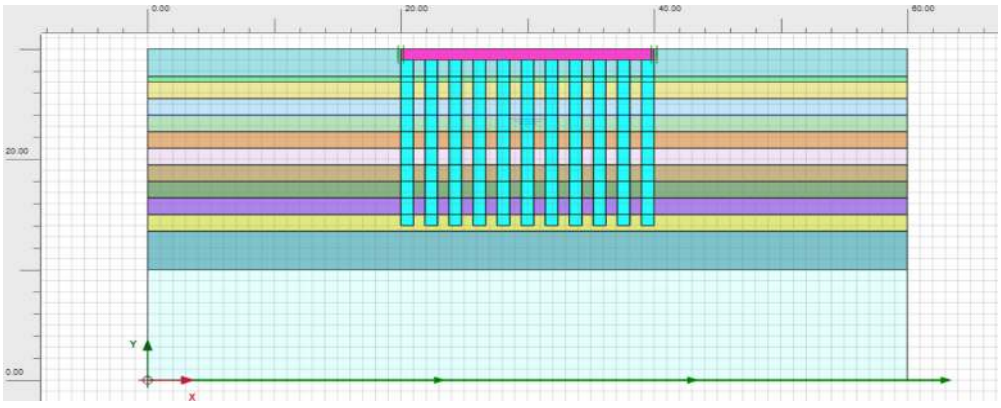

Figure 3.5 Improved model schematic view

As a result of the geophysical studies carried out in the field, V_s (m/s) values of the ground up to a depth of 30.00 m were obtained and it is observed that the Vs value of the lowest layer is 191 m/s. The logarithmic increase trends of the obtained SPT data in the ground were examined and graphed.

Geophysical Study Results:

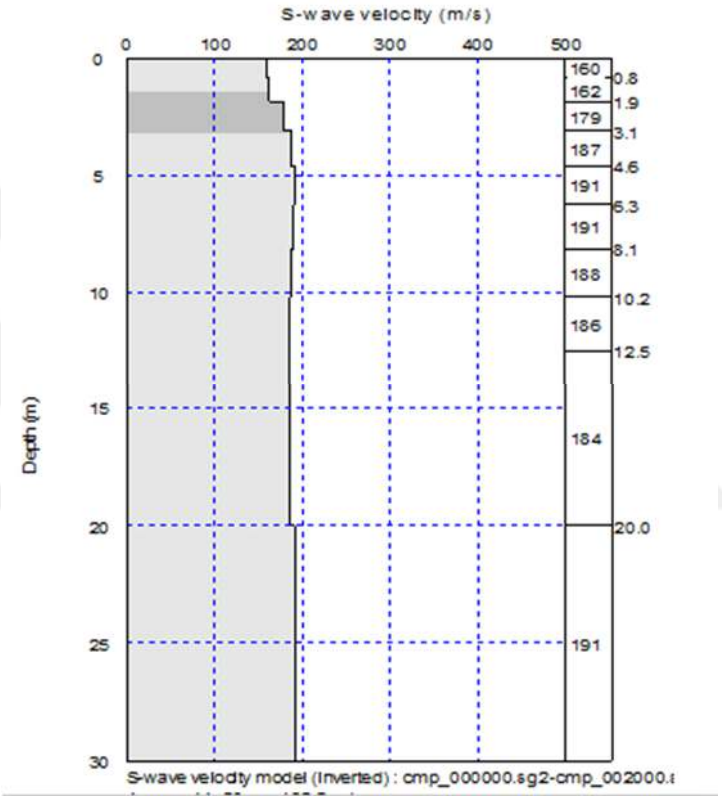

Figure 3.6 Vs values obtained as a result of geophysical studies in the field

3.4 Earthquake Selection

Considering the location of the modeled ground and considering the parameters of the layers in the ground, Response Spectrum values suitable for DD2-ZD values were obtained from AFAD Interactive Earthquake Reporting System. When the earthquake history of the city of Kayseri, which is the subject of this thesis, is examined, it is determined that the probability of an earthquake with a magnitude of 5.5 - 7.4 MW is high. Response spectra data from Afad interactive earthquake hazard map report and

these parameters were uploaded to the Peer database system and sample earthquake records suitable for the site I wanted to model were obtained.

The site of this thesis (Kayseri) is marked in AFAD interactive earthquake hazard map system. DD2 Earthquake Ground Motion characterizes the rare earthquake ground motion where the probability of exceeding the spectral magnitudes in 50 years is 10% and the corresponding recurrence period is 475 years. This earthquake ground motion is also referred to as the standard design earthquake ground motion. In the model, DD2 and ZC is chosen as the soil type. Because when the drilling data are examined, it is seen that the Vs values of the layers are categorized as ZD soil in the section where the earthquake load is affected by the V_s values of the layers as a result of V_s correlation.

According to TBEC 2018 site seismic values results:

Rapor Başlığı:	Kayseri Site Response Analysis	
Deprem Yer Hareketi Düzeyi	DD-2	50 yılda aşılma olasılığı %10 (tekrarlanma periyodu 475 yıl) olan deprem yer hareketi düzeyi
Yerel Zemin Sınıfı	ZD	Orta sıkı - sıkı kum, çakıl veya çok katı kil tabakaları
Enlem:	38.719675°	
Boylam	35.486319°	

Çıktılar

S_S = 0.432 S_1 = 0.110 PGA=0.187 PGV=10.785

S_S : Kısa periyot harita spektral ivme katsayısı [boyutsuz]

S_1 : 1.0 saniye periyot için harita spektral ivme katsayısı [boyutsuz]

PGA : En büyük yer ivmesi [g]

PGV : En büyük yer hızı [cm/sn]

Soil class	Soil type	Top 30 meter average		
		(V_s, m/s)	($\bar{N}_{ch}$, blows/30 cm)	($\bar{s}_u$, kPa)
ZA	Solid, hard rock	>1500	-	-
ZB	Low weathered, moderately strong rock	760-1500	-	-
ZC	Very tight layers of sand, gravel and hard clay or weathered, highly fractured weak rock	360-760	>50	>250
ZD	Medium firm – firm sand, gravel or very solid clay layers	180-360	15-50	70-250
ZE	Loose sand, gravel or soft solid clay layers or profiles with PI > 20 and w > 40%, containing a total layer of soft clay (su < 25 kPa) thicker than 3 meters in total	<180	<15	<70
ZF	Site-specific soil behaviour analysis will be carried out			

Yerel Zemin Sınıfı	Kısa periyot bölgesi için *Yerel Zemin Etki Katsayısı* F_S					
	$S_S \leq 0.25$	$S_S = 0.50$	$S_S = 0.75$	$S_S = 1.00$	$S_S = 1.25$	$S_S \geq 1.50$
ZA	0.8	0.8	0.8	0.8	0.8	0.8
ZB	0.9	0.9	0.9	0.9	0.9	0.9
ZC	1.3	1.3	1.2	1.2	1.2	1.2
ZD	1.6	1.4	1.2	1.1	1.0	1.0
ZE	2.4	1.7	1.3	1.1	0.9	0.8
ZF	*Sahaya özel zemin davranış analizi yapılacaktır.*					

Yerel Zemin Sınıfı ZD ve S_S =0.432 için F_S=1.454

Yerel Zemin Sınıfı	1.0 saniye periyot için *Yerel Zemin Etki Katsayısı* F_1					
	$S_1 \leq 0.10$	$S_1 = 0.20$	$S_1 = 0.30$	$S_1 = 0.40$	$S_1 = 0.50$	$S_1 \geq 0.60$
ZA	0.8	0.8	0.8	0.8	0.8	0.8
ZB	0.8	0.8	0.8	0.8	0.8	0.8
ZC	1.5	1.5	1.5	1.5	1.5	1.4
ZD	2.4	2.2	2.0	1.9	1.8	1.7
ZE	4.2	3.3	2.8	2.4	2.2	2.0
ZF	*Sahaya özel zemin davranış analizi yapılacaktır.*					

Yerel Zemin Sınıfı ZD ve S_1 =0.110 için F_1=2.380

$$S_{DS} = S_S F_S = 0.432 \text{ x } 1.454 = 0.628$$

$$S_{D1} = S_1 F_1 = 0.110 \text{ x } 2.380 = 0.262$$

S_{DS} : Kısa periyot tasarım spektral ivme katsayısı [boyutsuz]

S_{D1} : 1.0 saniye periyot için tasarım spektral ivme katsayısı [boyutsuz]

Horizontal Elastic Design Spectrum:

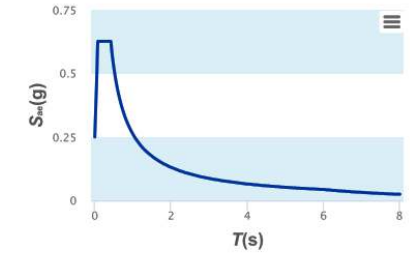

$$S_{ae}(T) = \left(0.4 + 0.6\frac{T}{T_A}\right) S_{DS} \qquad (0 \le T \le T_A)$$

$$S_{ae}(T) = S_{DS} \qquad (T_A \le T \le T_B)$$

$$S_{ae}(T) = \frac{S_{D1}}{T} \qquad (T_B \le T \le T_L)$$

$$S_{ae}(T) = \frac{S_{D1} T_L}{T^2} \qquad (T_L \le T)$$

$$T_A = 0.2\frac{S_{D1}}{S_{DS}} \qquad T_B = \frac{S_{D1}}{S_{DS}} \qquad T_L = 6s$$

T_A = 0.083 (s) T_B = 0.417 (s) T_L = 6.000 (s)

Vertical Elastic Design Spectrum:

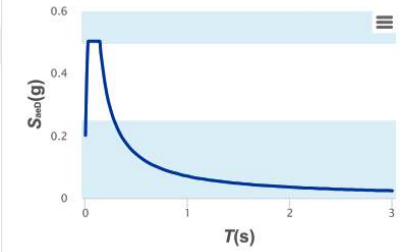

$$S_{aeD}(T) = \left(0.32 + 0.48\frac{T}{T_{AD}}\right) S_{DS} \qquad (0 \le T \le T_{AD})$$

$$S_{aeD}(T) = 0.8 S_{DS} \qquad (T_{AD} \le T \le T_{BD})$$

$$S_{aeD}(T) = 0.8 S_{DS}\frac{T_{BD}}{T} \qquad (T_{BD} \le T \le T_{LD})$$

$$T_{AD} = \frac{T_A}{3} \qquad T_{BD} = \frac{T_B}{3} \qquad T_{LD} = \frac{T_L}{2}$$

T_{AD} = 0.028 (s) T_{BD} = 0.139 (s) T_{LD} = 3.000 (s)

Earthquake response spectrum values obtained from AFAD Interactive Earthquake Map were introduced to the Peer database system and earthquakes suitable for the site were listed.

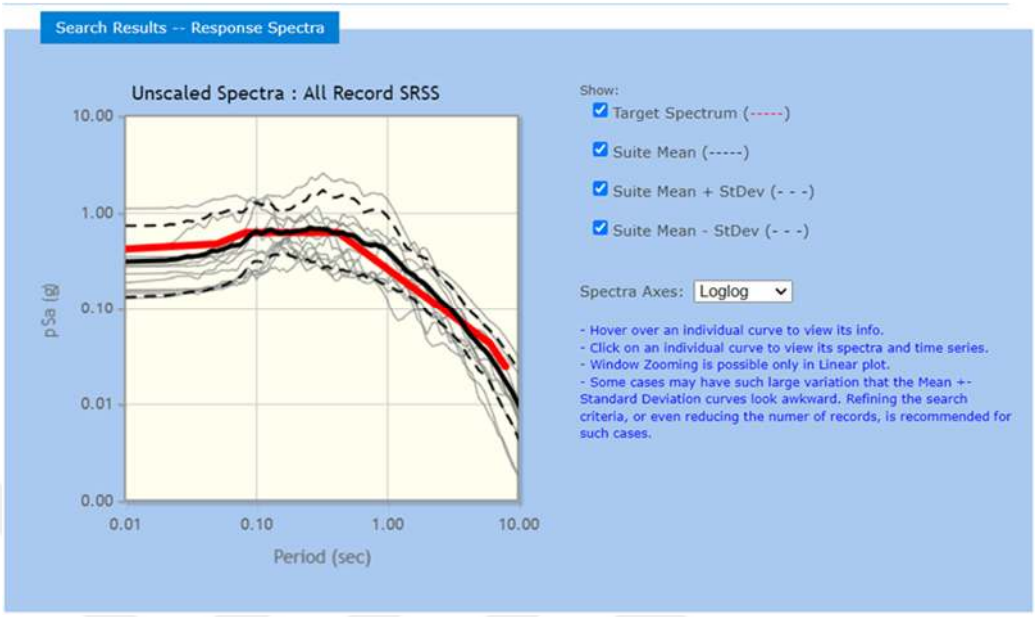

Figure 3.9 Spectral plot for special site area

After introducing the Response Spectrum values of the site to Peer, the properties of the fault line closest to the site subject to the model were entered and the list of earthquakes that occurred worldwide most similar to the site was obtained. Since the Erciyes Fault and Ercin Fault, which are closest to Kasyeri province, are Strike Slip fault lines, the selected earthquakes were determined as earthquakes that occurred on the Strike Slip Fault line. R_{jb} (Joyner-Boore distance to rupture plane) and Rrup (Closest distance to rupture plane) values were taken between 0 - 60 km. Since Vs_{30} value was determined according to ZD soil parameters, earthquakes in the range of 180-360 m/s were asked to be ranked.

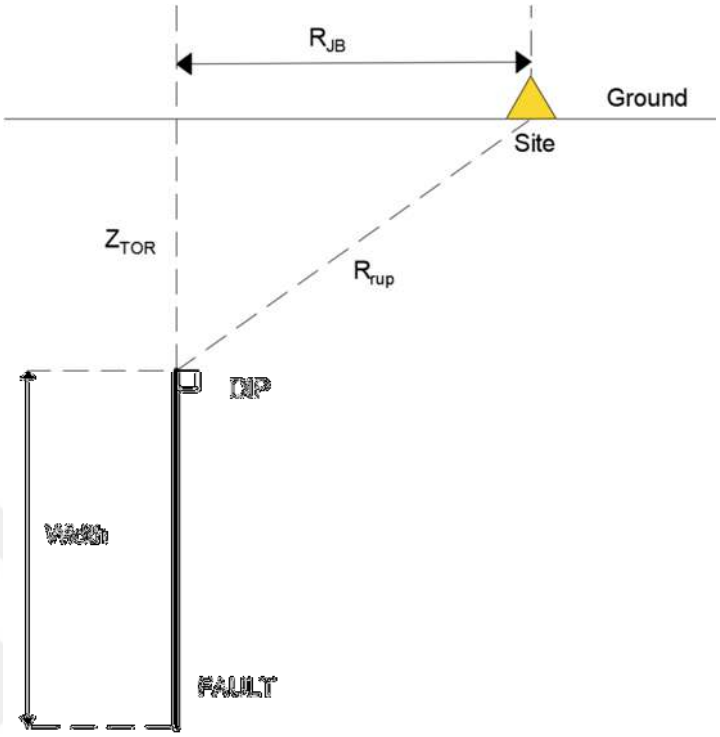

Figure 3.10 Strike Slip faulting parameter schematic view

Results -- Metadata

Click heading of the column to be sorted in ascending order

Rescale Using Checked Records

	Result ID	Spectral Ordinate	Record Seq. #	MSE	Scale Factor	Tp(s)	D5-75(s)	D5-95(s)	Arias Intensity (m/s)	Event	Year	Station	Mag	Me
view	1	SRSS	6	0.1651	1.0	-	17.7	24.2	1.6	Imperial Valley-02	1940	El Centro Array #9	6.95	str
view	2	SRSS	158	0.3026	1.0	-	6.1	9.8	1.2	Imperial Valley-06	1979	Aeropuerto Mexicali	6.53	str
view	3	SRSS	209	0.4199	1.0	-	6.2	14.3	0.2	Imperial Valley-08	1979	Westmorland Fire Sta	5.62	str
view	4	SRSS	316	0.2693	1.0	4.309	6.2	10.7	0.7	Westmorland	1901	Parachute Test Site	5.9	str
view	5	SRSS	544	0.7924	1.0	-	12.1	21.7	0.1	Chalfant Valley-01	1986	Bishop - LADWP South St	5.77	str
view	6	SRSS	850	0.2079	1.0	-	22.6	31.7	0.7	Landers	1992	Desert Hot Springs	7.28	str
view	7	SRSS	930	0.7662	1.0	-	11.7	22.0	0.2	Big Bear-01	1992	San Bernardino - 2nd & Arrowhead	6.46	str
view	8	SRSS	1602	1.0951	1.0	0.882	2.6	9.0	3.7	Duzce, Turkey	1999	Bolu	7.14	str
view	9	SRSS	3758	0.3871	1.0	-	26.2	38.7	0.5	Landers	1992	Thousand Palms Post Office	7.28	str

Figure 3.11 Output earthquake list window in Peer database

Table 3.1 Choosen earthquake records

Result ID	Spectral Ordinate	Record Sequence Number	Mean Squared Error	Scale Factor	5-75% Duration (sec)	5-95% Duration (sec)	Arias Intensity (m/sec)	Earthquake Name	Year	Station Name	Magnitude	Mechanism	Rjb (km)	Rrup (km)	Vs30 (m/sec)	Lowest Useable Frequency (Hz)	Initial-search Scale Factor
1	SRSS	6	0.0478	0.6344	17.7	24.2	1.6	"Imperial Valley-02"	1940	"El Centro Array #9"	6.95	strike slip	6.09	6.09	213.44	0.25	0.6564
5	SRSS	158	0.103	0.631	6.1	9.8	1.2	"Imperial Valley-06"	1979	"Aeropuerto Mexicali"	6.53	strike slip	0	0.34	259.86	0.2875	0.6529
23	SRSS	209	0.0748	1.8175	6.2	14.3	0.2	"Imperial Valley-08"	1979	"Westmorland Fire Sta"	5.62	strike slip	9.39	9.76	193.67	0.0875	1.8805
25	SRSS	316	0.1089	0.747	6.2	18.7	0.7	"Westmorland"	1981	"Parachute Test Site"	5.9	strike slip	16.54	16.66	348.69	0.1125	0.7729
30	SRSS	544	0.0848	1.6949	12.1	21.7	0.1	"Chalfant Valley-01"	1986	"Bishop - LADWP South St"	5.77	strike slip	23.38	23.47	303.47	0.15	1.7536
37	SRSS	850	0.0796	1.0079	22.6	31.7	0.7	"Landers"	1992	"Desert Hot Springs"	7.28	strike slip	21.78	21.78	359	0.07	1.0428
43	SRSS	930	0.0809	1.5815	11.7	22	0.2	"Big Bear-01"	1992	"San Bernardino - 2nd & Arrowhead"	6.46	strike slip	33.56	33.79	325.83	0.16	1.6363
50	SRSS	1602	0.1053	0.2961	2.6	9	3.7	"Duzce_ Turkey"	1999	"Bolu"	7.14	strike slip	12.02	12.04	293.57	0.0625	0.3064
56	SRSS	3758	0.0992	1.2531	26.2	38.7	0.5	"Landers"	1992	"Thousand Palms Post Office"	7.28	strike slip	36.93	36.93	333.89	0.1125	1.2965
59	SRSS	3969	0.0877	1.2871	5.9	21.7	0.5	"Tottori_ Japan"	2000	"TTRH04"	6.61	strike slip	32.75	32.75	254.26	0.035	1.3317
89	SRSS	6930	0.0955	1.6777	13.8	23.8	0.2	"Darfield_ New Zealand"	2010	"LRSC"	7	strike slip	9.38	12.52	295.74	0.375	1.7359

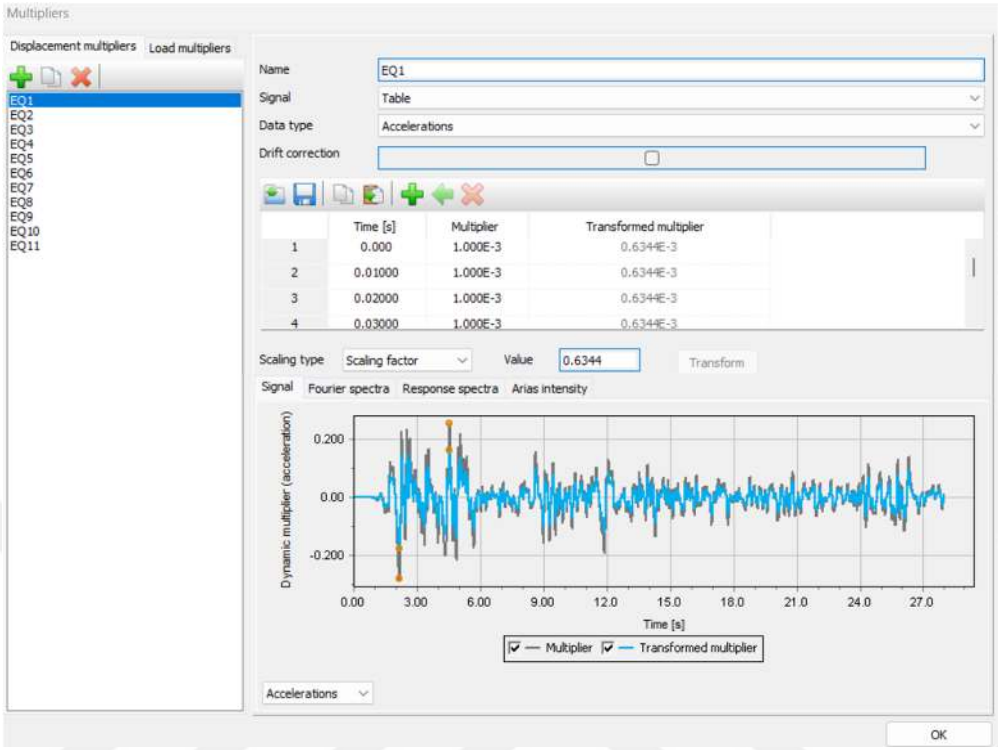

Figure 3.12 Earthquake 1 scaled according to Peer

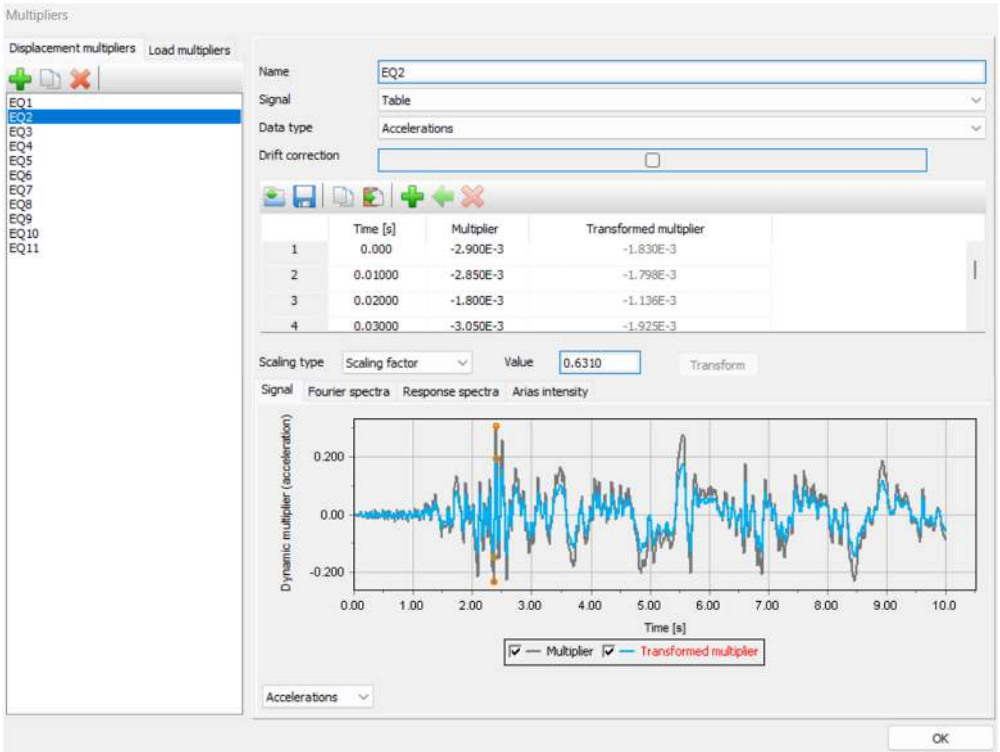

Figure 3.13 Earthquake 2 scaled according to Peer

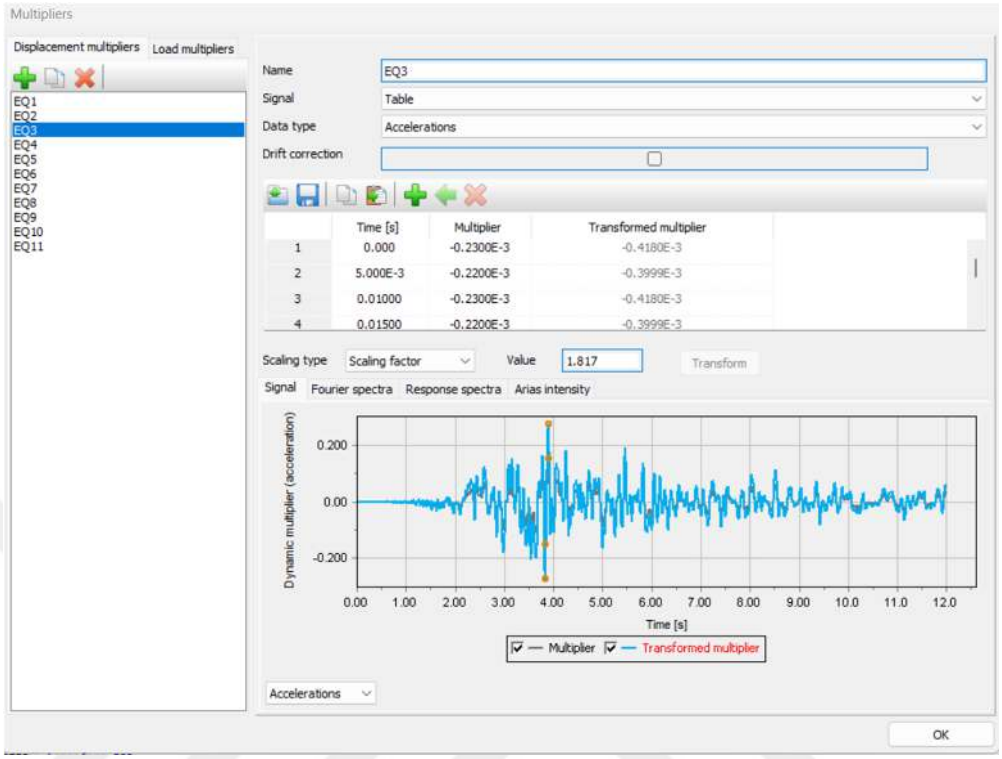

Figure 3.14 Earthquake 3 scaled according to Peer

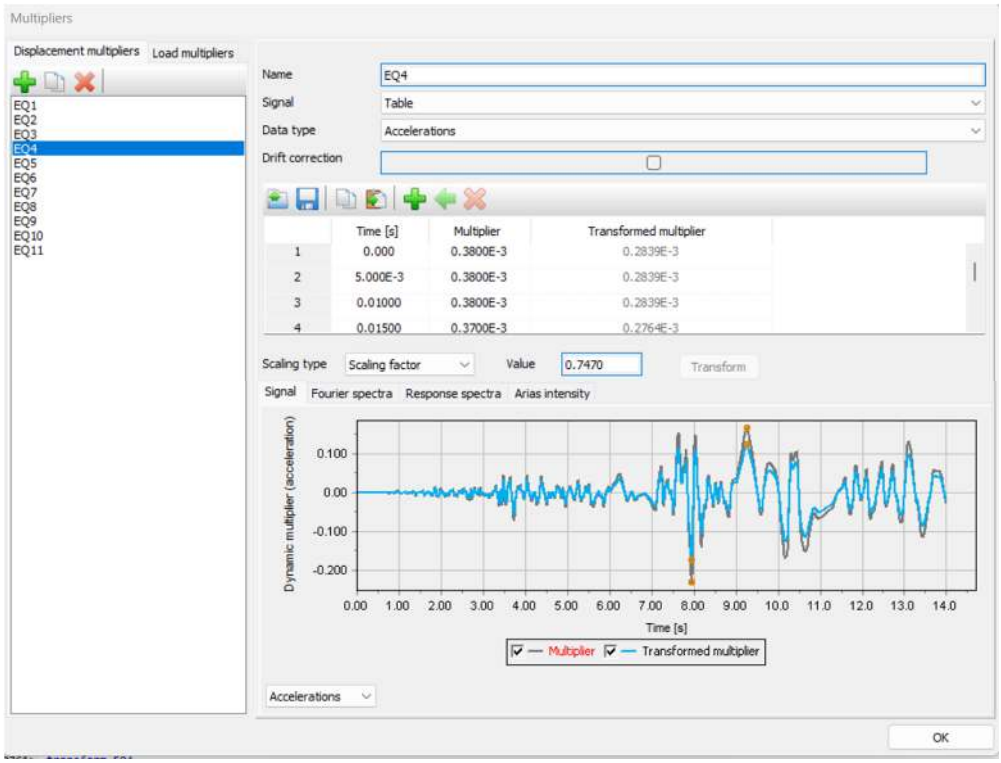

Figure 3.15 Earthquake 4 scaled according to Peer

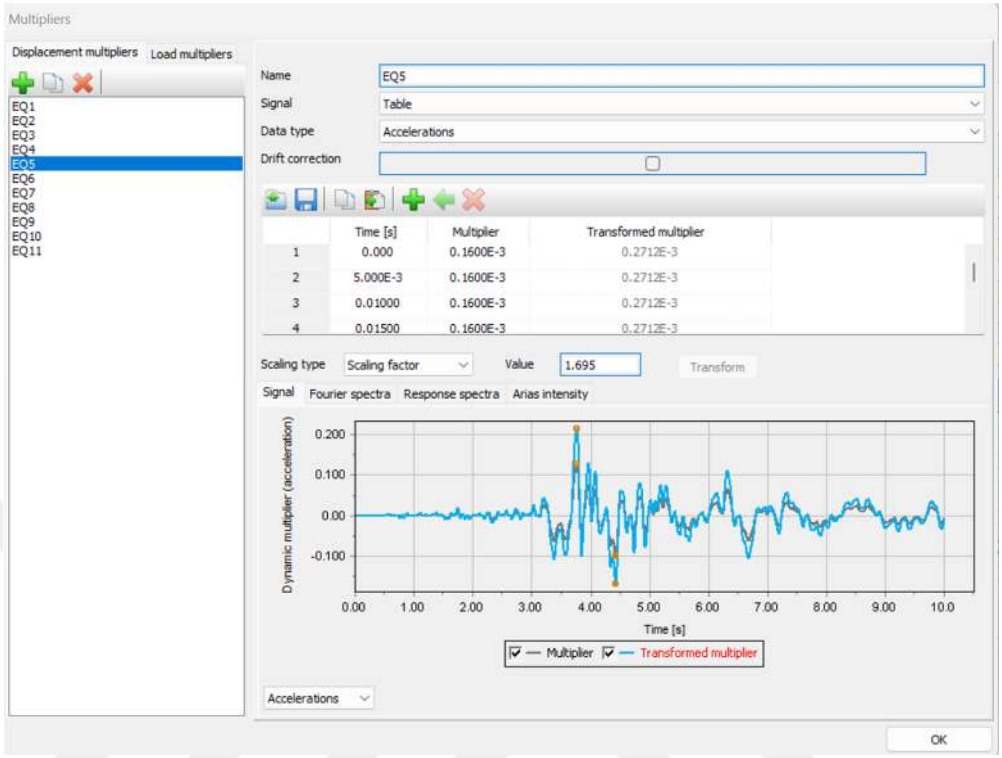

Figure 3.16 Earthquake 5 scaled according to Peer

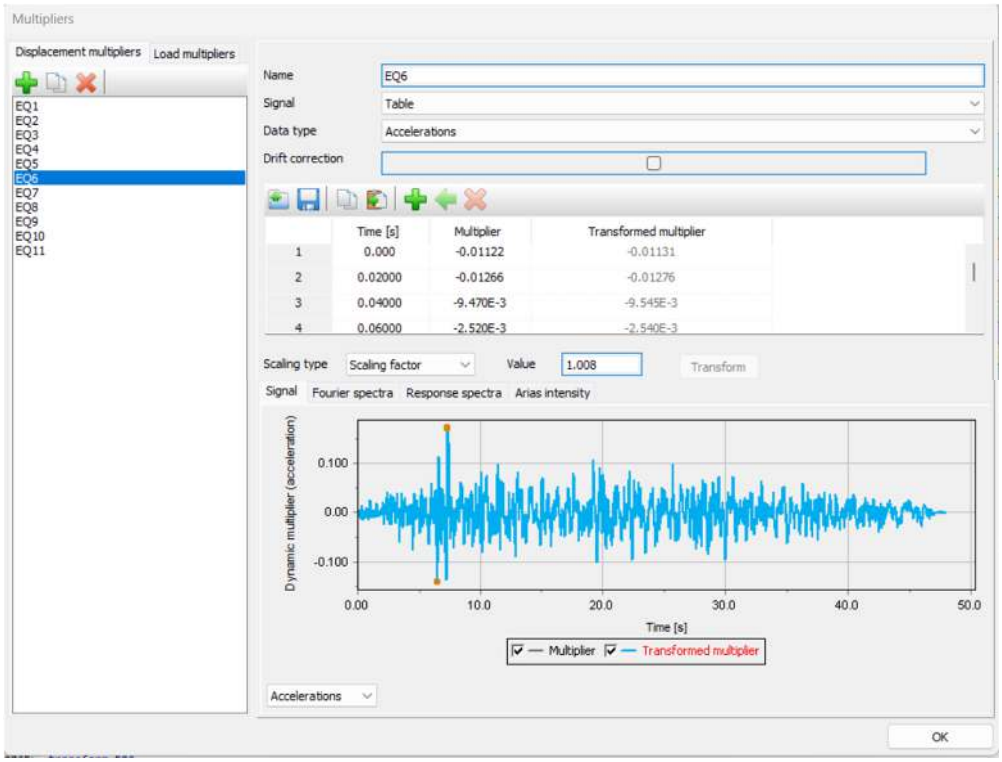

Figure 3.17 Earthquake 6 scaled according to Peer

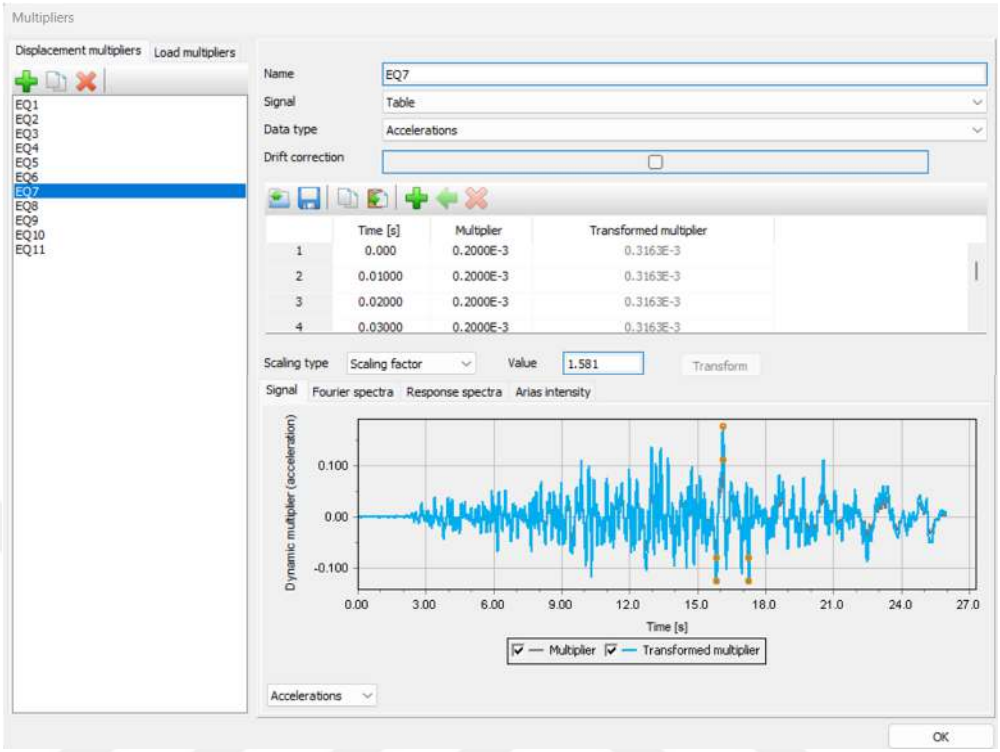

Figure 3.18 Earthquake 7 scaled according to Peer

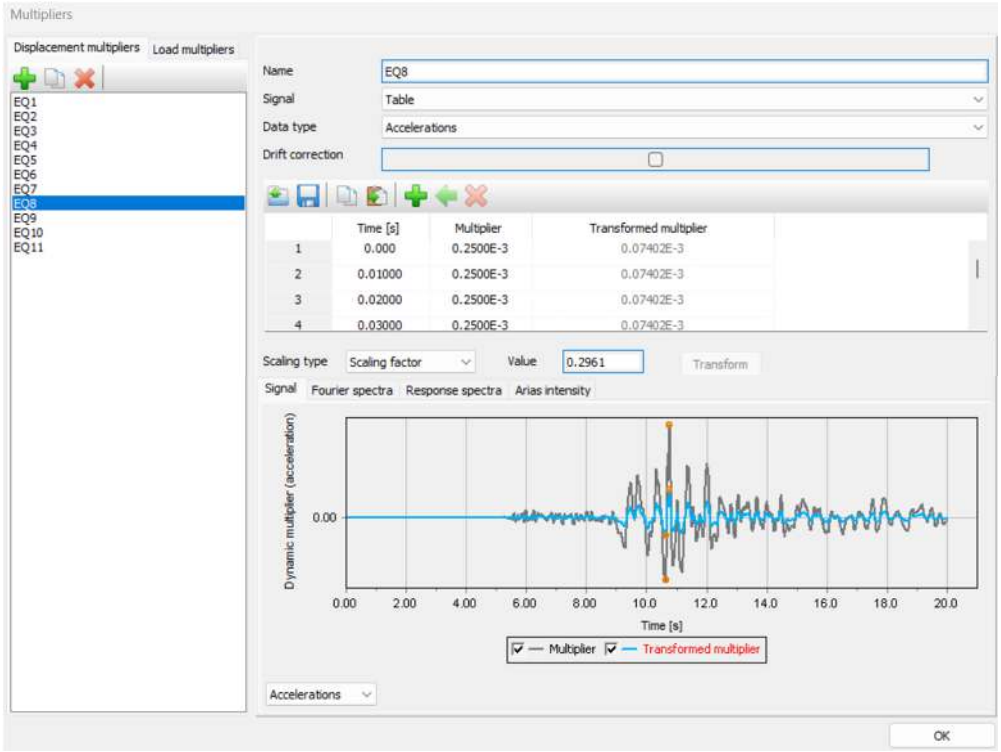

Figure 3.19 Earthquake 8 scaled according to Peer

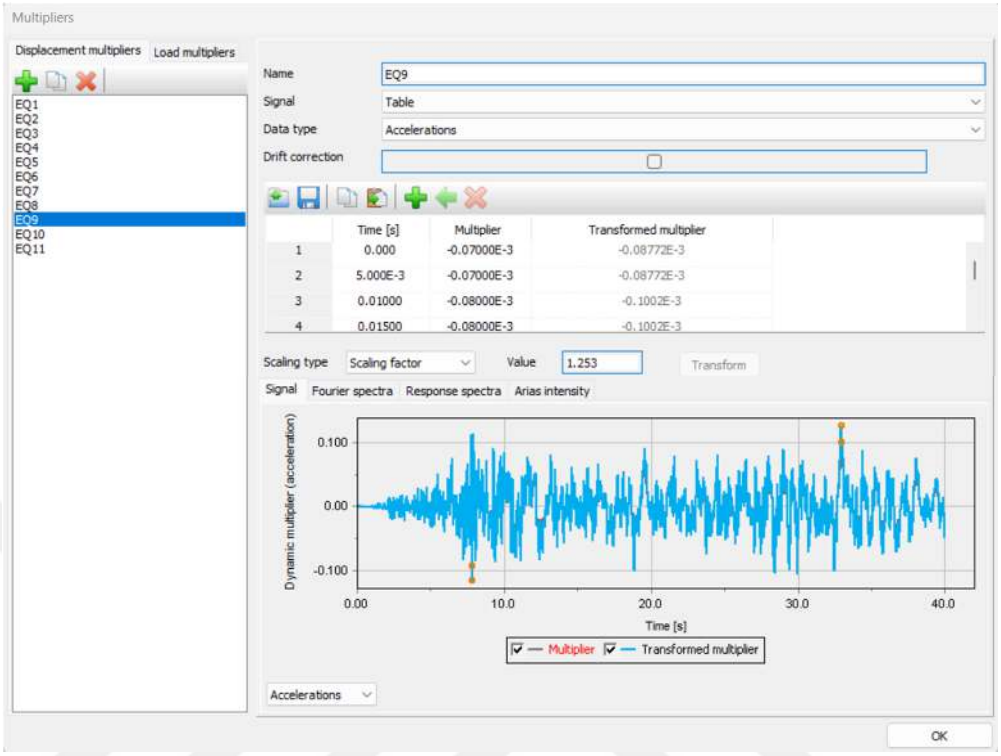

Figure 3.20 Earthquake 9 scaled according to Peer

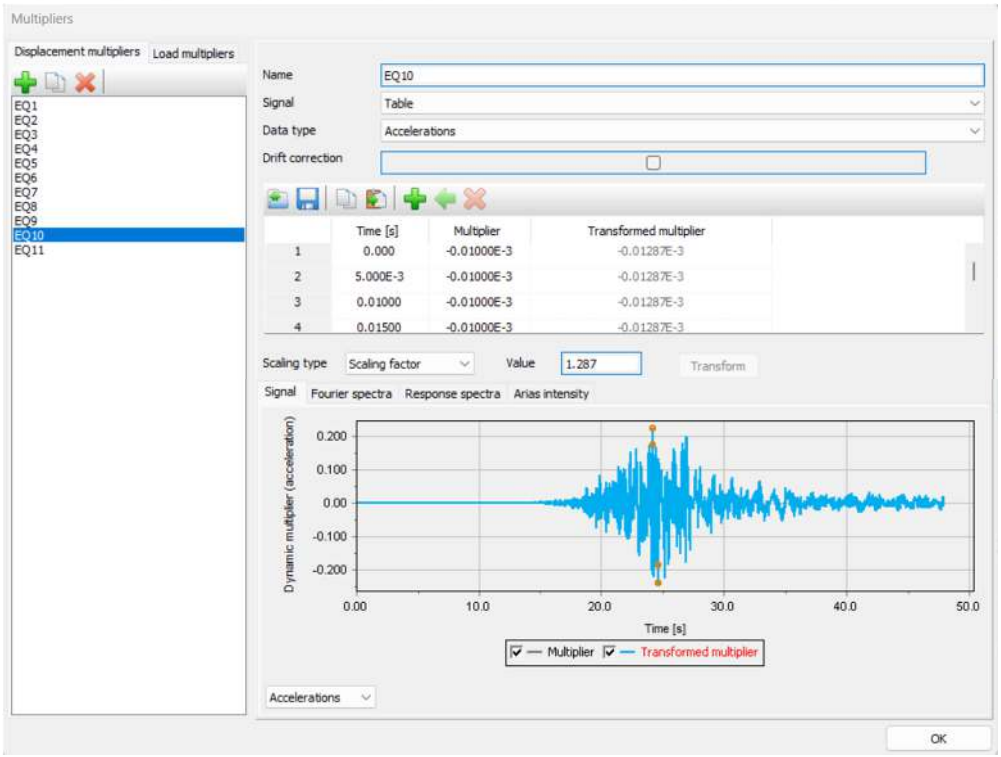

Figure 3.21 Earthquake 10 scaled according to Peer

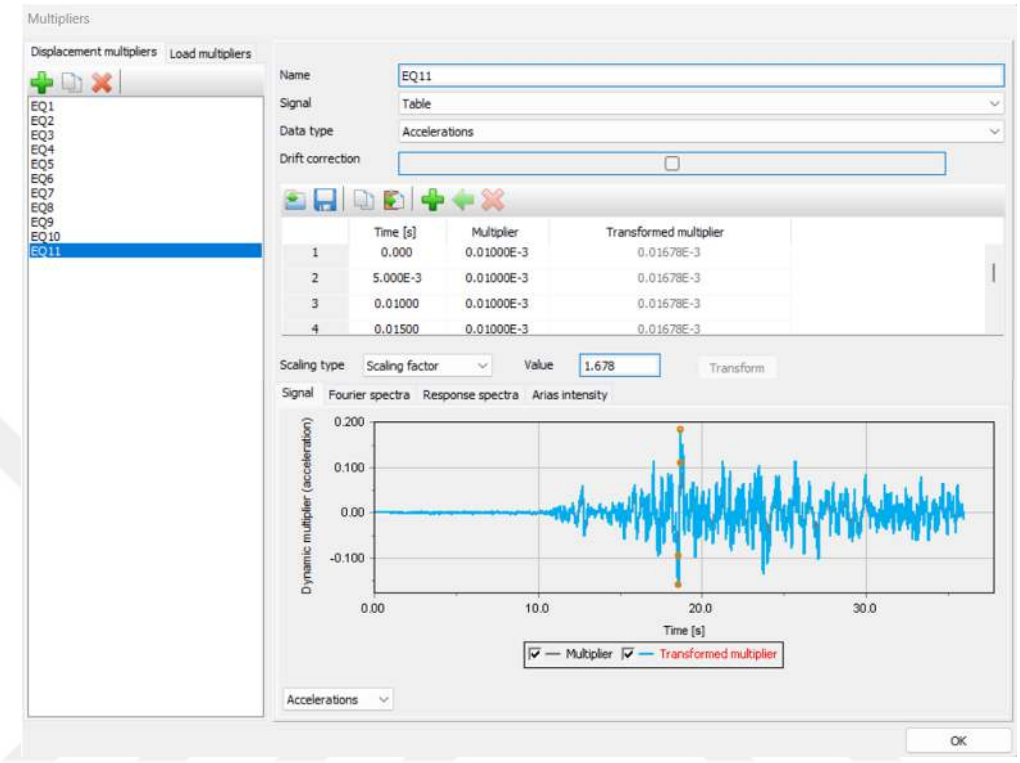

Figure 3.22 Earthquake 11 scaled according to Peer

3.5 FEM Model Material Properties

The soil parameters subject to the model were obtained as a result of the correlation of the data obtained as a result of the SPT test. These data were calculated and entered into the Plaxis 2D software using the UBC3D-PLM module of the Plaxis 2D program to provide liquefaction control in the field as mentioned in Chapter 2, and the parameters of the HSSmall Module to determine the Site response analysis. There are 13 different kind of soils, 20.00 m long foundation and 15.00 m long 1.00 m diameter jet grout columns connected to the foundation. The foundation subject to the model is defined as a reinforced structure with C_{30} (European standard) class concrete as concrete area in Plaxis 2D software. In addition, jet grout columns were parameterized and added to the model as Concrete Model elements as unreinforced momentless structural elements.

Table 3.2 UBC3D-PLM Model soil properties

Layer No.	Unit	Thickness	Depth (m)		z	γ	$(N_1)_{60}$	Calculated Parameter											φcv	φp
		(m)	Top	Bottom	(m)	(kN/m^3)		k^{*e}_B	k^{*e}_G	k^{*P}_G	m_e	n_e	n_p	R_f	f_{dens}	f_{Epost}	c	(deg.)	(deg.)
1	Stiff CIL	2.50	0.00	2.50	1.25	14.20	8	607.6	867.9	266.6	0.5	0.5	0.4	0.81	1	1	35	4	5
2	Medium SiSa	0.50	2.50	3.00	2.75	14.20	11	675.6	965.1	450.3	0.5	0.5	0.4	0.77	1	1	5	34	35
3	Loose SiSa	1.50	3.00	4.50	3.75	14.20	6	552.0	788.6	185.2	0.5	0.5	0.4	0.84	1	1	1	30	31
4	Well Graded Sil	1.50	4.50	6.00	5.25	14.20	11	675.6	965.1	450.3	0.5	0.5	0.4	0.77	1	1	50	5	6
5	Loose SiSa	1.50	6.00	7.50	6.75	18.30	6	552.0	788.6	185.2	0.5	0.5	0.4	0.84	1	1	5	29	30
6	Medium CIL	1.50	7.50	9.00	8.25	18.30	5	519.5	742.1	155.7	0.5	0.5	0.4	0.86	1	1	50	5	6
7	Medium CIL	1.50	9.00	10.50	9.75	18.30	5	519.5	742.1	155.7	0.5	0.5	0.4	0.86	1	1	50	5	6
8	Medium SiSa	1.50	10.50	12.00	11.25	18.30	5	519.5	742.1	155.7	0.5	0.5	0.4	0.86	1	1	40	4	5
9	CIL	1.50	12.00	13.50	12.75	18.30	7	581.1	830.2	222.0	0.5	0.5	0.4	0.82	1	1	35	5	6
10	CiSa	1.50	13.50	15.00	14.25	18.30	10	654.5	935.0	380.5	0.5	0.5	0.4	0.78	1	1	25	5	6
11	SIL	1.50	15.00	16.50	15.75	18.30	9	631.9	902.7	319.4	0.5	0.5	0.4	0.79	1	1	15	25	26
12	SiSa	3.50	16.50	20.00	18.25	18.30	6	552.0	788.6	185.2	0.5	0.5	0.4	0.84	1	1	5	31	32
13	CiSa	10.00	20.00	30.00	25.00	18.3	6	552.0	788.6	185.2	0.5	0.5	0.4	0.84	1	1	5	30	31

Table 3.3 HSSmall Model soil properties

Layer No.	Name	Thickness	Bottom	Top	Vs	γ	ν_{ur}	Pref	m	c	ϕ	G_0^{REF}	γ0.7	E_{oed}^{ref}	E_{oed}^{ref}	E_{ur}^{ref}
		(m)	(m)	(m)	m/s	(kN/m^3)		kPa		kPa	(°)	Mpa		Mpa	Mpa	Mpa
1	Stiff ClL	2.50	0.00	2.50	160	14.16	0.4	100.0	0.7	35.0	4	41	3.89E-04	5.49	16.46	16.46
2	Medium SiSa	0.50	2.50	3.00	179	14.16	0.4	100.0	0.7	5.0	34.3	131	5.59E-05	44.47	133.42	133.42
3	Loose SiSa	1.50	3.00	4.50	187	14.16	0.4	100.0	0.7	1.0	30	124	6.48E-05	30.13	120.50	120.50
4	Well Graded Sil	1.50	4.50	6.00	191	14.16	0.4	100.0	0.7	50.0	5	55	0.000454	5.45	27.25	27.25
5	Loose SiSa	1.50	6.00	7.50	191	18.27	0.4	100.0	0.7	5.0	29	90	0.000214	11.34	68.06	68.06
6	Medium ClL	1.50	7.50	9.00	191	18.27	0.4	100.0	0.7	50.0	5	65	0.00017	5.41	37.88	37.88
7	Medium ClL	1.50	9.00	10.50	188	18.27	0.4	100.0	0.7	50.0	5	62	0.000179	4.28	34.21	34.21
8	Medium SiSa	1.50	10.50	12.00	186	18.27	0.4	100.0	0.7	40.0	4	59	0.000151	3.48	31.35	31.35
9	ClL	1.50	12.00	13.50	184	18.27	0.4	100.0	0.7	35.0	5	55	0.000142	2.74	27.36	27.36
10	ClSa	1.50	13.50	15.00	184	18.27	0.4	100.0	0.7	25.0	5	51	0.000109	2.18	24.02	24.02
11	SIL	1.50	15.00	16.50	184	18.27	0.4	100.0	0.7	15.0	25	47	7.02E-05	1.76	21.12	21.12
12	SiSa	3.50	16.50	20.00	184	18.27	0.4	100.0	0.7	5.0	31	46	0.000316	1.53	19.94	19.94
13	ClSa	10.00	20.00	30.00	191	18.27	0.4	100.0	0.7	5.0	30	39	0.000485	1.13	15.75	15.75

CHAPTER 4

RESULTS

4.1 Overview

In this section, analysis verification and comparision studies were carried out. Analysis results of the site responses are given with graphics and figures.

4.2 Unimproved Model Dynamic Analysis

In this chapter, the seismic response of a natural soil without any structures, using SPT (Standard Penetration Test) data obtained from the field, has been investigated. First, the liquefaction potential of the soil during an earthquake was evaluated. In other words, the possibility of the soil behaving like a liquid during an earthquake and posing a threat to structures was examined. Subsequently, the changes in the forces generated within different layers of the soil during an earthquake and their path to the ground surface were shown in detail using graphs and figures. In this way, important information such as how the natural soil transmits, reflects, or attenuates seismic waves has been obtained.

4.2.1 Liquefaction Evaluation for Model

A numerical model of the site was developed using field-measured SPT data liquefaction potential was evaluated for 11 earthquake records. Results indicated that all earthquakes except earthquake 3 posed a higher liquefaction risk at the site. Liquefaction was considered to occur when the excess pore water pressure ratio (R_u) exceeded 1, as calculated using the Plaxis software. This finding is consistent with the criterion proposed by Beaty and Perlea (2011), who suggested that a maximum Ru value greater than 0.7 indicates liquefaction potential.

Looking at Figures 4.1-11, it is determined that liquefaction potential exists in the areas indicated by the “+” symbol in the figures and that liquefaction usually occurs on the ground and in layer 2.

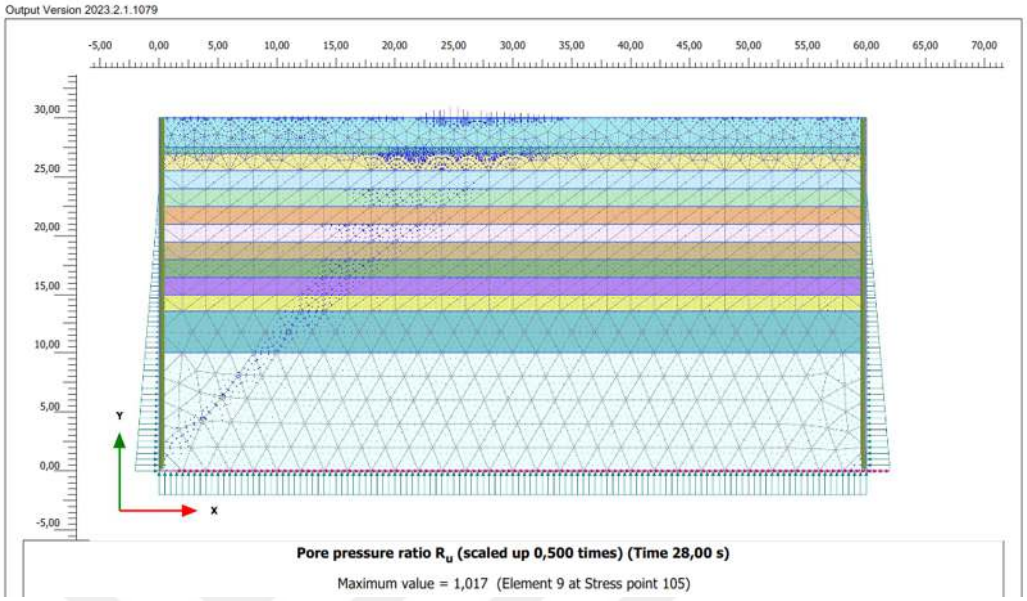

Figure 4.1 Earthquake 1 liquefaction result

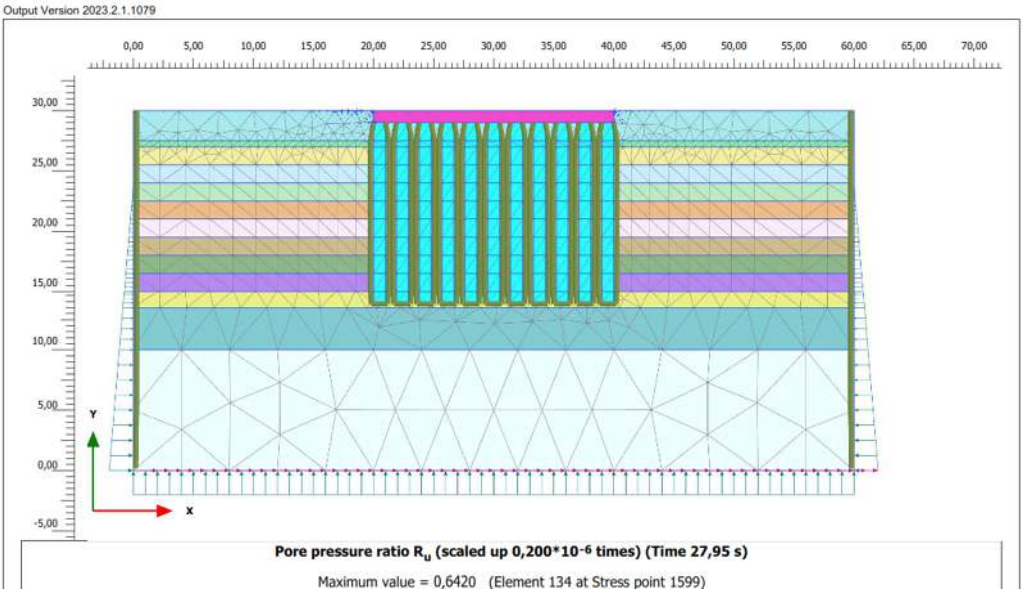

Figure 4.2 Earthquake 1 improved model liquefaction result

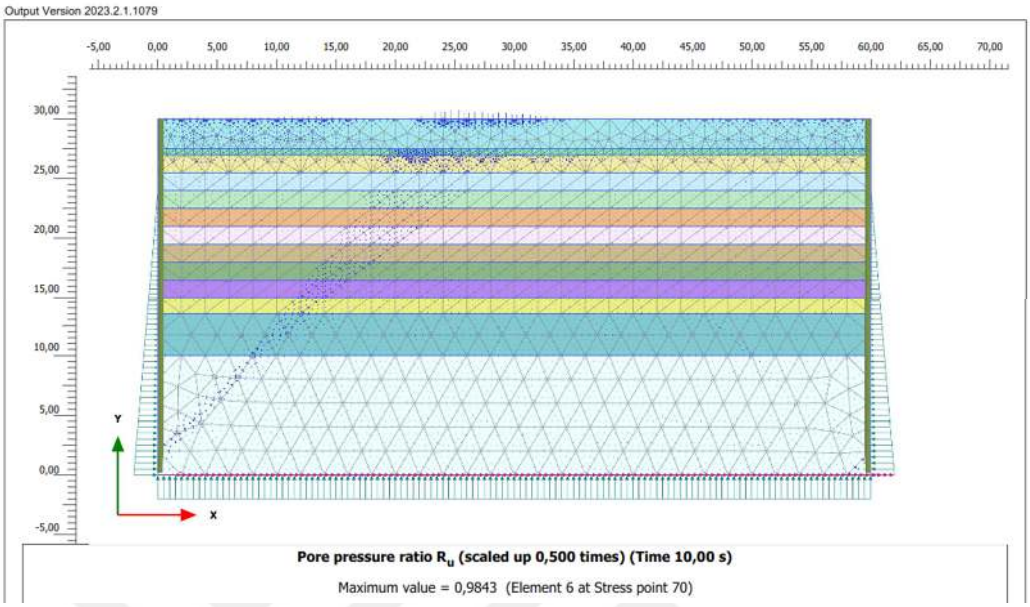

Figure 4.3 Earthquake 2 liquefaction result

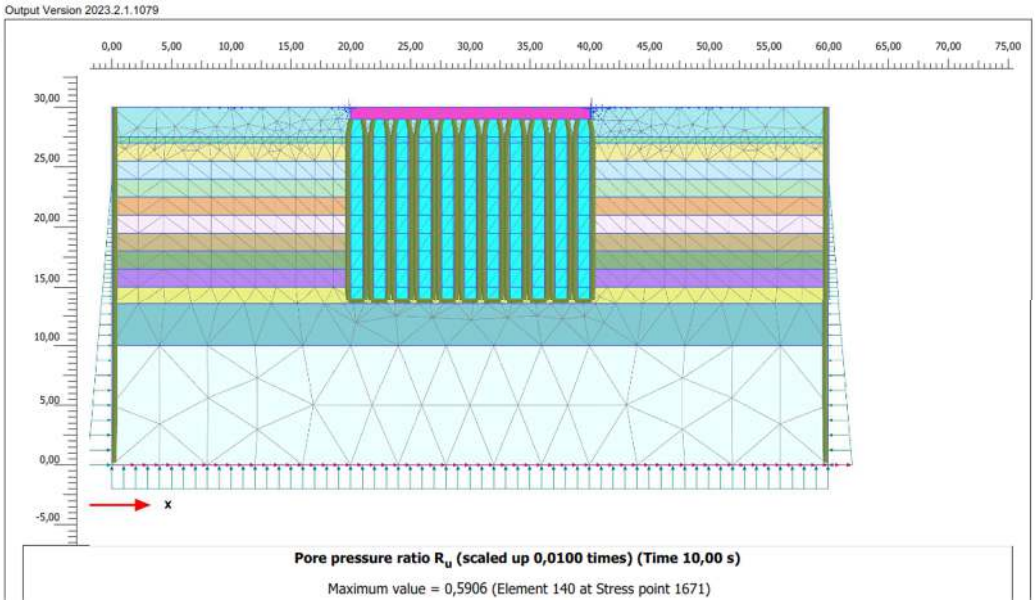

Figure 4.4 Earthquake 2 improved model liquefaction result

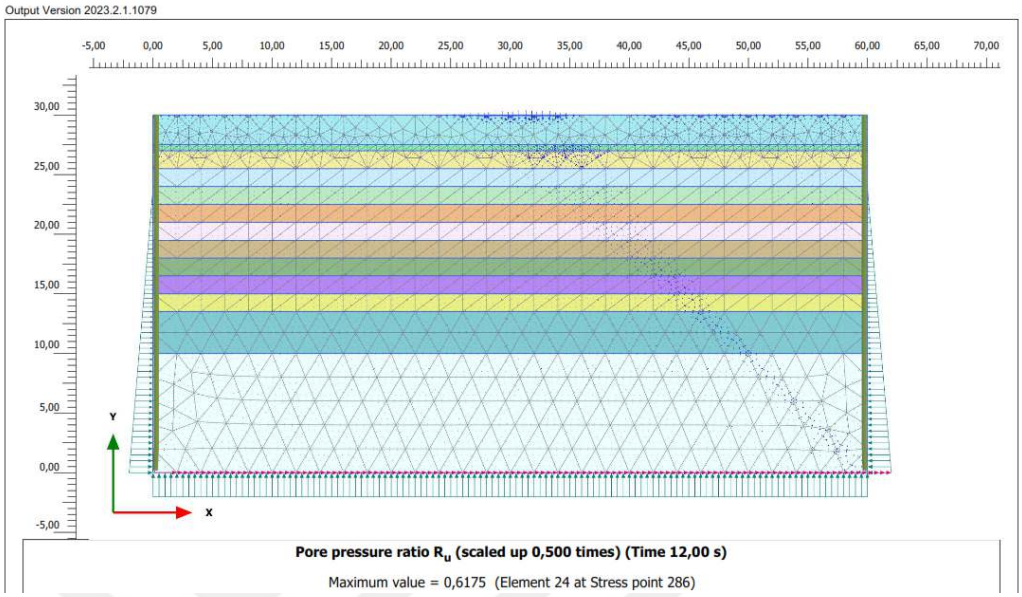

Figure 4.5 Earthquake 3 liquefaction result

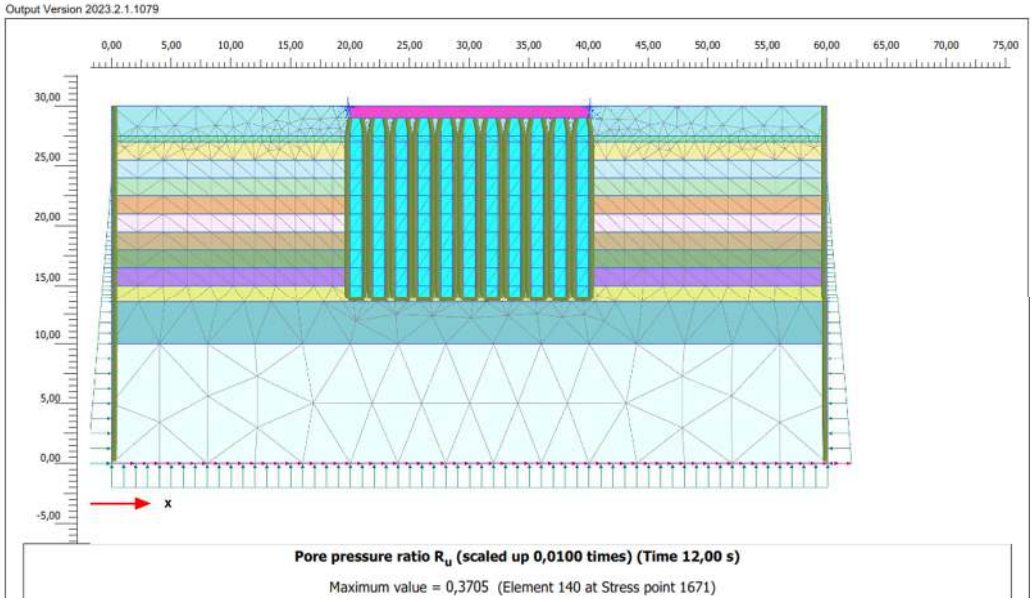

Figure 4.6 Earthquake 3 improved model liquefaction result

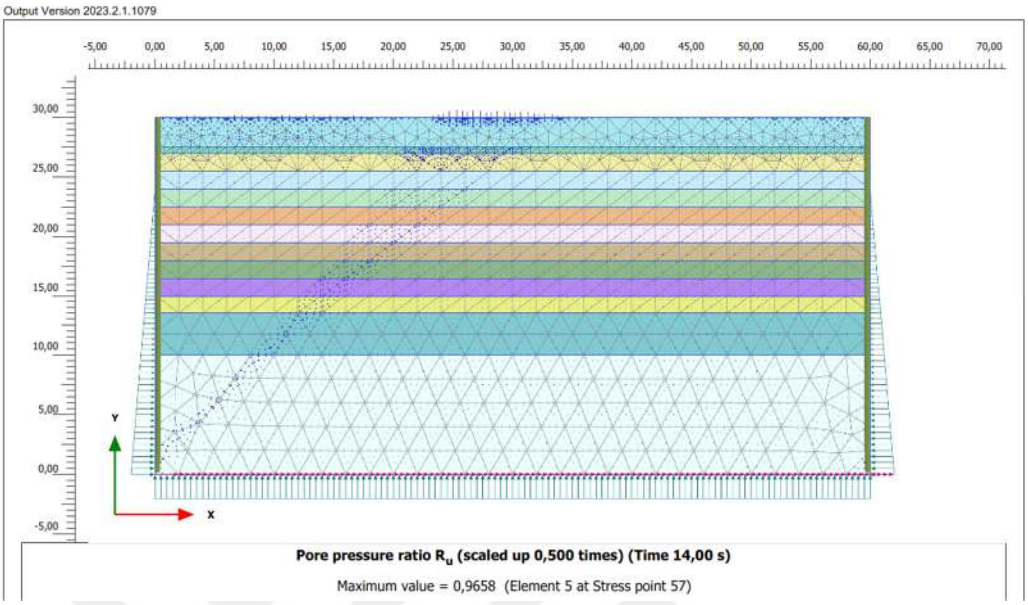

Figure 4.7 Earthquake 4 liquefaction result

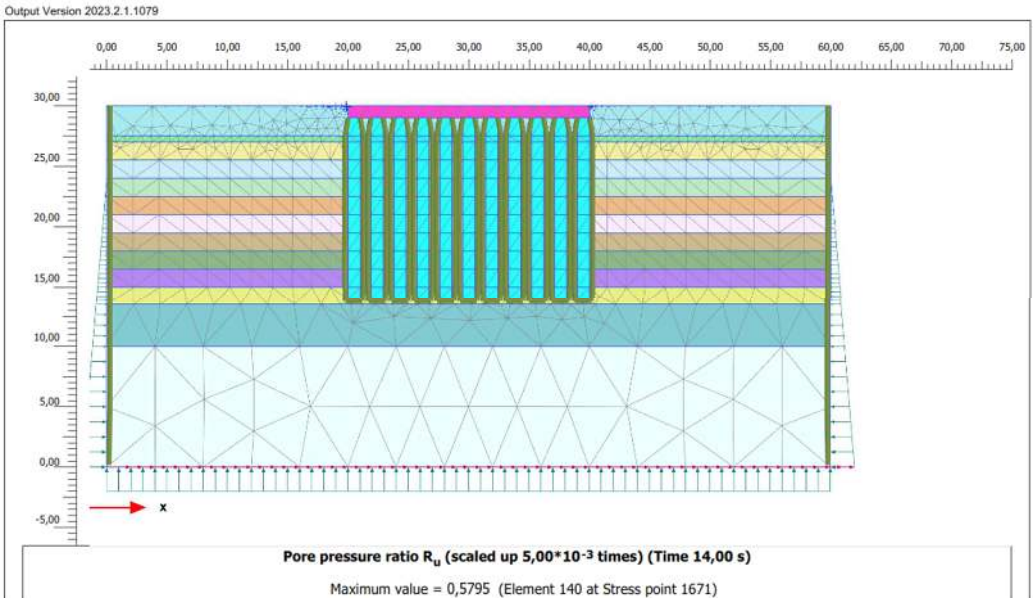

Figure 4.8 Earthquake 4 improved model liquefaction result

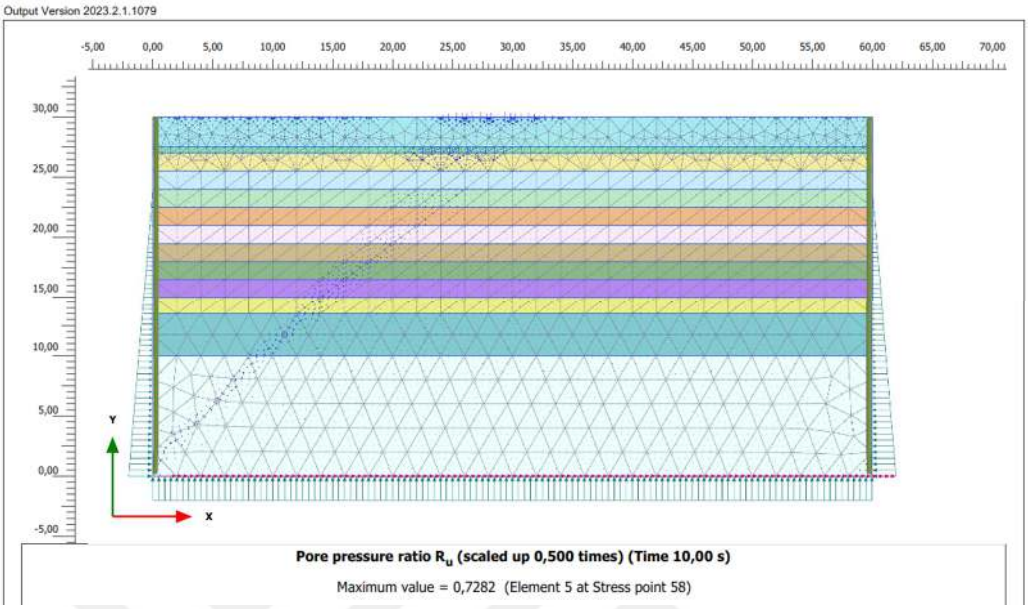

Figure 4.9 Earthquake 5 liquefaction result

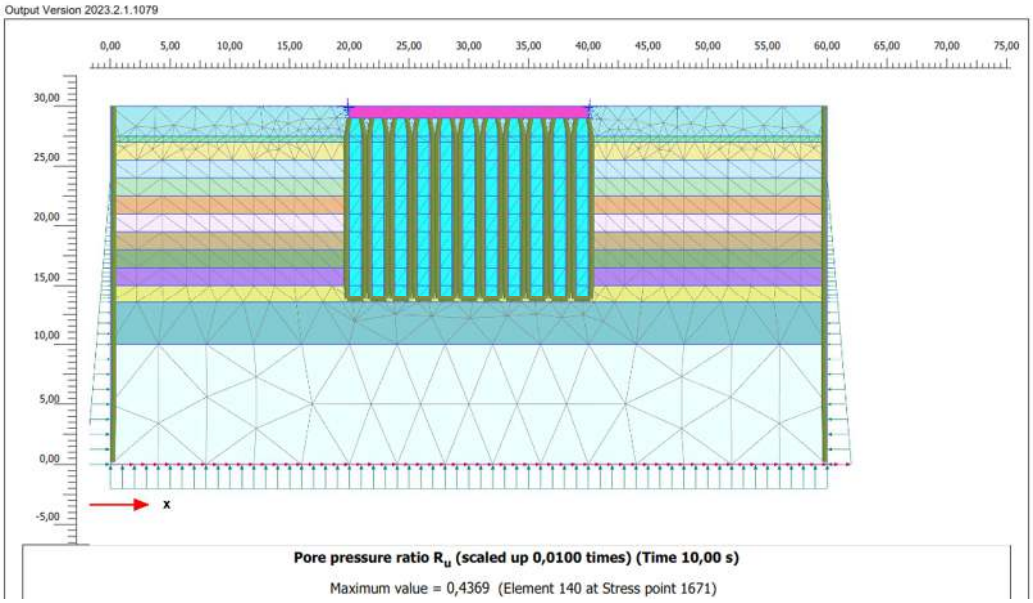

Figure 4.10 Earthquake 5 improved model liquefaction result

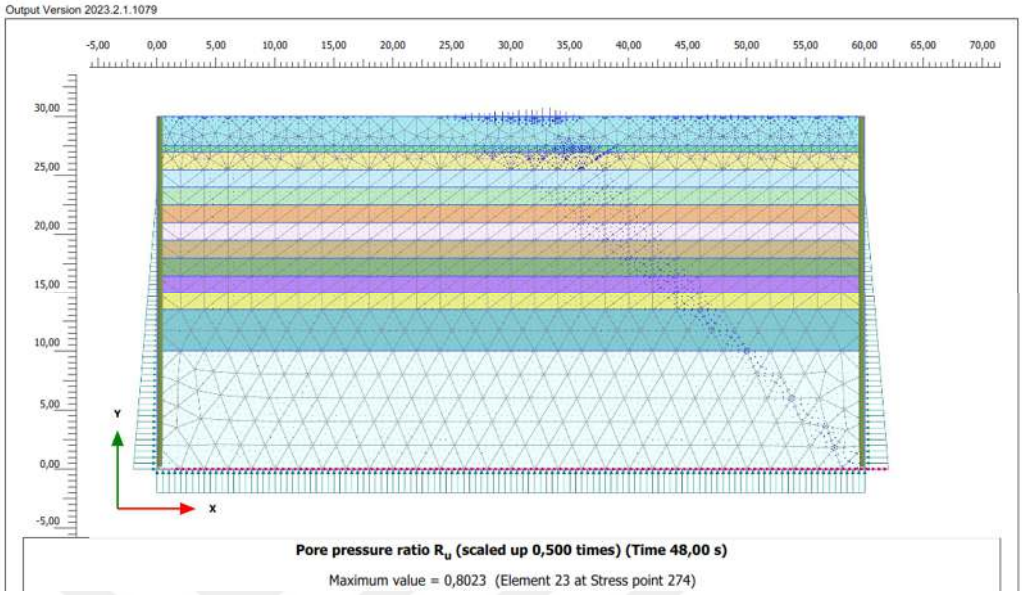

Figure 4.11 Earthquake 6 liquefaction result

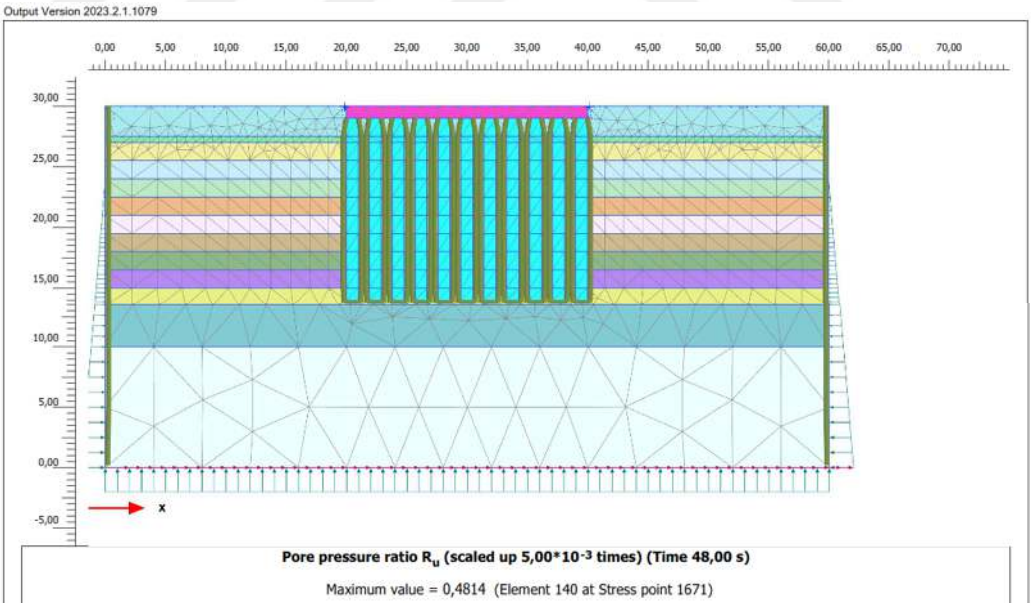

Figure 4.12 Earthquake 6 improved model liquefaction result

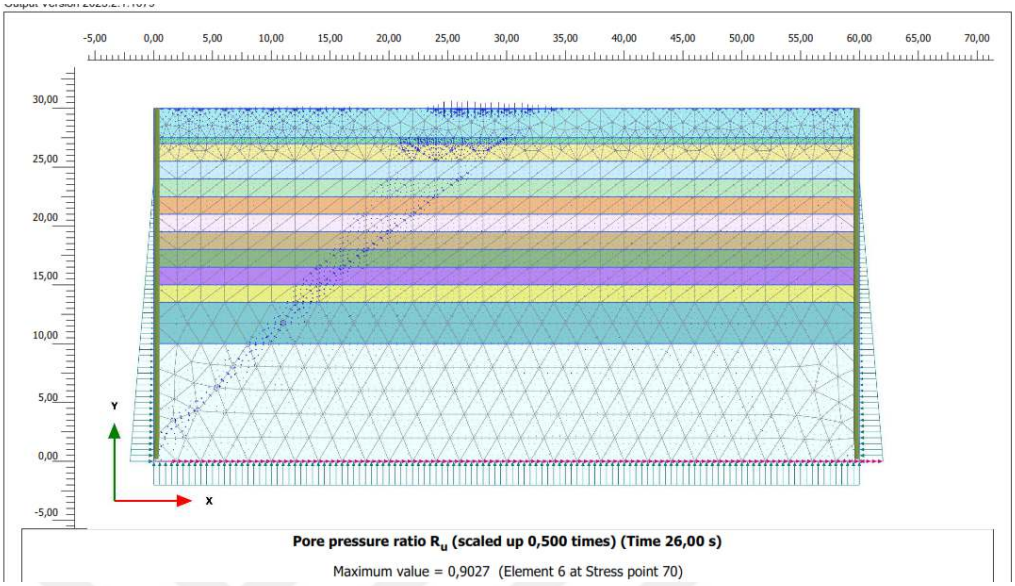

Figure 4.13 Earthquake 7 liquefaction result

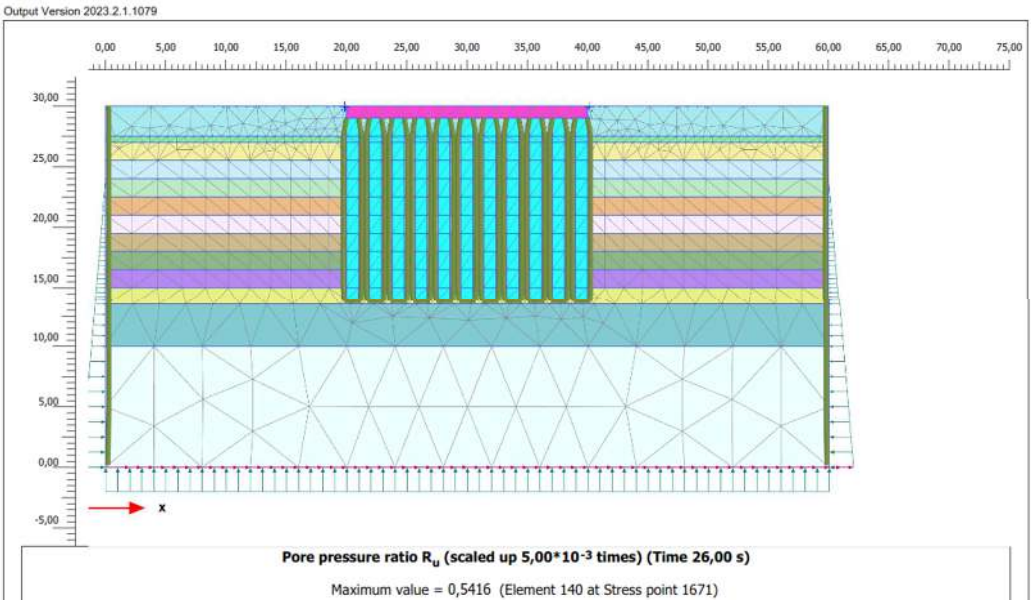

Figure 4.14 Earthquake 7 improved model liquefaction result

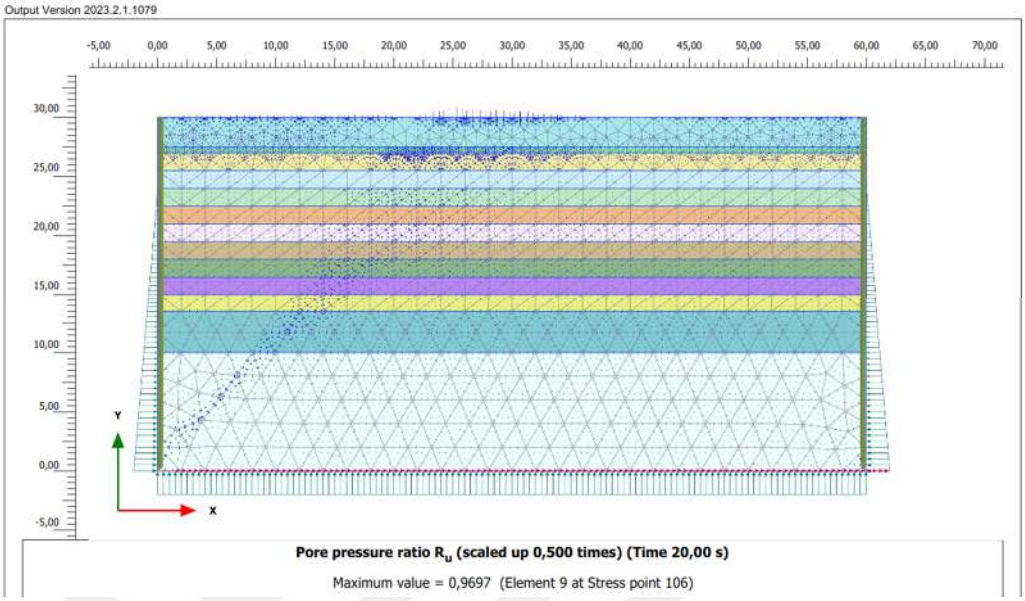

Figure 4.15 Earthquake 8 liquefaction result

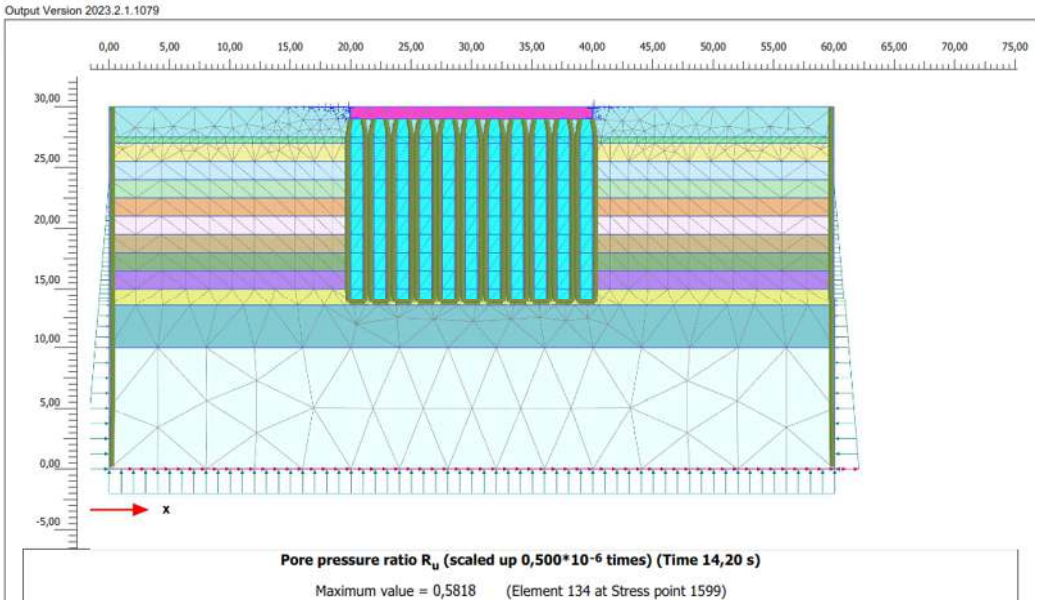

Figure 4.16 Earthquake 8 improved model liquefaction result

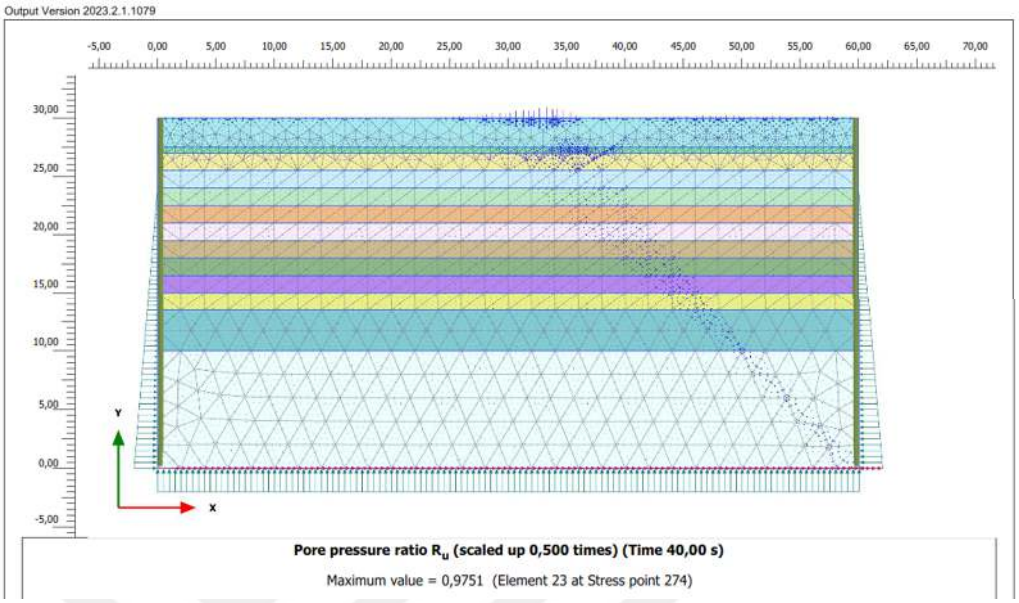

Figure 4.17 Earthquake 9 liquefaction result

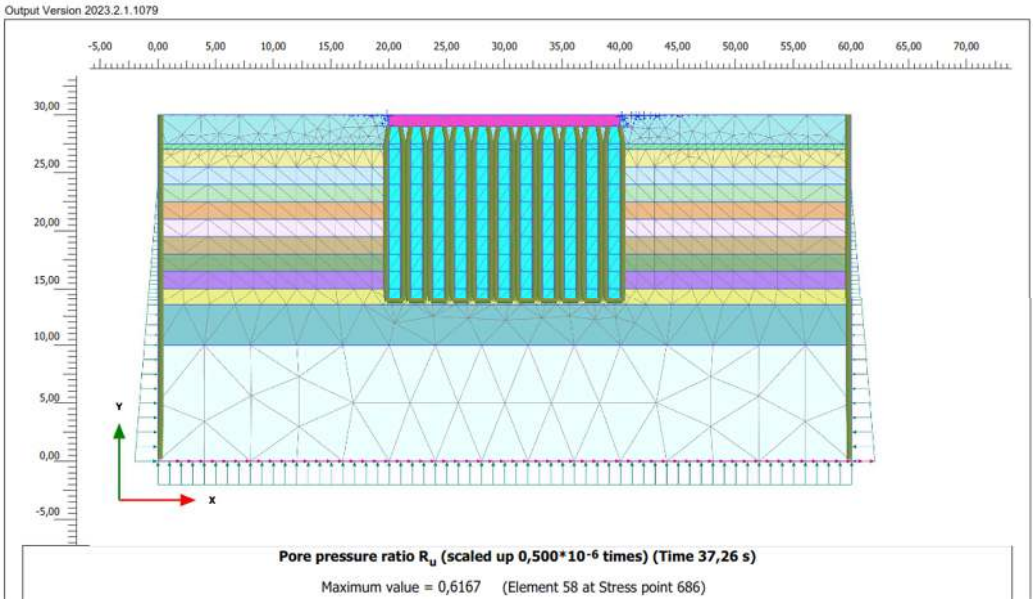

Figure 4.18 Earthquake 9 improved model liquefaction result

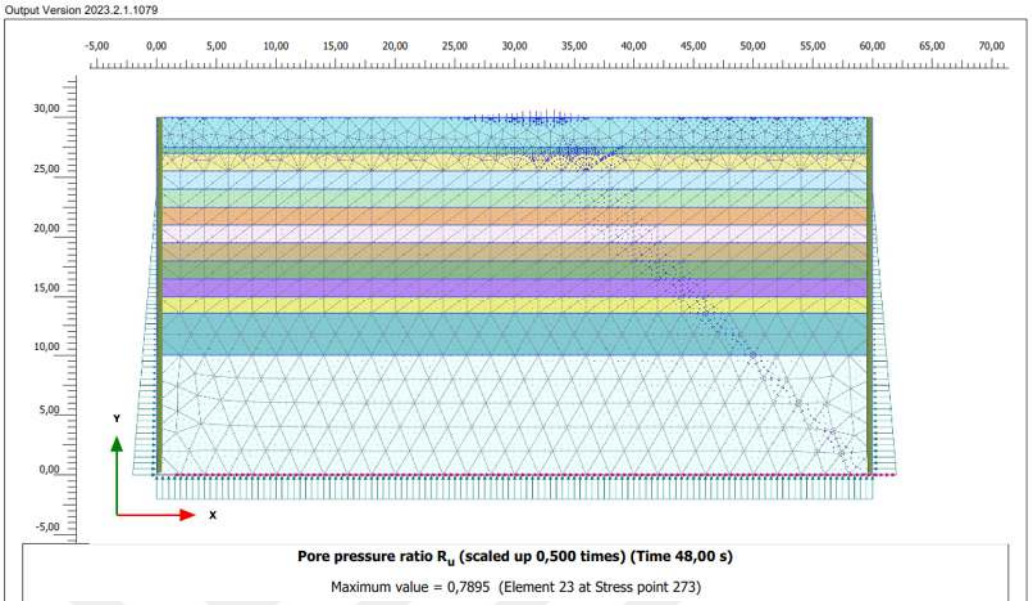

Figure 4.19 Earthquake 10 liquefaction result

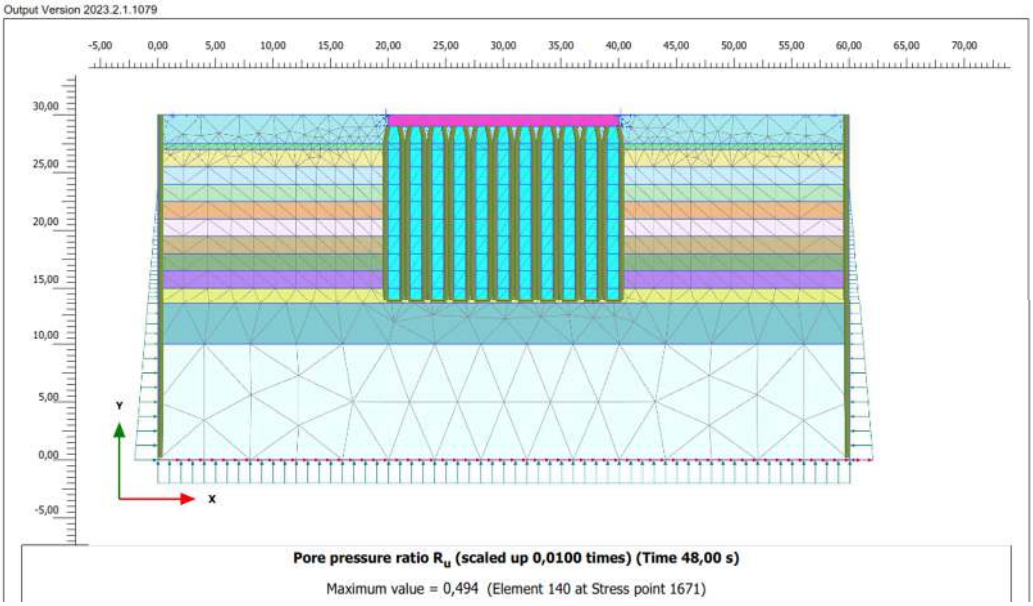

Figure 4.20 Earthquake 10 improved model liquefaction result

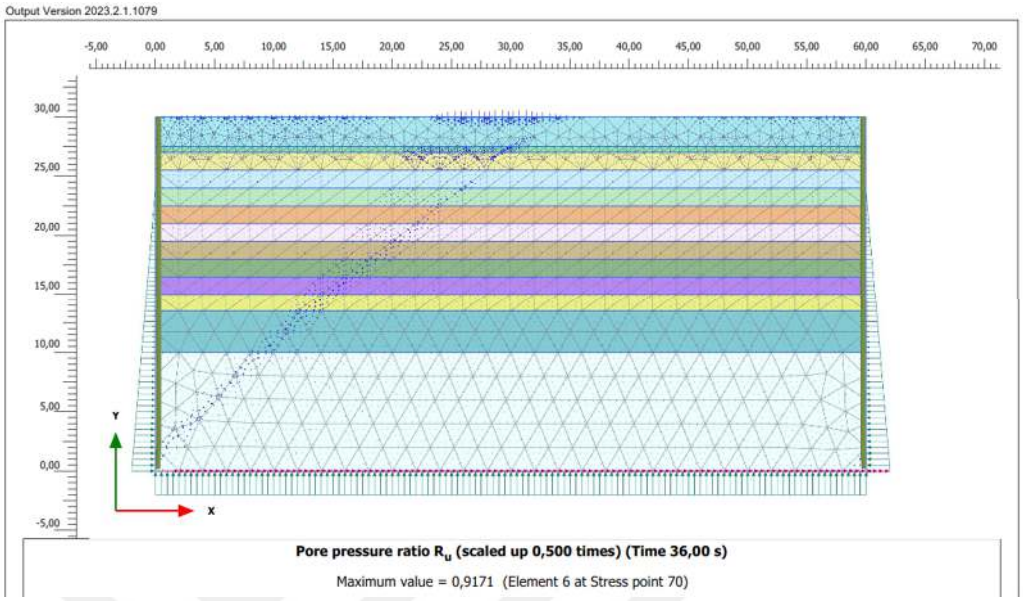

Figure 4.21 Earthquake 11 liquefaction result

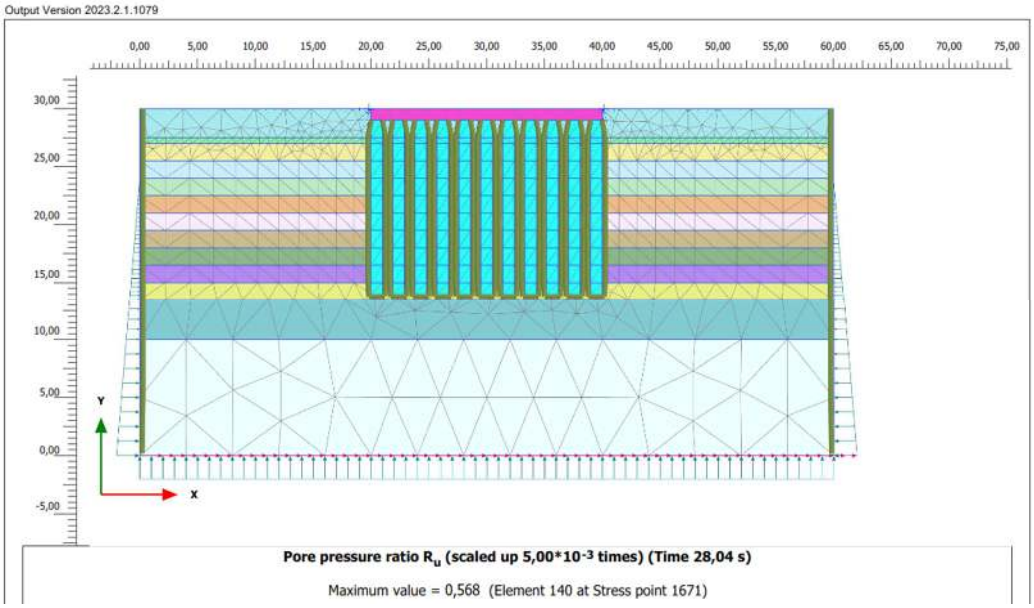

Figure 4.22 Earthquake 11 improved model liquefaction result

As seen in the figures, the liquefaction risk was found to be located in the upper and middle parts (30, 30) of the model in the unimproved models. Later, when the foundation and jet grout were added to the model, it was observed that the liquefaction potential spread to the lateral parts of the foundation element (location coordinate: (20,30) & (40, 30)) , but this did not have the potential to damage the foundation and superstructure.

4.3 Site Response Analysis

4.3.1 Response Analysis Evaluation for Unimproved Model

To understand how soil layers will respond to a given seismic motion at the ground surface, it is essential to analyze the propagation of shear waves from bedrock to the surface. This analysis, known as site amplification, provides the input acceleration to the soil layer at the location. By estimating the necessary natural frequency of a structure and understanding the amplified seismic wave that the structure will experience, site amplification is crucial for seismic design. Accurate modeling should result in a reasonable correlation between the results of site amplification analysis and the actual seismic response of the structure. However, discrepancies may arise due to differences in analytical methods and underlying assumptions.

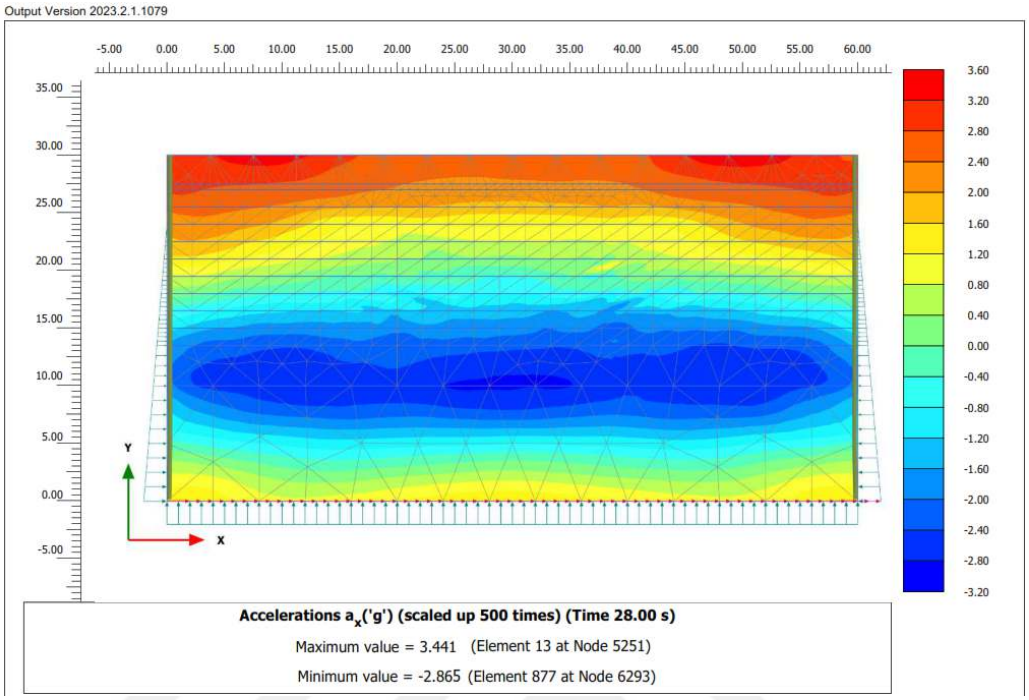

Figure 4.23 Earthquake 1 acceleration (ax) result

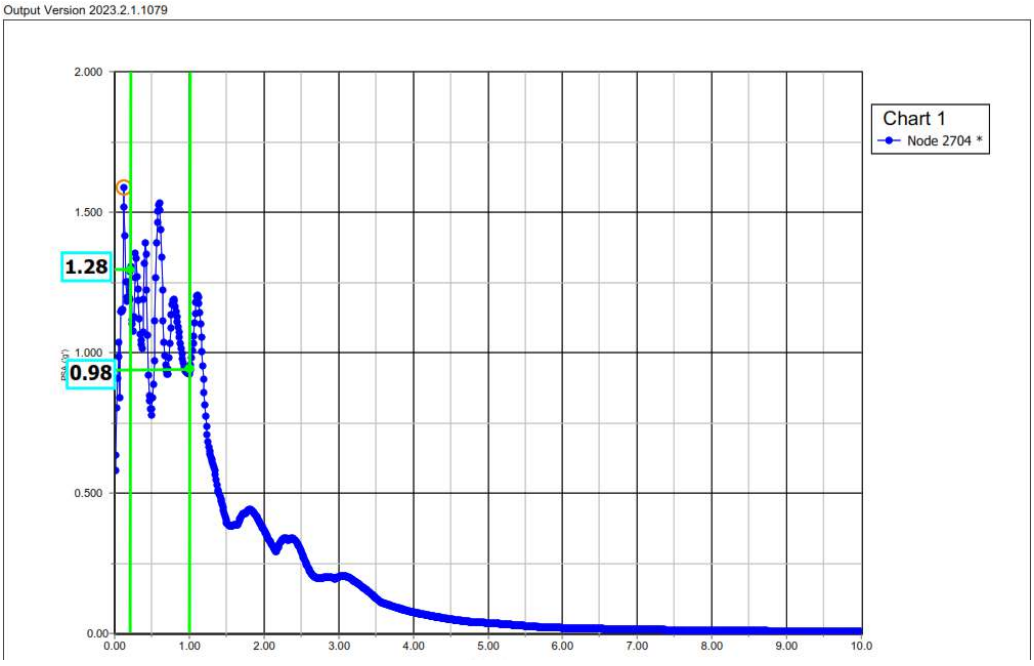

Figure 4.24 Earthquake 1 ground surface PSA graph

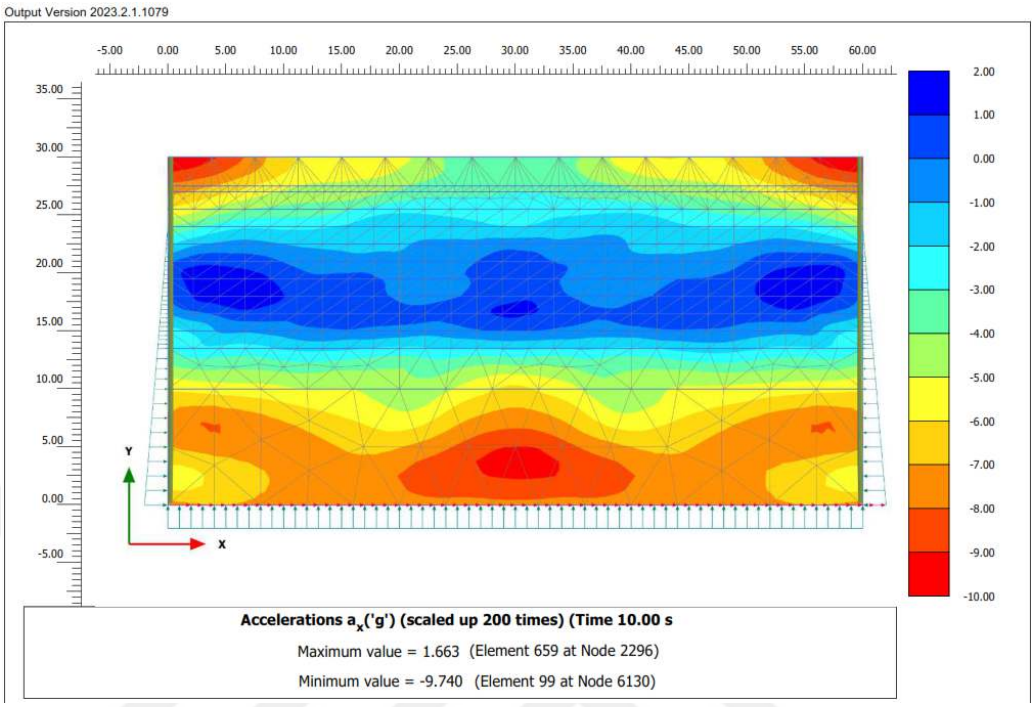

Figure 4.25 Earthquake 2 acceleration (ax) result

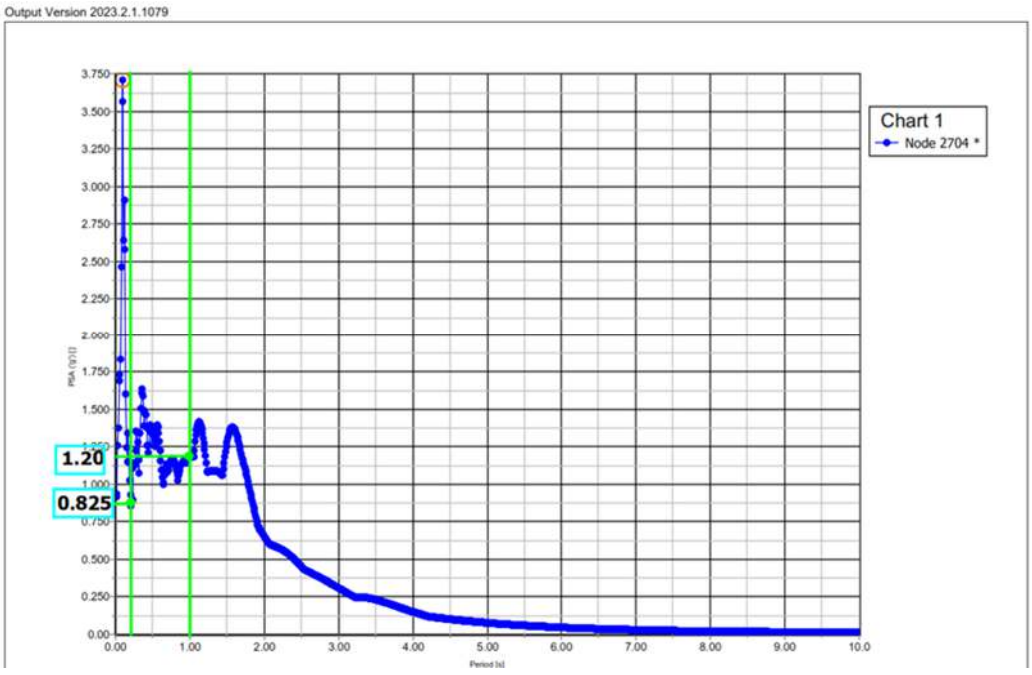

Figure 4.26 Earthquake 2 ground surface PSA result

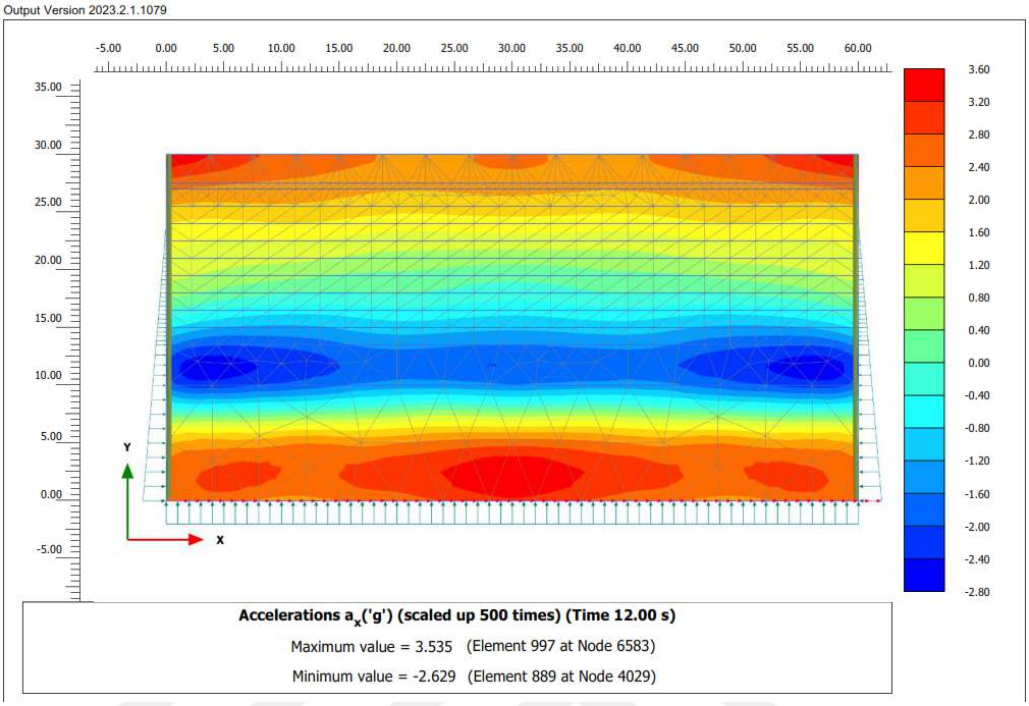

Figure 4.27 Earthquake 3 acceleration (ax) result

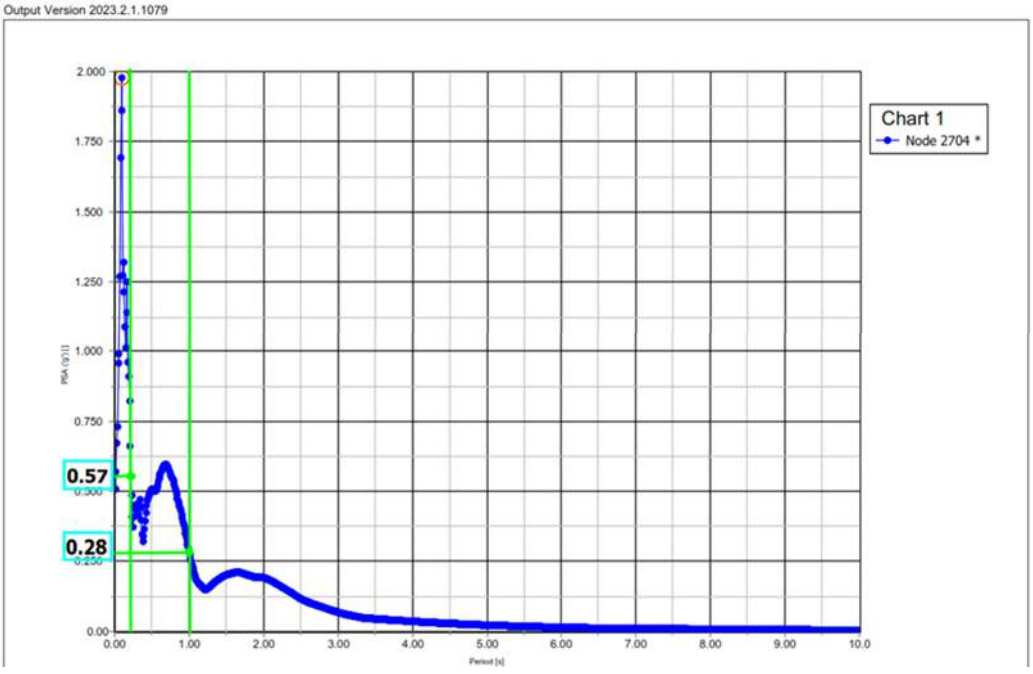

Figure 4.28 Earthquake 3 ground surface PSA result

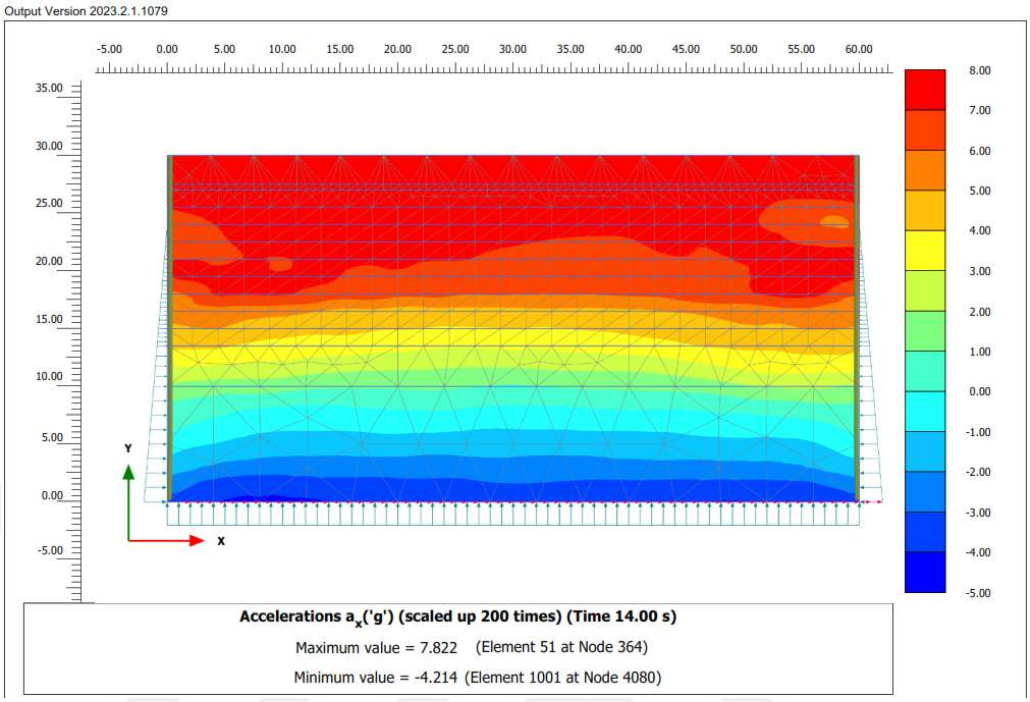

Figure 4.29 Earthquake 4 acceleration (ax) result

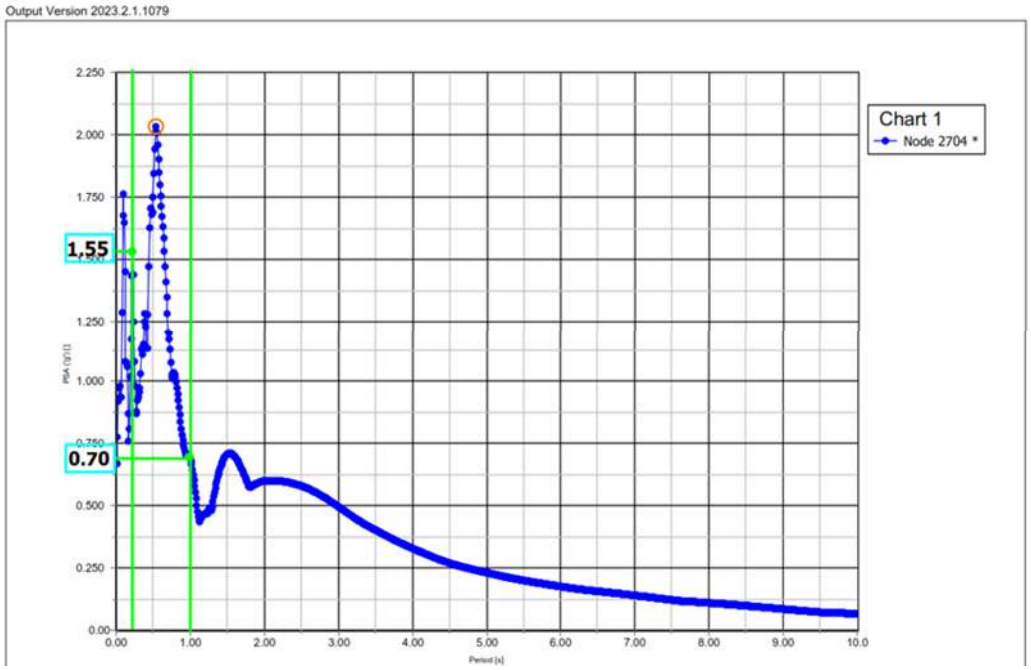

Figure 4.30 Earthquake 4 ground surface PSA result

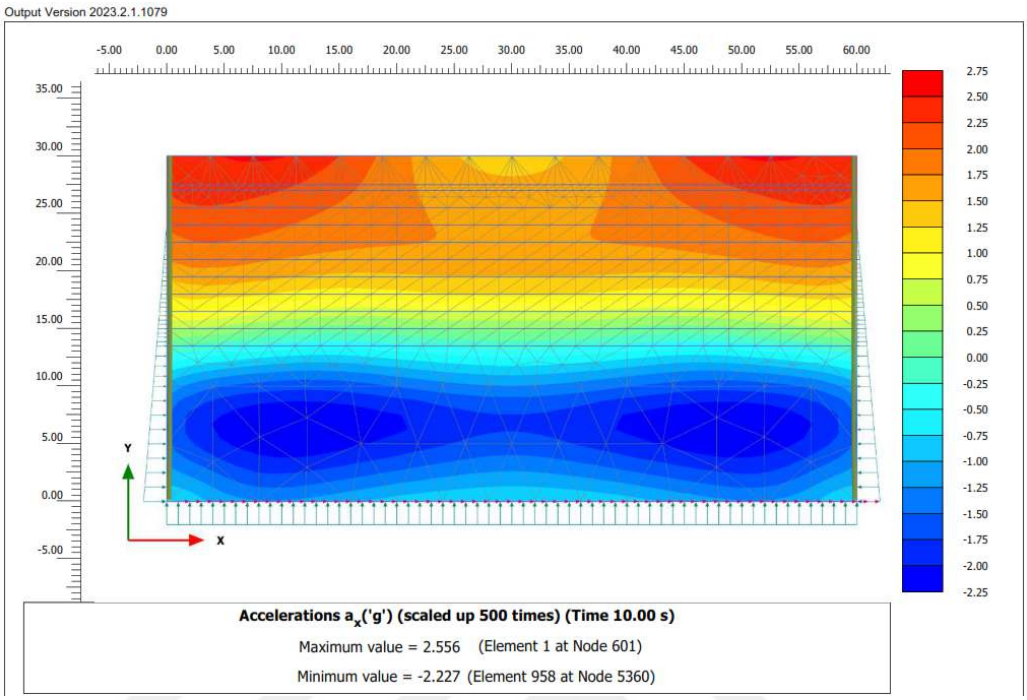

Figure 4.31 Earthquake 5 acceleration (ax) result

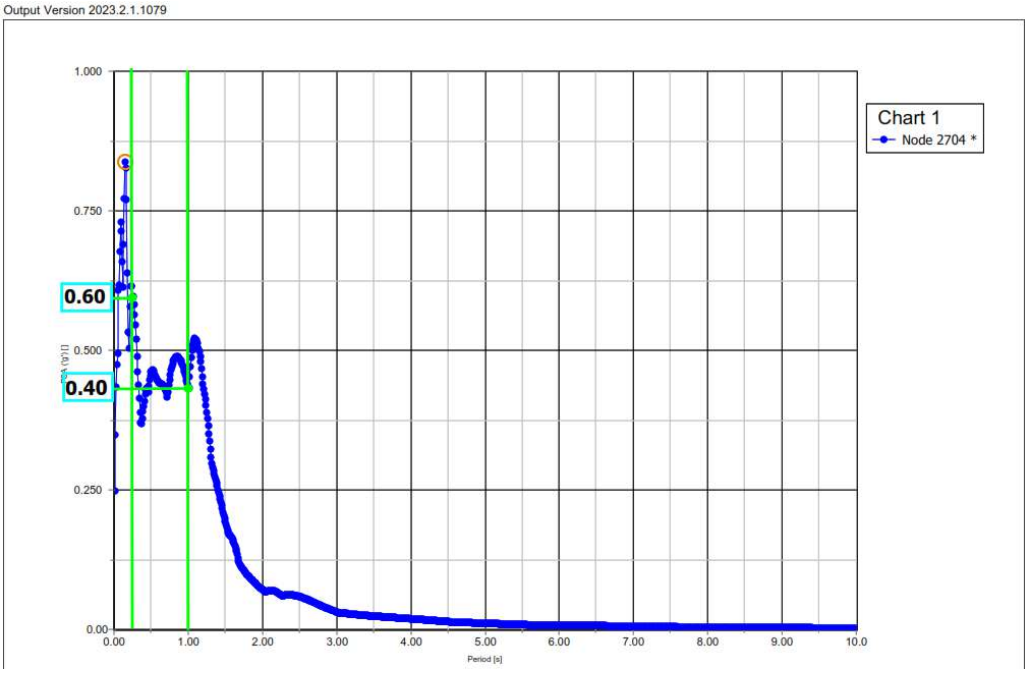

Figure 4.32 Earthquake 5 ground surface PSA result

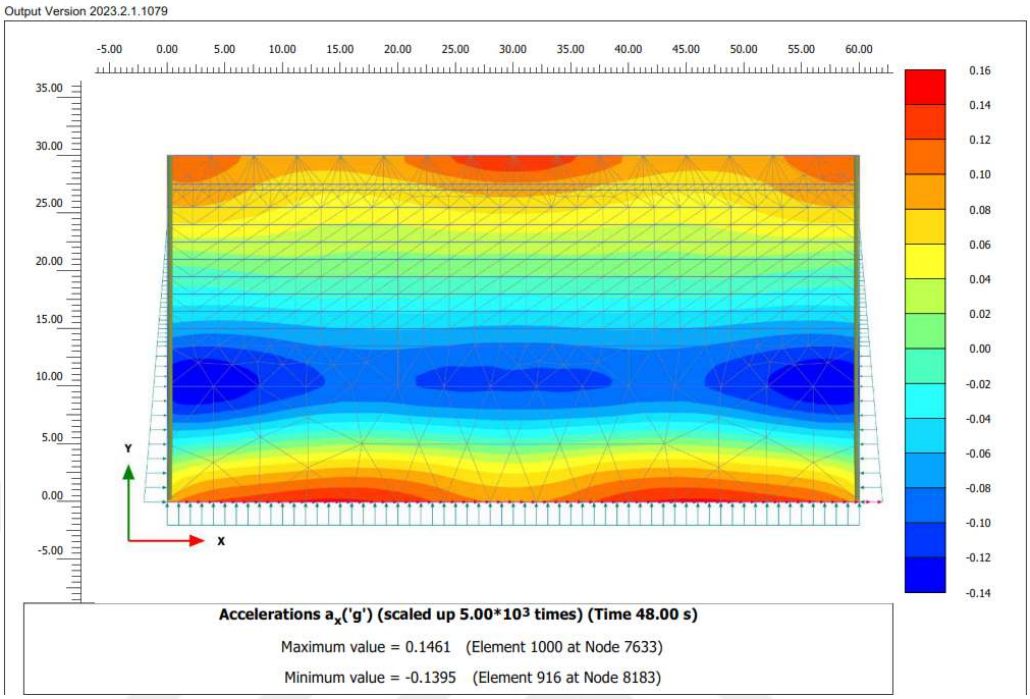

Figure 4.33 Earthquake 6 acceleration (ax) result

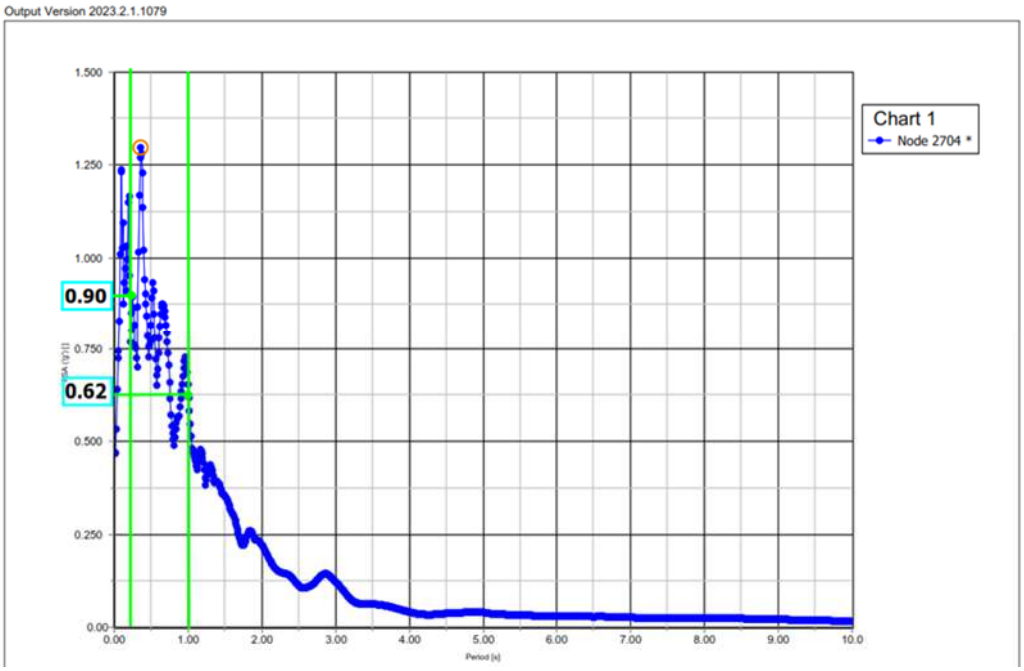

Figure 4.34 Earthquake 6 ground surface PSA result

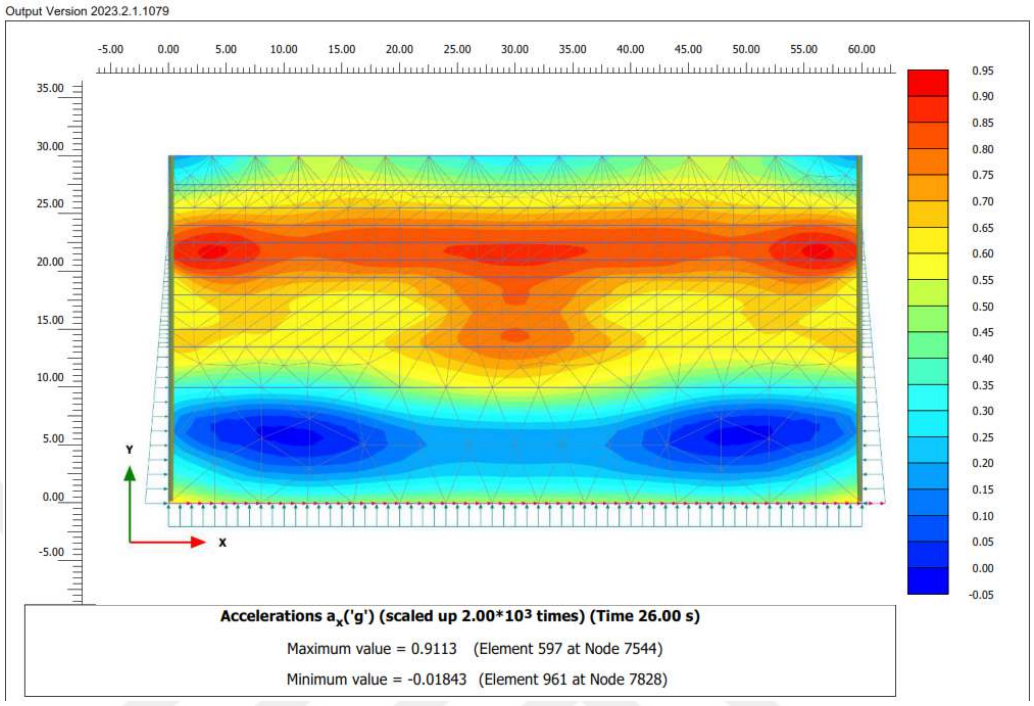

Figure 4.35 Earthquake 7 acceleration (ax) result

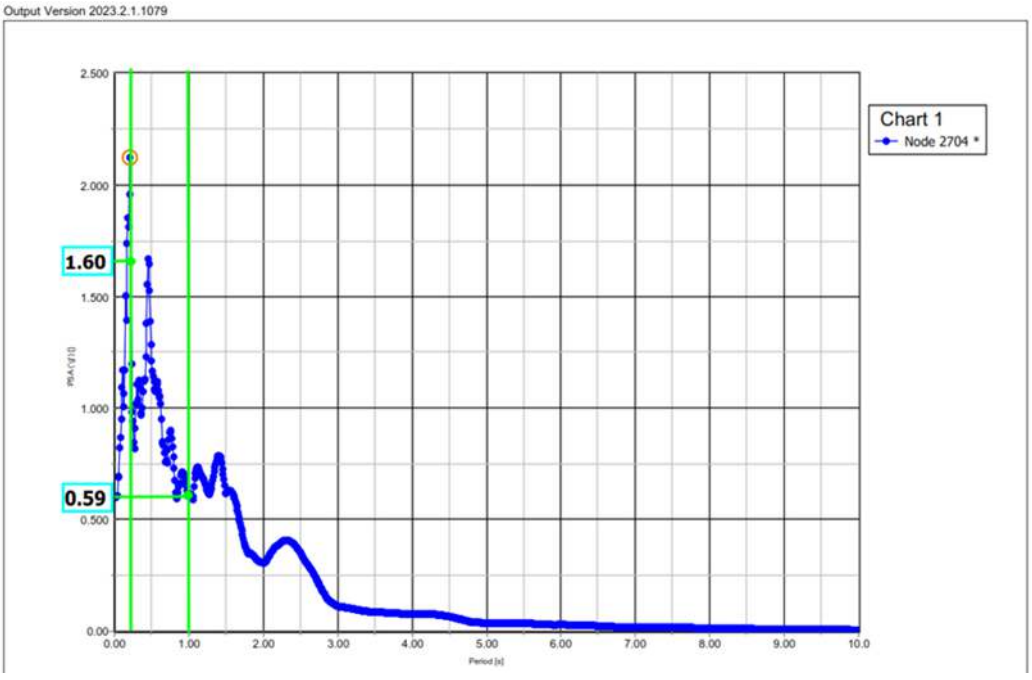

Figure 4.36 Earthquake 7 ground surface PSA result

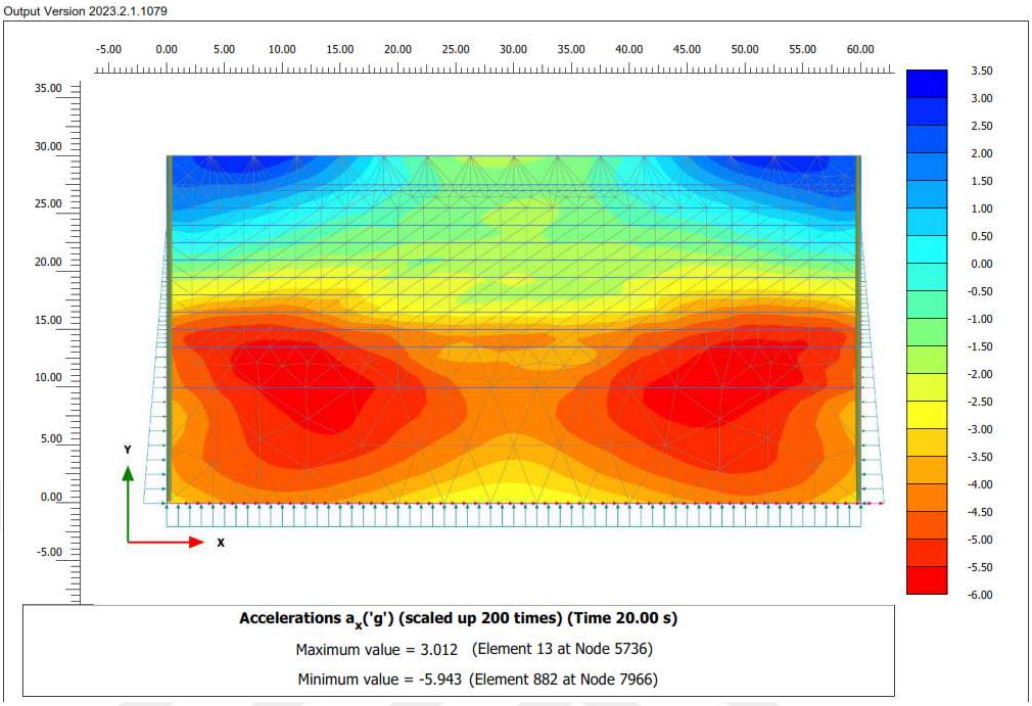

Figure 4.37 Earthquake 8 acceleration (ax) result

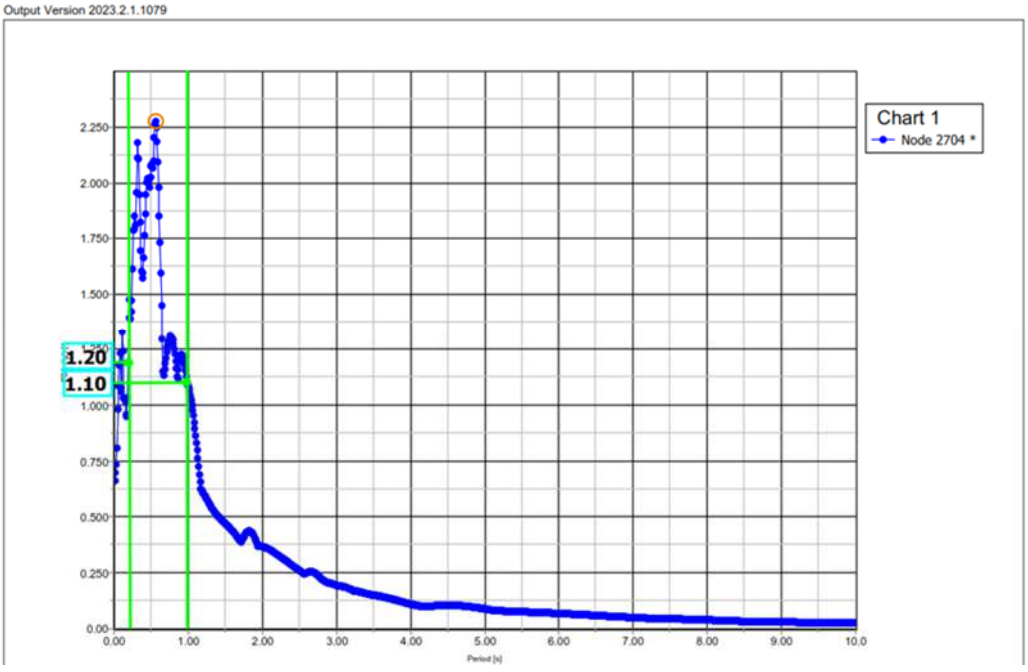

Figure 4.38 Earthquake 8 ground surface PSA result

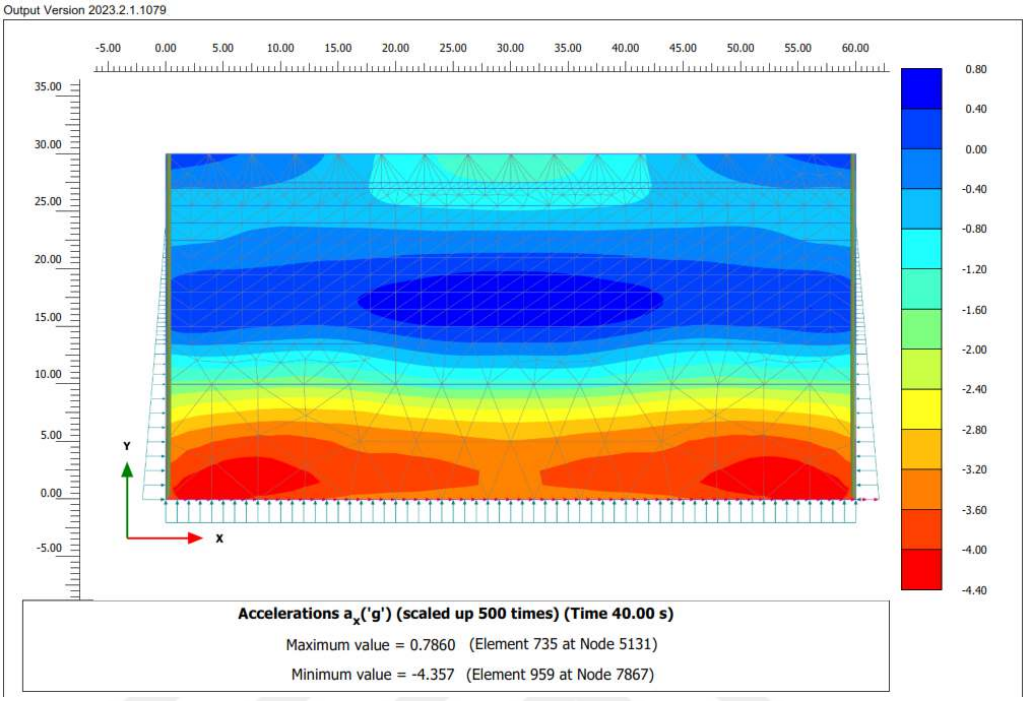

Figure 4.39 Earthquake 9 acceleration (ax) result

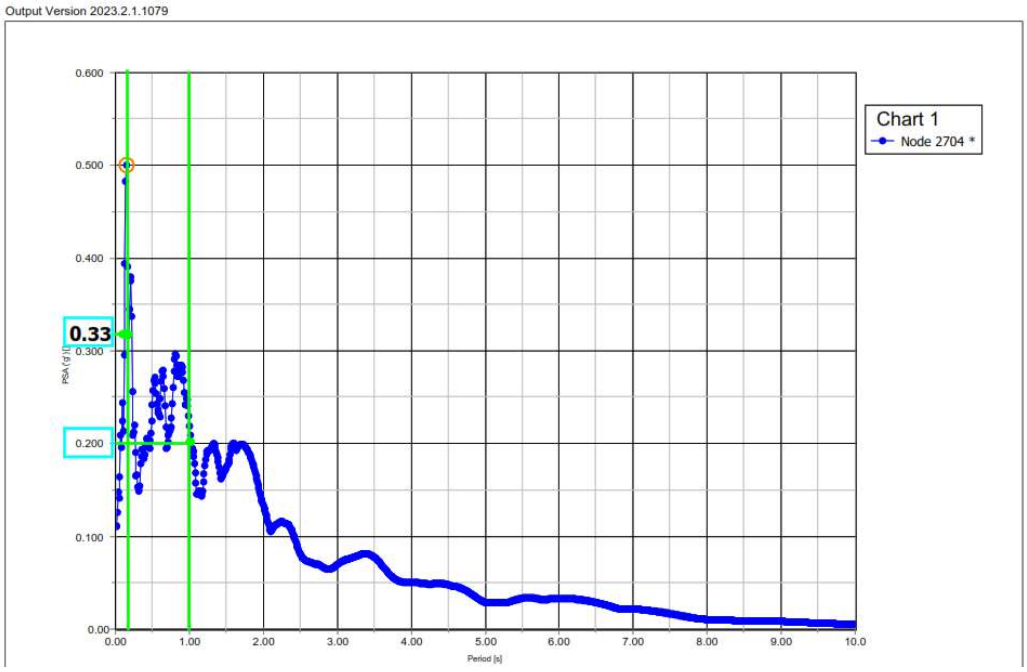

Figure 4.40 Earthquake 9 ground surface PSA result

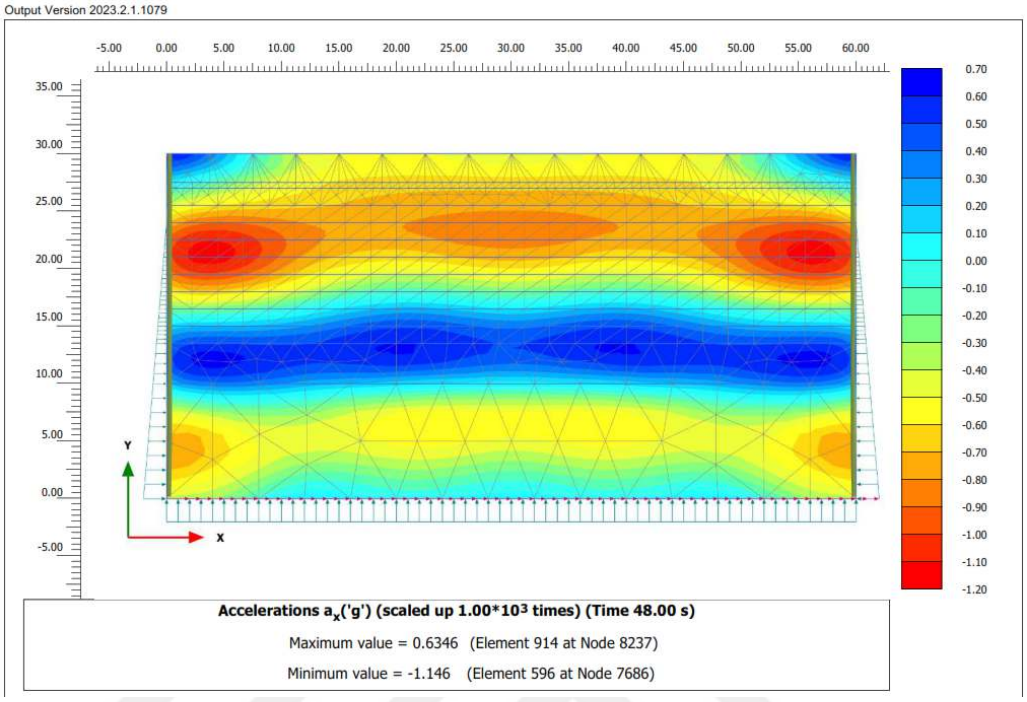

Figure 4.41 Earthquake 10 acceleration (ax) result

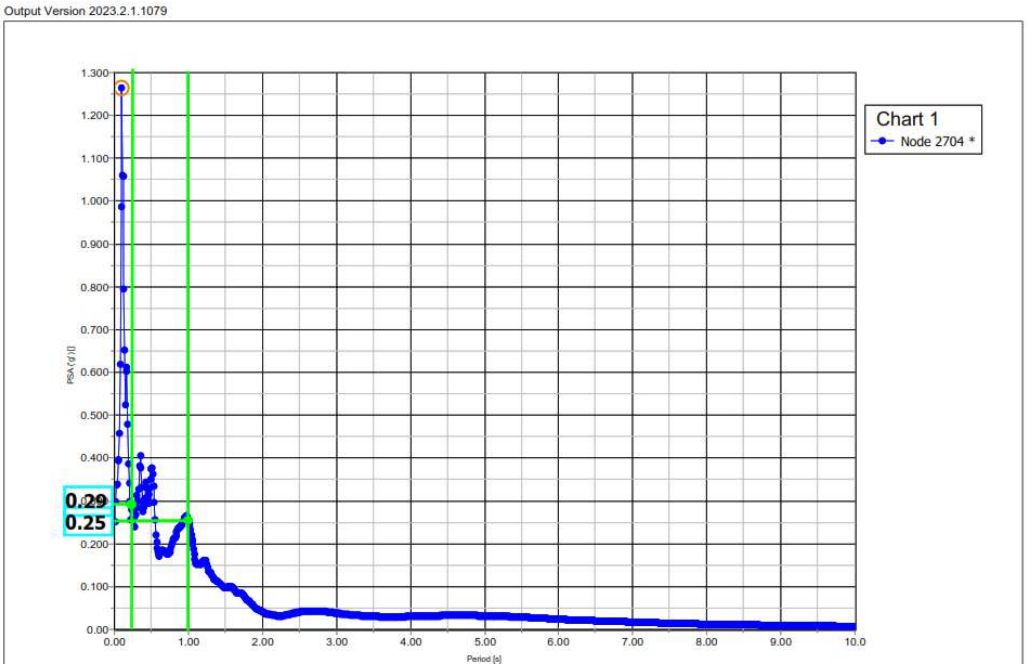

Figure 4.42 Earthquake 10 ground surface PSA result

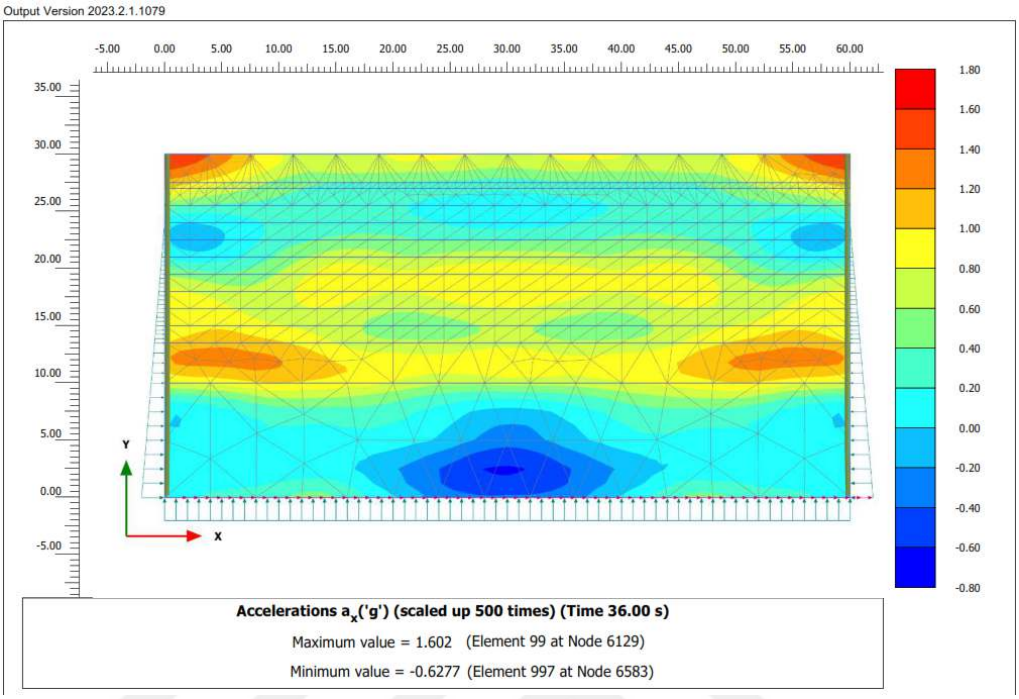

Figure 4.43 Earthquake 11 acceleration (ax) result

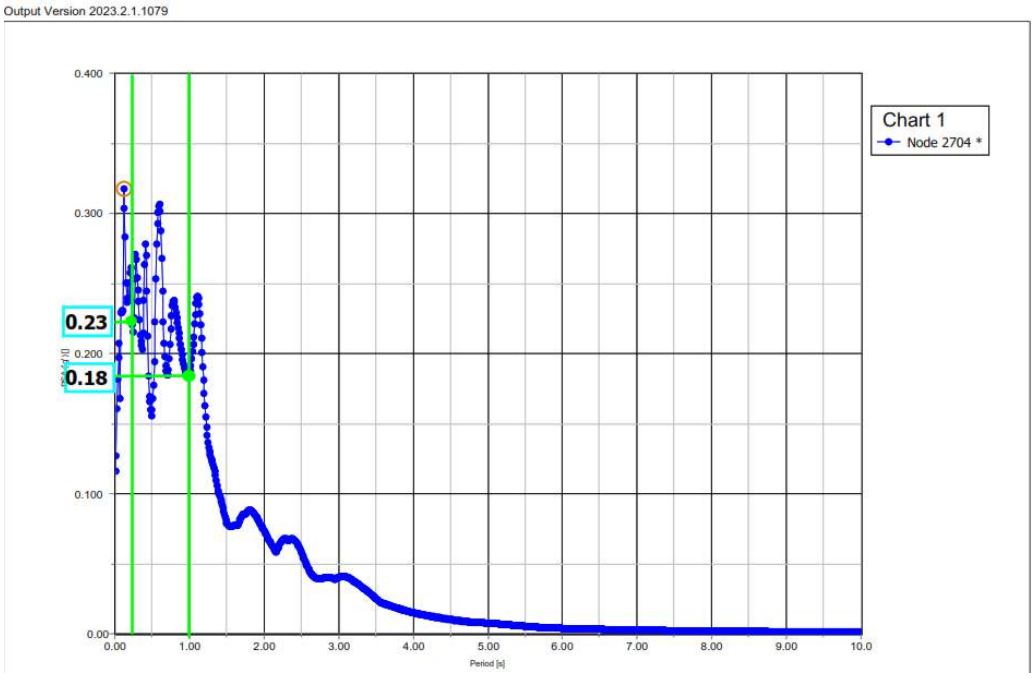

Figure 4.44 Earthquake 11 ground surface PSA result

4.3.2 Response Analysis Evaluation for Improved Model

In the previous analyses, the earthquake acceleration values between the layers were analyzed according to the natural structure of the ground. The earthquake effect was improved with jet grout column and ground improvement was made to support the reinforced concrete building to be built on it. The magnitudes of the acceleration felt on the foundation of this ground improvement were analyzed and the earthquake acceleration values to be felt in the superstructure of the ground improvement were compared in the report.

In earthquake-prone regions such as Kayseri, the choice of ground improvement methods is of great importance, especially in constructions to be built in areas with liquefaction risk. In this site, it would be a very correct decision to prefer jet grouting application.

The jet grouting method is based on the principle of creating columns by injecting a high-pressure mixture of water and cement into the ground. In this way, the bearing capacity is increased by improving the soil and the risk of liquefaction is significantly reduced. Bored piling, on the other hand, is the method of digging a hole in the ground and placing reinforced concrete piles in it.

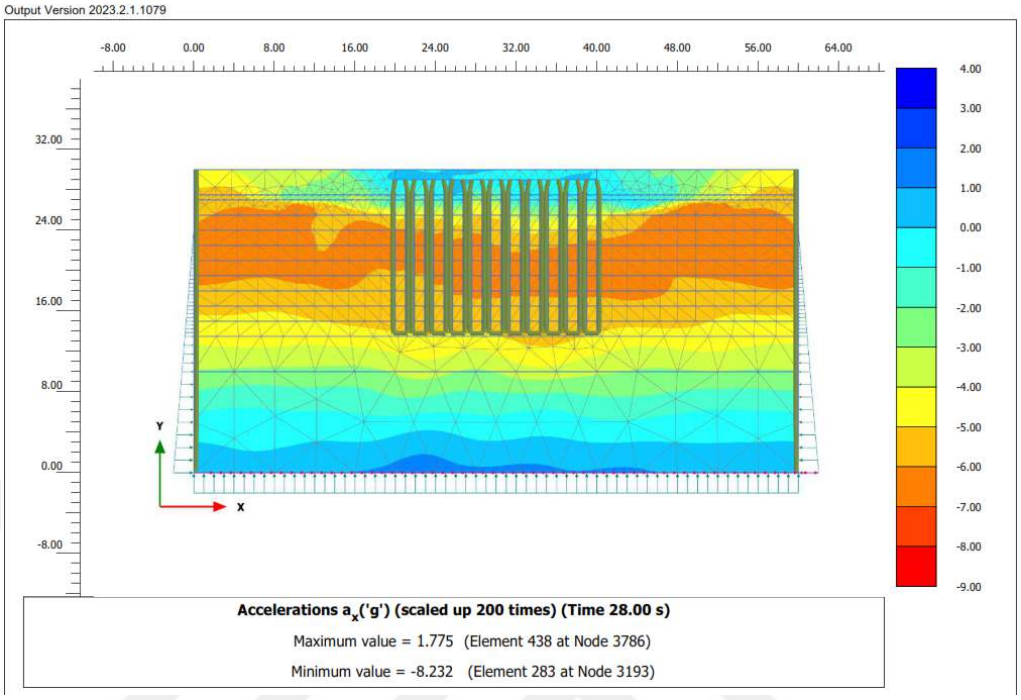

Figure 4.45 Earthquake 1 improved model acceleration (ax) result

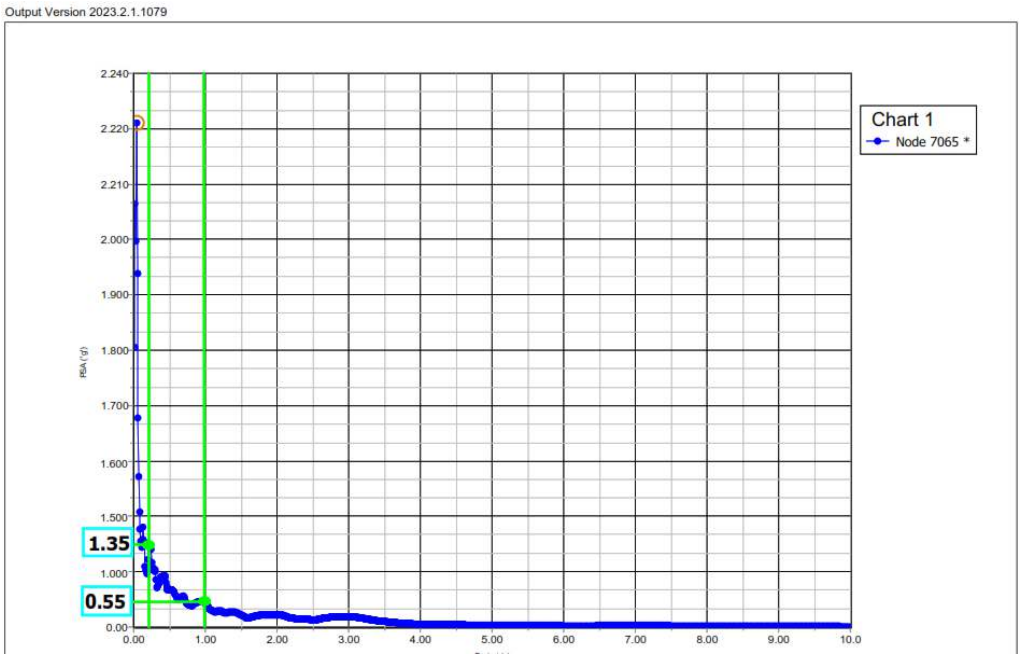

Figure 4.46 Earthquake 1 improved model ground surface PSA graph

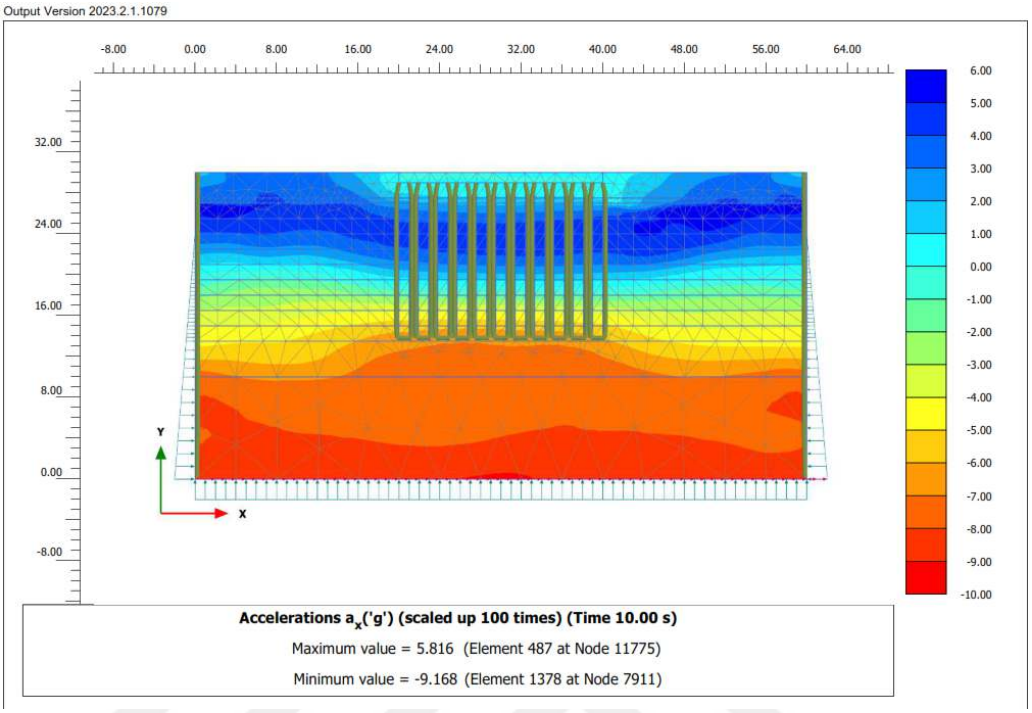

Figure 4.47 Earthquake 2 improved model acceleration (ax) result

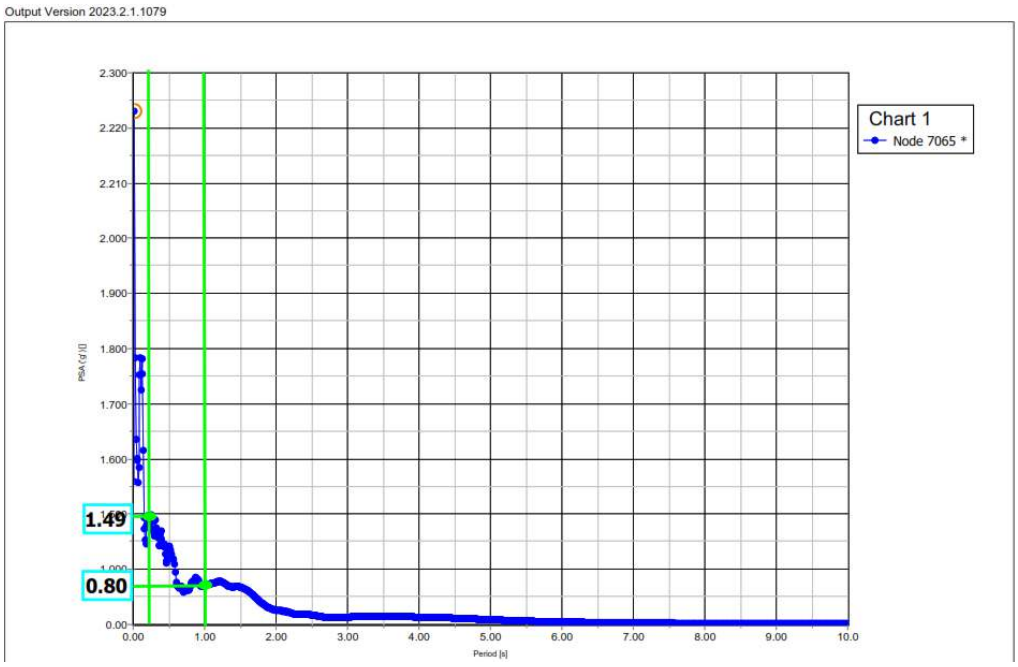

Figure 4.48 Earthquake 2 improved model ground surface PSA result

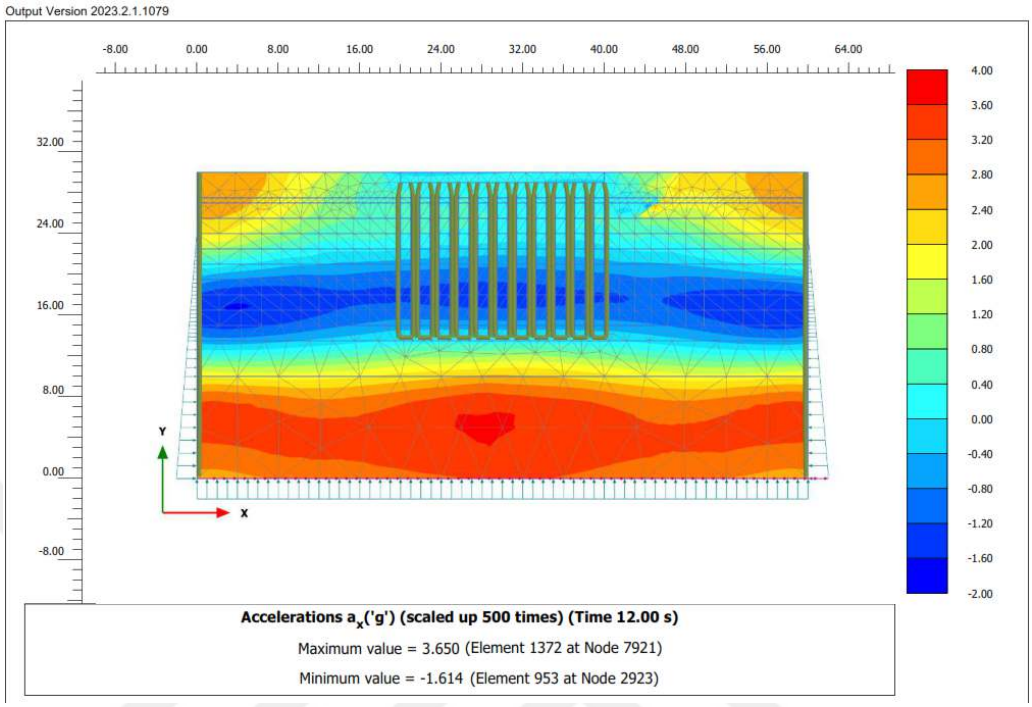

Figure 4.49 Earthquake 3 improved model acceleration (ax) result

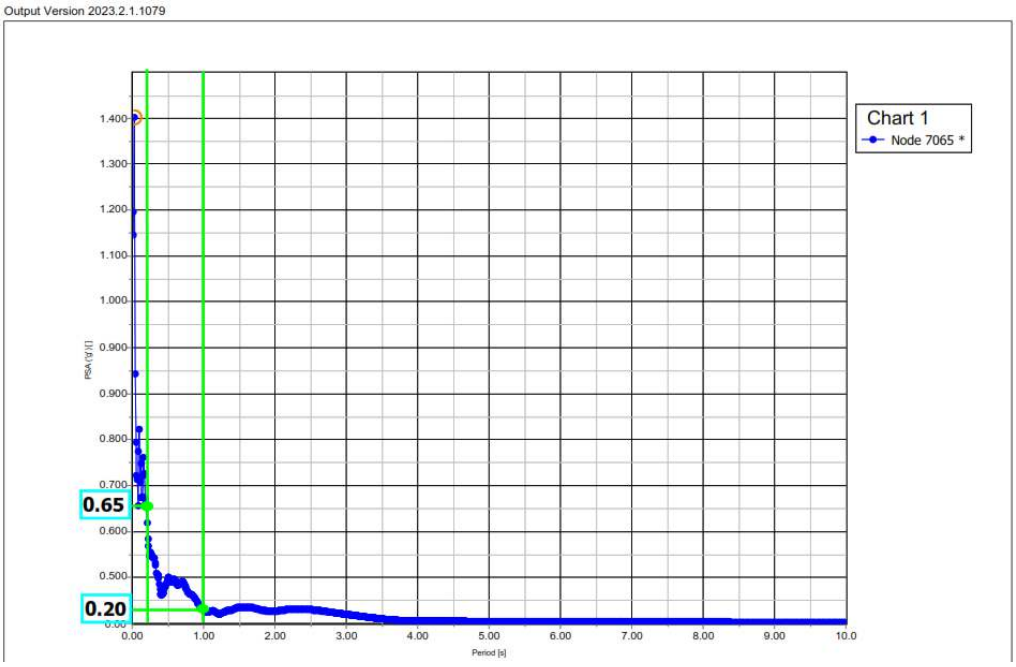

Figure 4.50 Earthquake 3 improved model ground surface PSA result

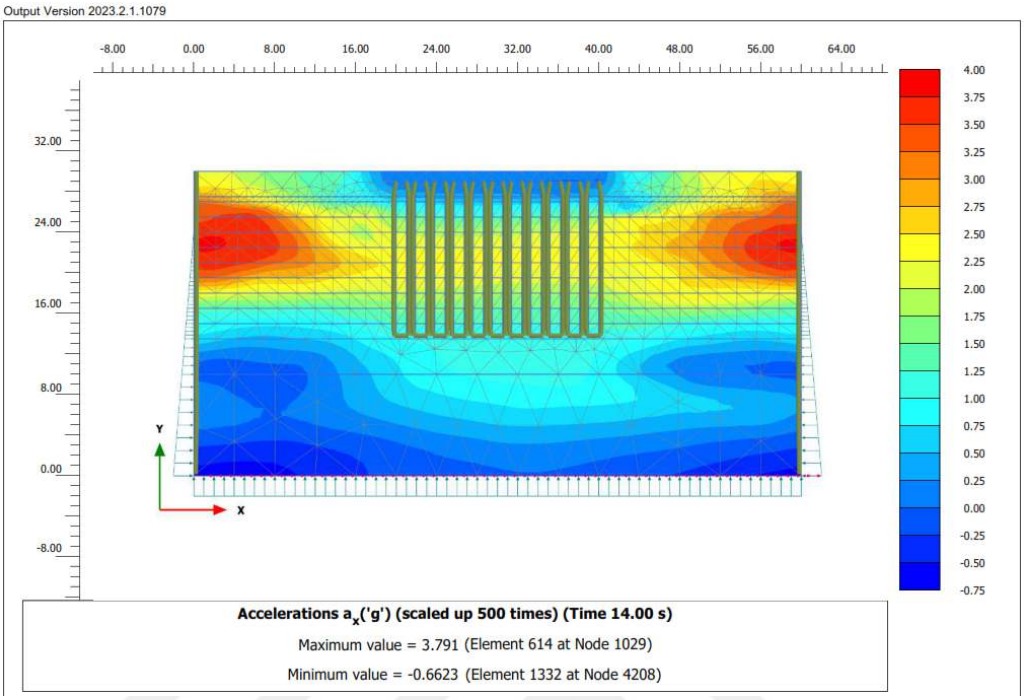

Figure 4.51 Earthquake 4 improved model acceleration (ax) result

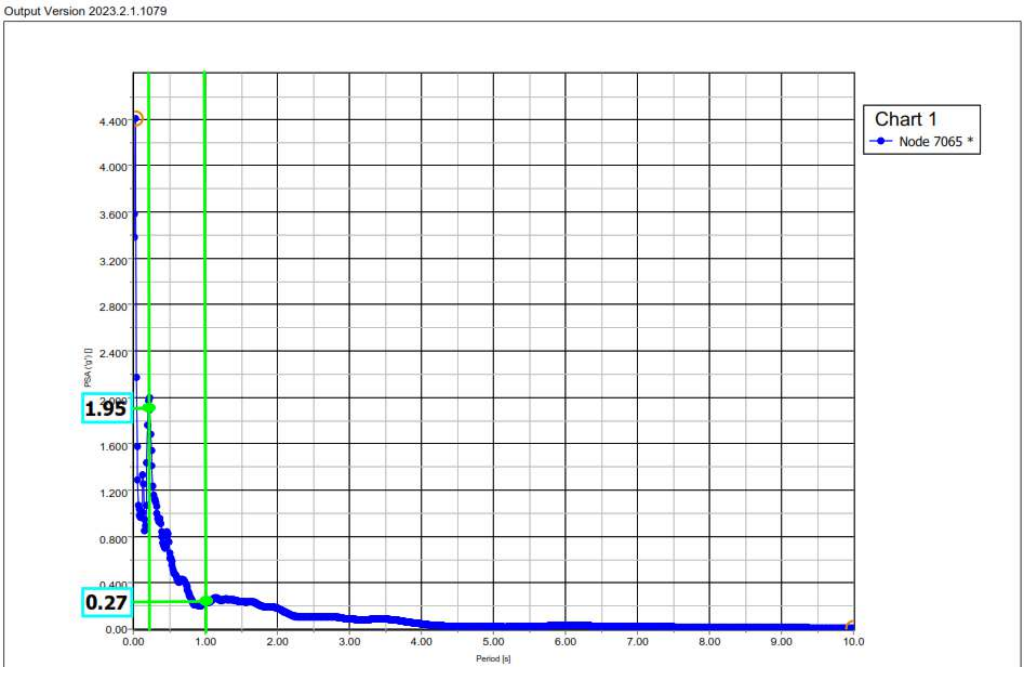

Figure 4.52 Earthquake 4 improved model ground surface PSA result

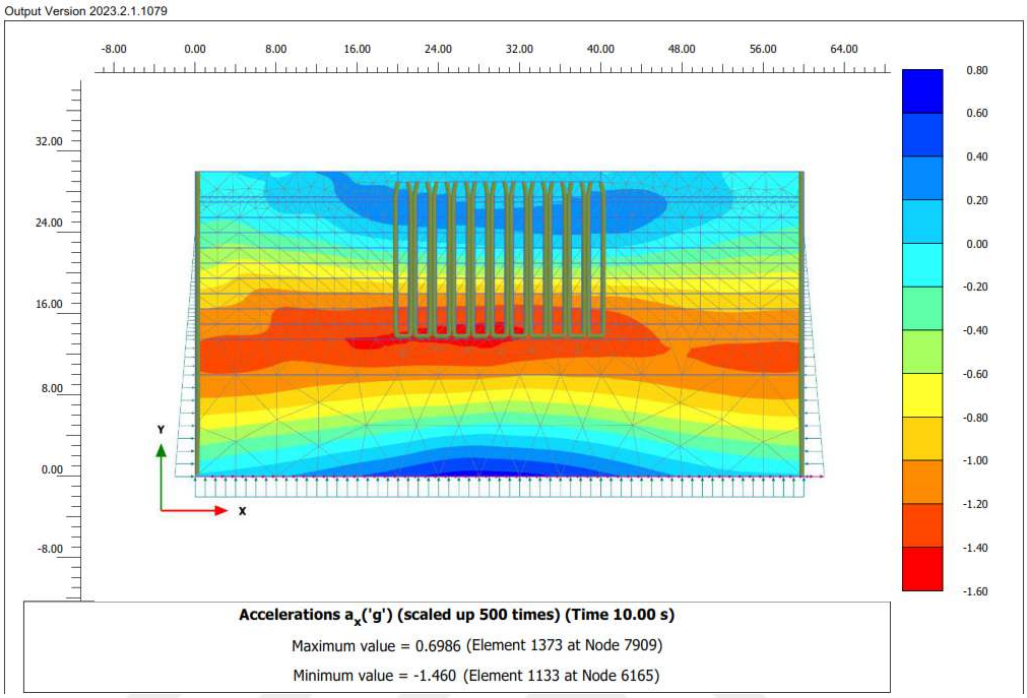

Figure 4.53 Earthquake 5 improved model acceleration (ax) result

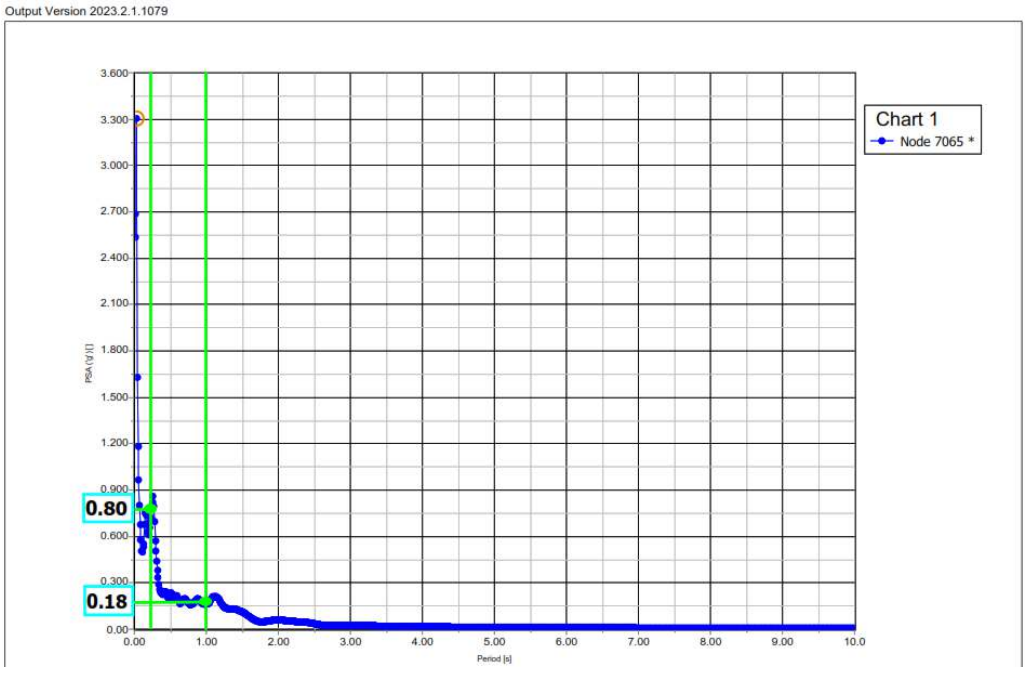

Figure 4.54 Earthquake 5 improved model ground surface PSA result

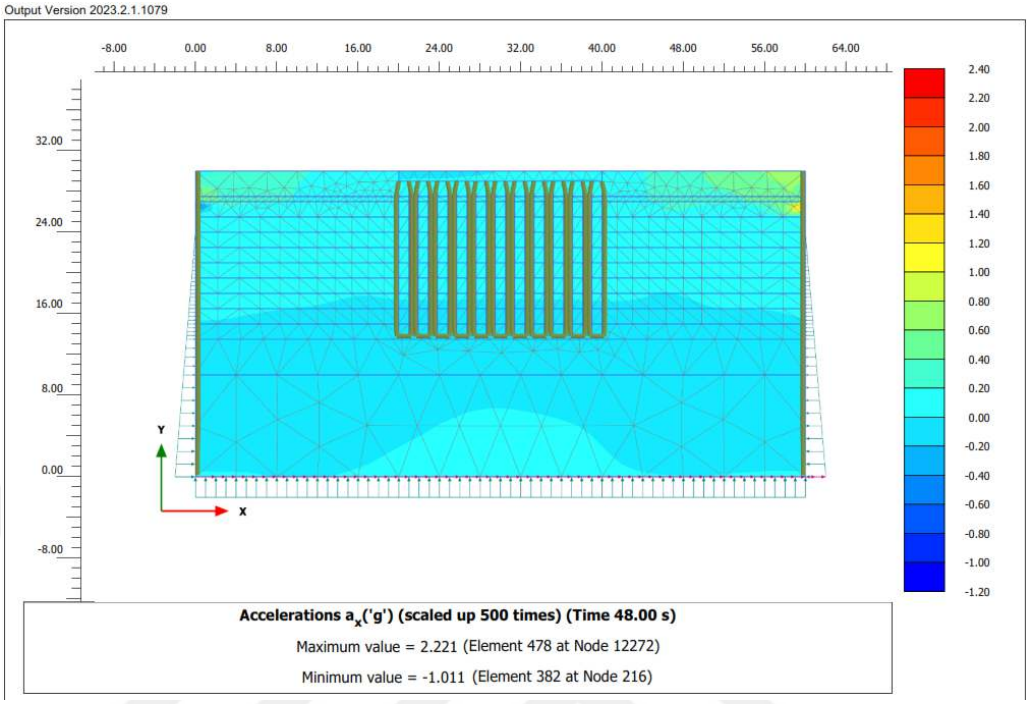

Figure 4.55 Earthquake 6 improved model acceleration (ax) result

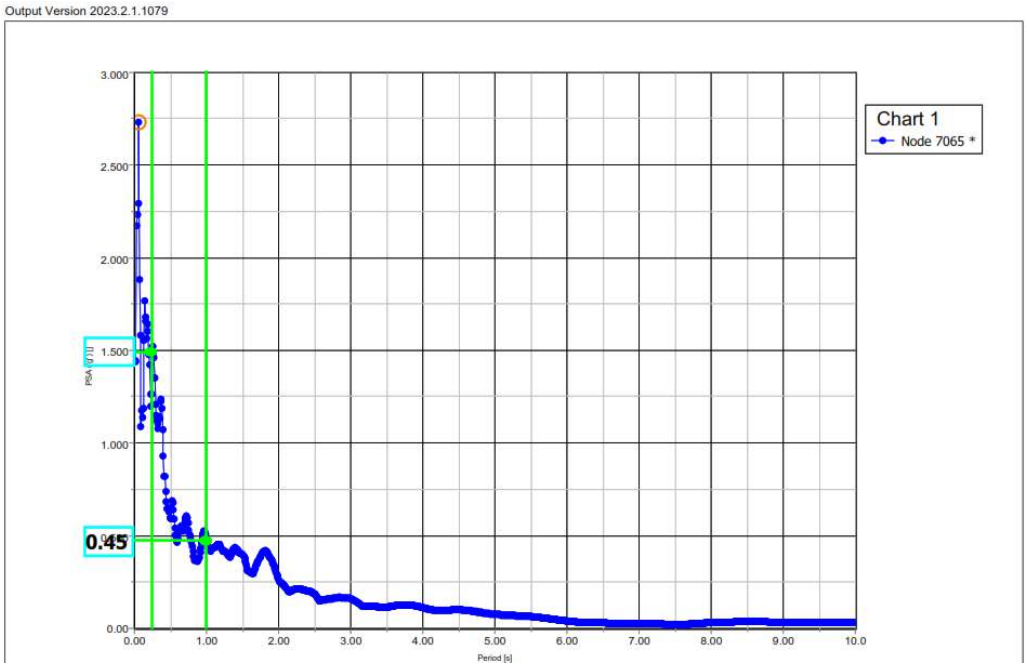

Figure 4.56 Earthquake 6 improved model ground surface PSA result

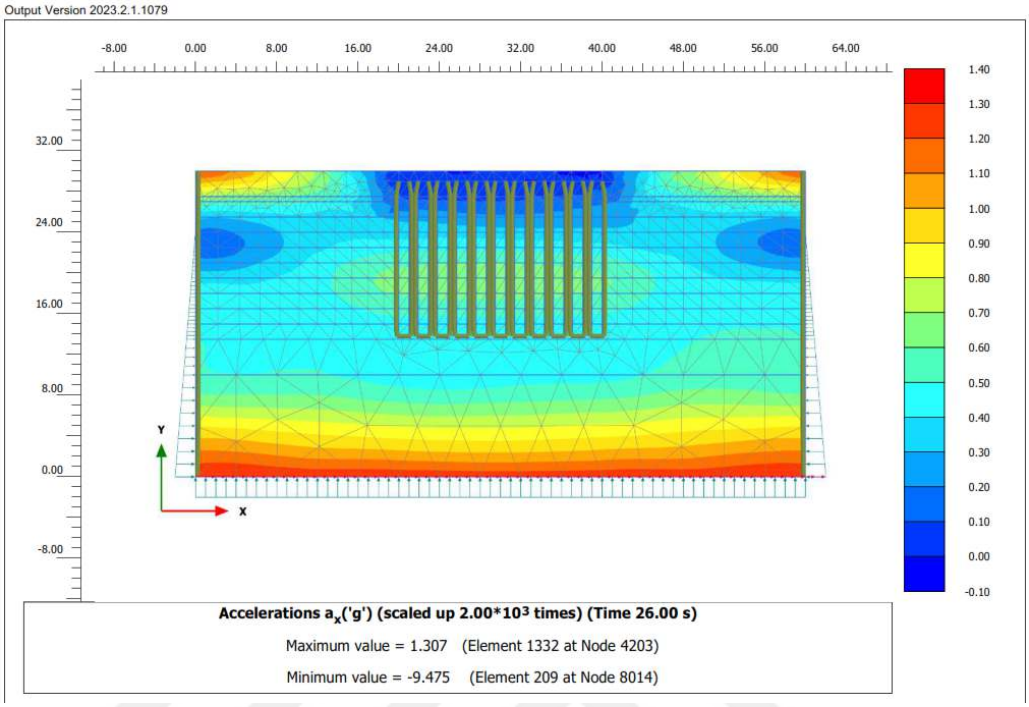

Figure 4.57 Earthquake 7 improved model acceleration (ax) result

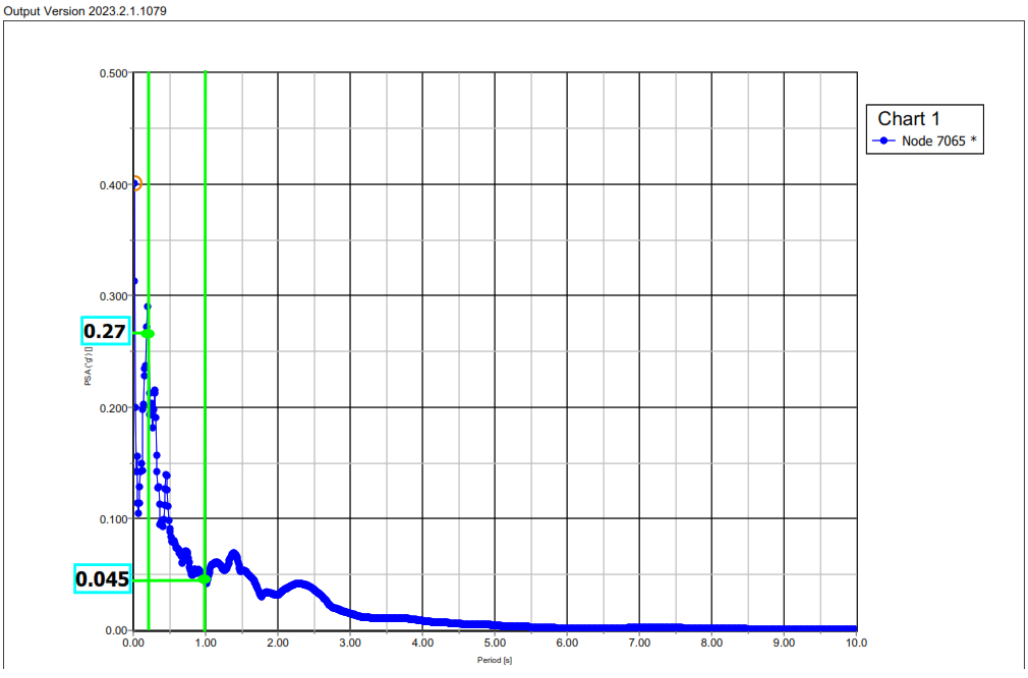

Figure 4.58 Earthquake 7 improved model ground surface PSA result

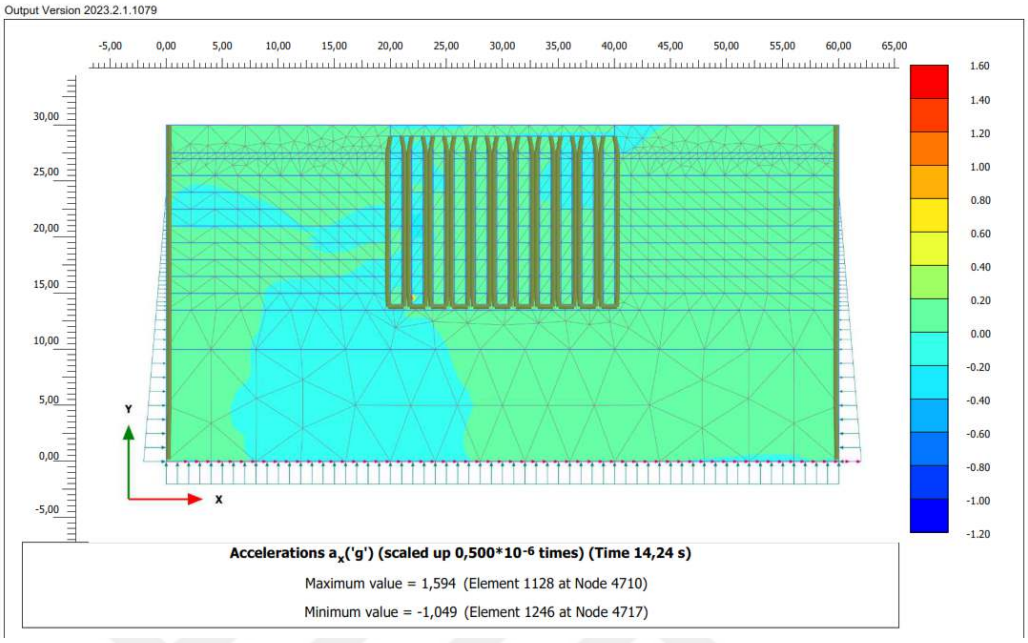

Figure 4.59 Earthquake 8 improved model acceleration (ax) result

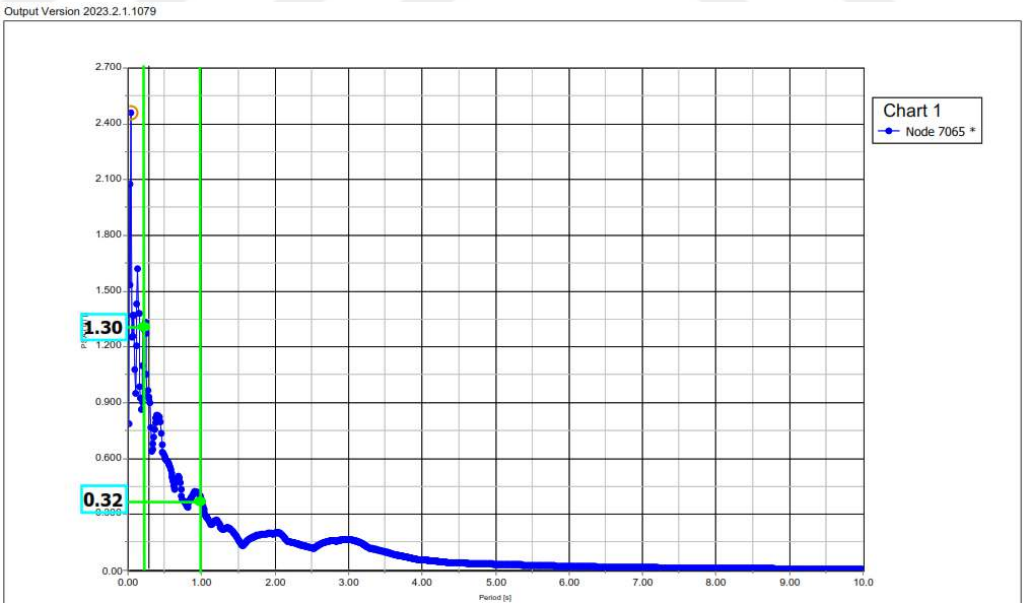

Figure 4.60 Earthquake 8 improved model ground surface PSA result

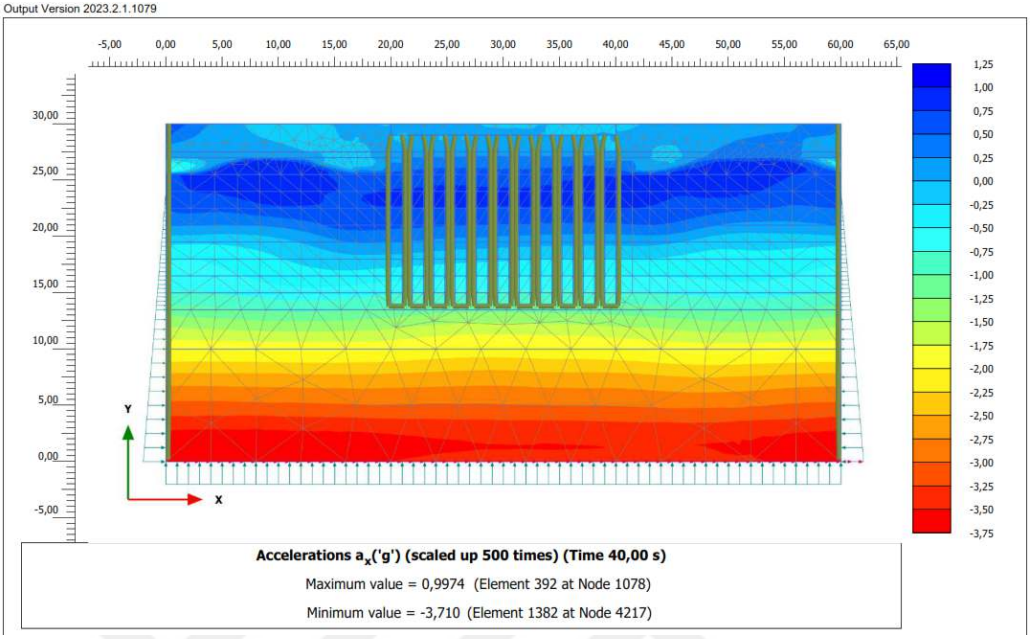

Figure 4.61 Earthquake 9 improved model acceleration (ax) result

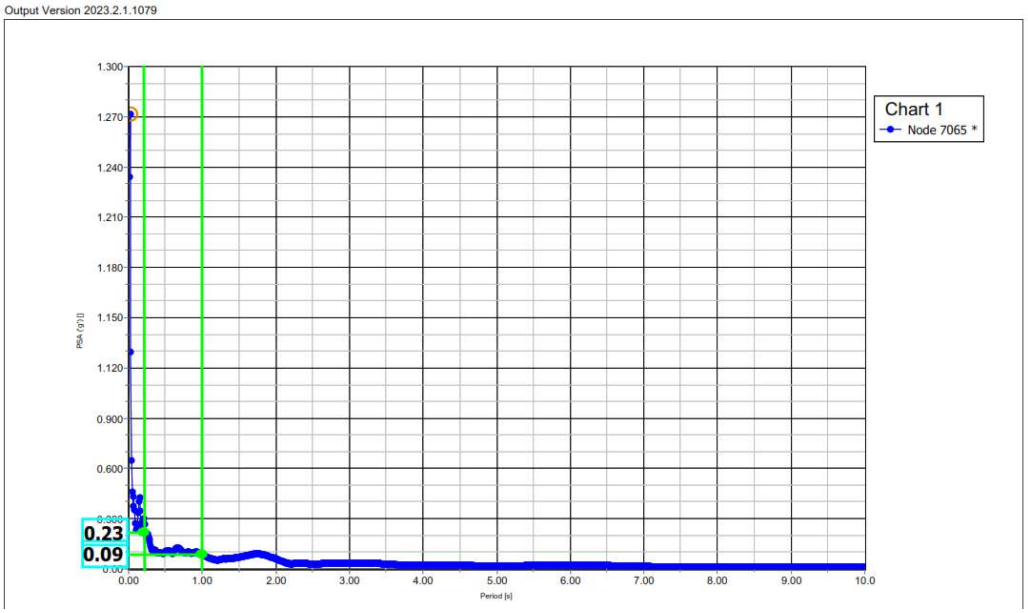

Figure 4.62 Earthquake 9 improved model ground surface PSA result

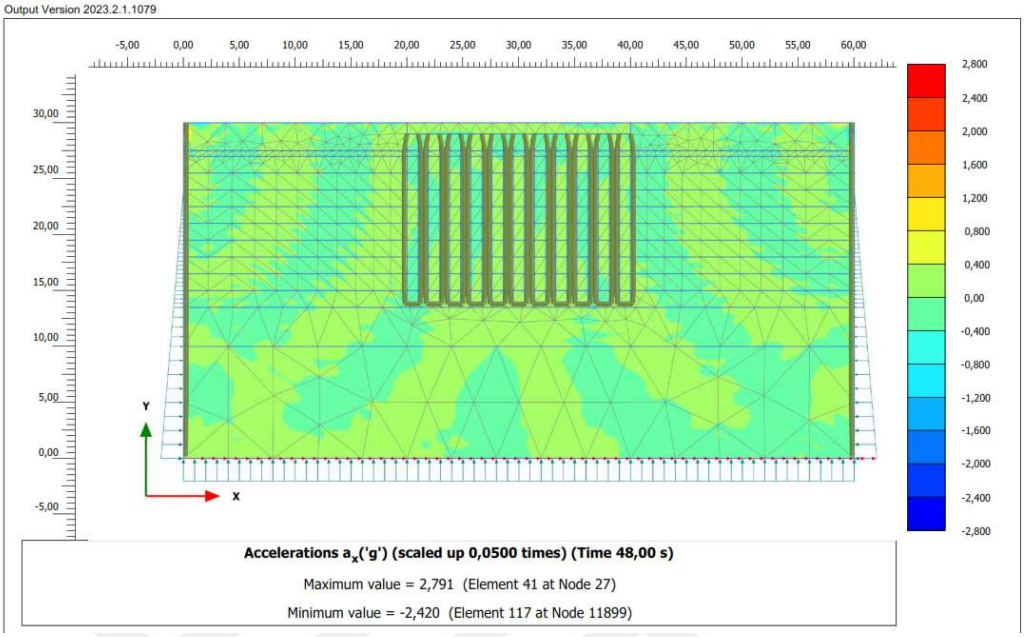

Figure 4.63 Earthquake 10 improved model acceleration (ax) result

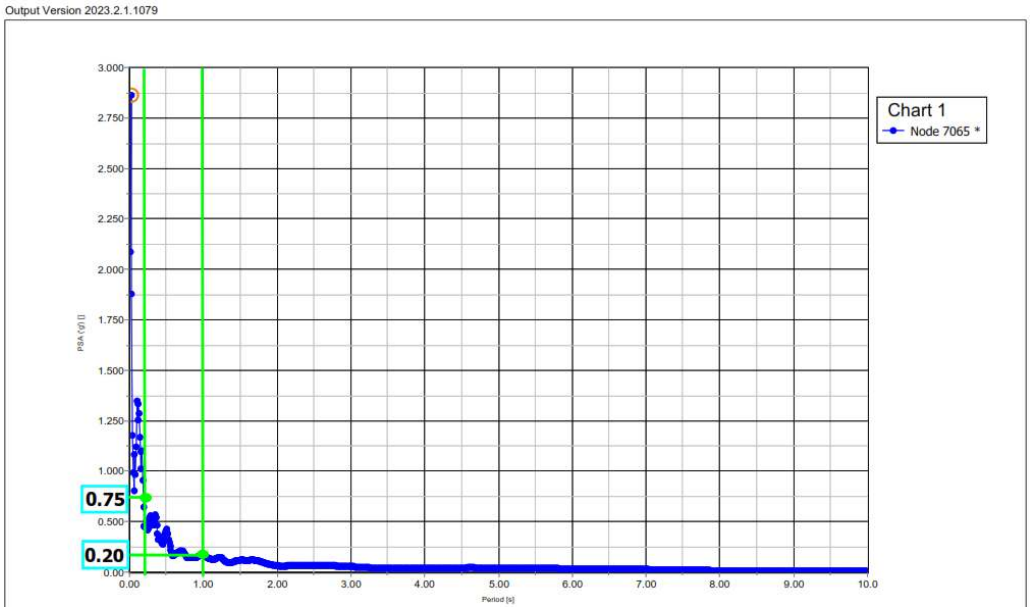

Figure 4.64 Earthquake 10 improved model ground surface PSA result

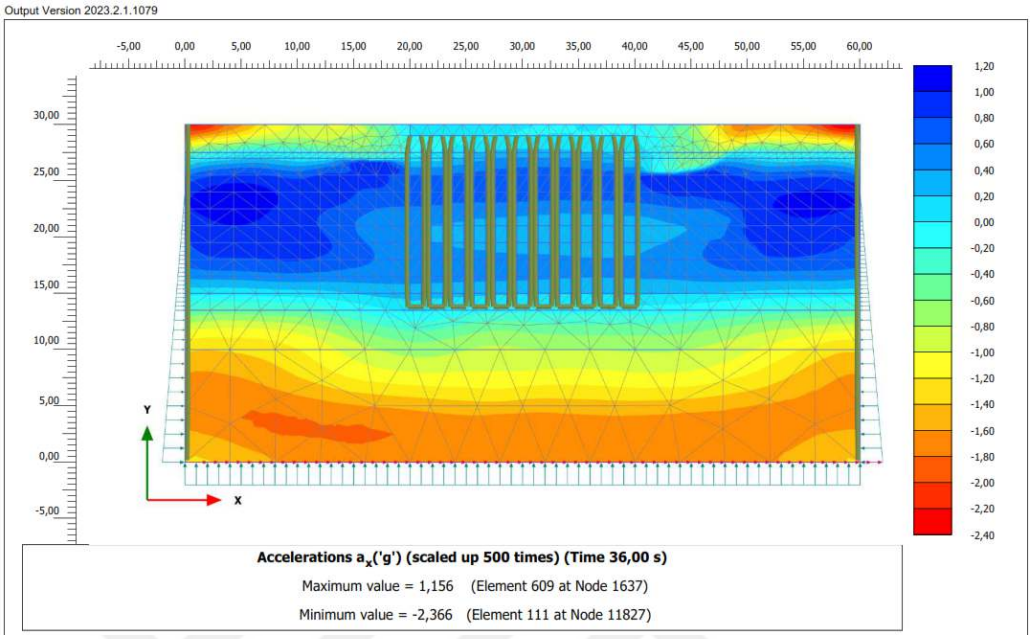

Figure 4.65 Earthquake 11 improved model acceleration (ax) result

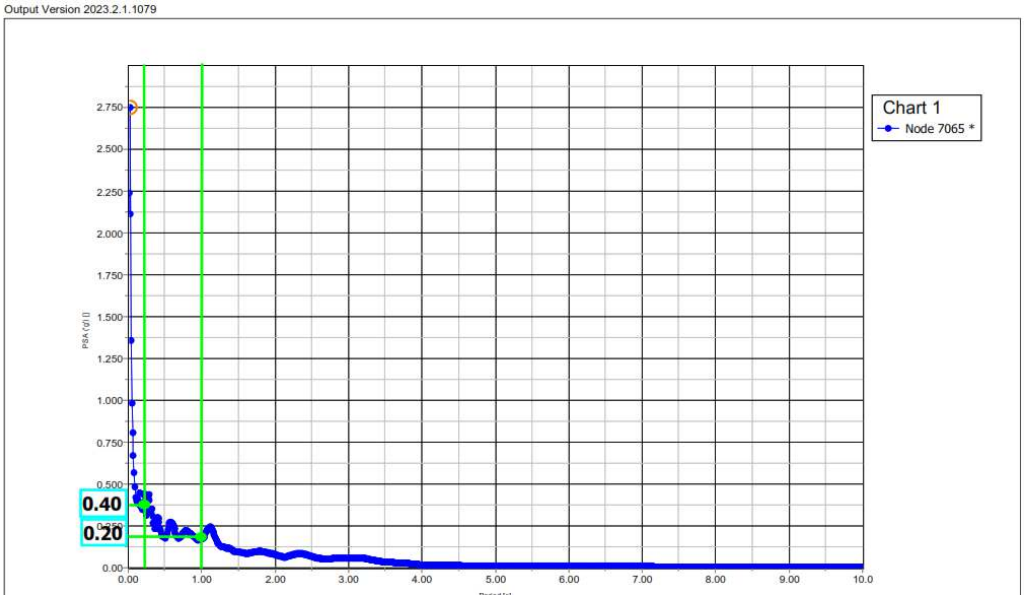

Figure 4.66 Earthquake 11 improved model ground surface PSA result

Table 4.1 0.2 secand ground surface PSA values

0.2 sec.			
Earthquake	**Unimproved Model**	**Improved Model**	**Unit**
1	1.28	1.35	g
2	1.2	1.49	g
3	0.57	0.65	g
4	1.55	1.95	g
5	0.6	0.8	g
6	0.9	1.5	g
7	1.6	1.9	g
8	1.2	1.3	g
9	0.33	0.4	g
10	0.29	0.75	g
11	0.23	0.4	g
Average:	0.89	1.14	**g**

Table 4.2 1.0 secand ground surface PSA values

1 sec.			
Earthquake	**Unimproved Model**	**Improved Model**	**Unit**
1	0.98	0.55	g
2	0.825	0.8	g
3	0.28	0.2	g
4	0.7	0.27	g
5	0.4	0.18	g
6	0.62	0.45	g
7	0.59	0.3	g
8	1.1	0.32	g
9	0.2	0.23	g
10	0.25	0.2	g
11	0.18	0.2	g
Average:	0.56	0.34	**g**

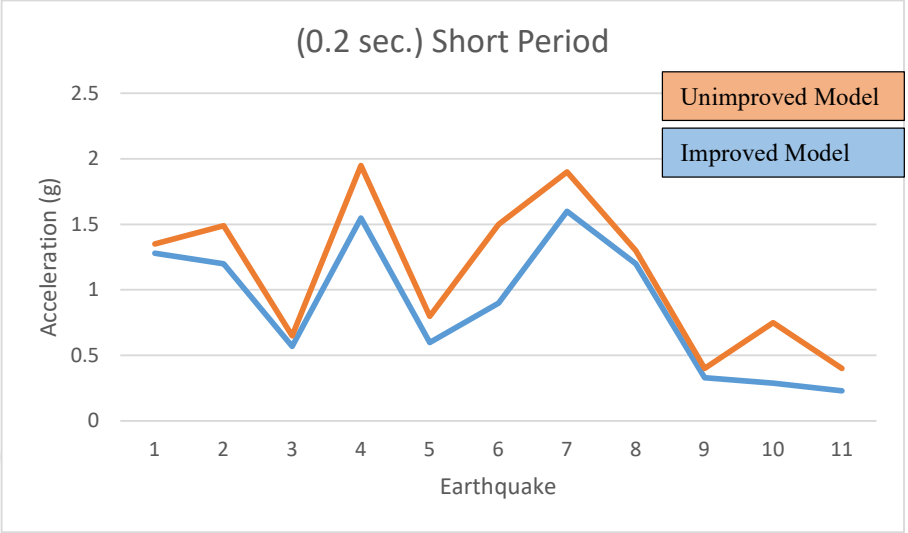

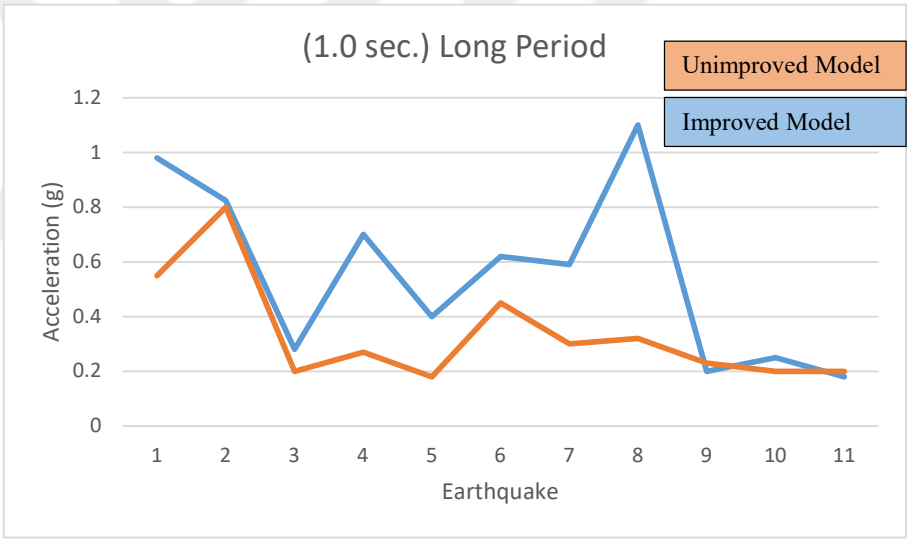

Table 4.3 Comparision of the PSA values

Results			
	TBEC 2018	Unimproved Model	Improved Model
S_S:	0.432	0.432	0.432
S_1:	0.11	0.11	0.11
F_S:	1.454	0.89	1.14
F_1:	2.38	0.56	0.34
S_{DS}:	0.628	0.383	0.491
S_{D1}:	0.262	0.061	0.037
TA:	0.0834	0.0320	0.0151
TB:	0.4168	0.1600	0.0754
TL:	6	6	6

CHAPTER 5

CONCLUSION

The determination of design response spectrum, liquefaction assessment, and seismic load applied to structures essential for seismic design, it is imperative to detect ground amplification during earthquakes. Consequently, Site Response Analysis (SRA) is of paramount importance, and ensuring the reliability of this analysis can be considered the most critical factor. In this article, SRA was conducted under various scenarios, leading to the following conclusions.

This research presents the findings of a two-dimensional site response study using PLAXIS 2D, which is designed to simulate the non-linear dissipative behavior of soils subjected to seismic stress. In this context, the selection of the soil's constitutive model is crucial. The results of the fully dynamic analysis performed with PLAXIS 2D are compared to those of an enhanced soil site response study, where the secant shear modulus and damping ratio are adjusted in successive iterations to match the strain level induced in each layer.

In PLAXIS, the Hardening Soil model with small-strain stiffness (HSsmall) was employed to demonstrate its capability to reflect soil behavior during seismic shaking for earthquakes with moderate peak accelerations. The outcomes of both techniques are compared, showing reliable agreement.

The HSsmall model has limitations when used with strong ground motions. Identifying a threshold peak acceleration for the input motion is challenging due to multiple factors such as frequency, soil properties, and boundary conditions. In this scenario, one option may be to employ the user-defined soil model known as the generalized HSSmall model.

Through this study, it has been understood that designing according to TBEC-2018 data will not compromise the durability of structures. In addition, as can be seen in this study, it is observed that the earthquake effects show a certain level of increase in the short period in the improved ground, but have a downward trend in the long period. However, when considering project economics, this approach may lead to the

construction of durable but uneconomical structures. This “Site Response Analysis” has demonstrated that it enables the design of both durable and economical projects in a shorter timeframe.

However, it has been shown that the jet injection method increases the liquefaction resistance and is useful in ensuring the stability of the soil in the sections where the possibility of liquefaction is high in the field. As indicated in the analyses here, it was determined that jet injection columns placed at the bottom of the foundation significantly reduced the risk of liquefaction.

This research emphasizes the importance of “Site Response Analysis” in seismic design and illustrates that more reliable and economical structural designs can be achieved through the comparison of different analysis methods. Future studies could focus on further developing these analysis under various soil conditions and earthquake scenarios.

REFERENCES

[1] Tsai, Chi-Chin, and Chun-Wei Chen. "A comparison of site response analysis method and its impact on earthquake engineering practice." 2nd European Conference on EarthquaNe Engineering and Seismology, Istanbul. 2014.

[2] Cai, Jing, Jianqi Lu, and Shanyou Li. "Summary of Research on Site Response Analysis." E3S Web of Conferences. Vol. 276. EDP Sciences, 2021.

[3] Ansal, Atilla, Gökçe Tönük, and Shima Sadegzadeh. "Site response analysis in performance based approach." Soil Dynamics and Earthquake Engineering 178 (2024): 108480.

[4] Yıldız, Özgür. "Nonlinear and equivalent linear site response analysis of Istanbul soils." NATURENGS 2.1 (2021): 88-101.

[5] Seed, R.B., Dickenson, S.E., Rau, G.A., White, R.K., and Mok, C.M. (1994). "Observations regarding seismic response analyses for soft and deep clay sites." Proceedings of the 1992 NCEER/SEAOC/BSSC Workshop on Site Response During Earthquakes and Seismic Code Provisions, G. R. Martin, ed., University of Southern California, Los Angeles, November 18-20, 1992, National Center for Earthquake Engineering Research Special Publication NCEER-94-SP01, Buffalo, NY.

[6] Romero, Salome, and Rix, Glenn J. (2001). "Regional variations in near surface shear wave velocity in the Greater Memphis area." Engineering Geology, 62(1-3), 137-158.

[7] Hashash, Y.M.A., Dashti, S., Romero, M.I., Ghayoomi, M., and Musgrove, M. (2015). Evaluation of 1-D seismic site response modeling of sand using centrifuge experiments, Soil Dynamics and Earthquake Engineering, 78, 19–31.

[8] Ansal, Atilla, Gökçe Tönük, and Shima Sadegzadeh. "Site response analysis in performance based approach." Soil Dynamics and Earthquake Engineering 178 (2024): 108480.

[9] Silva, W. J. (2005). Site response simulations for the NGA project: Report prepared for the Pacific Earthquake Engineering Research Center.

[10] Akin, Mutluhan, et al. "Impact of jet-grouting pressure on the strength and deformation characteristics of sandy and clayey soils in the compression zone." *KSCE Journal of Civil Engineering* 23 (2019): 3340-3352.

[11] Sedighi, Pouya, Helmut F. Schweiger, and Wolfgang Jimmy Wehr. "Effect of jet-grout columns on the seismic response of layered soil deposits." *International Journal of Geomechanics* 17.3 (2017): 04016085.

[12] El-Emam, Magdi, et al. "Local site effects on seismic ground response of major cities in UAE." *Natural Hazards* 79 (2015): 791-814.

[13] Schertmann, H.G. (1975). The correlation of SPT and penetration test results with the geotechnical parameters of soils. Canadian Geotechnical Journal, 12(4), 581-594.

[14] AFAD. (2018). Türkiye Bina Deprem Yönetmeliği. Ankara: AFAD Başkanlığı.

[15] Brinkgreve, R. B. J., W. M. Swolfs, and E. Engin. *Plaxis Introductory: Student Pack and Tutorial Manual 2010*. CRC Press, Inc., 2011.

[16] Choobbasti, Asskar Janalizadeh, et al. "Evaluation of site response characteristic using nonlinear method (Case study: Babol, Iran)." *Frontiers of structural and civil engineering* 8 (2014): 69-82.

[17] Galavi, Vahid, Alexandros Petalas, and R. B. J. Brinkgreve. "Finite element modelling of seismic liquefaction in soils." *Geotechnical Engineering Journal of the SEAGS & AGSSEA* 44.3 (2013): 55-64.

[18] MANUAL, Tutorial. PLAXIS 2D. *Deft University of Technology & PLAXIS, Netherlands*, 2016.

[19] Türkiye Afet ve Acil Durum Yönetimi Başkanlığı. (2023). *AFAD Türkiye İvme Veri Tabanı ve Analiz Sistemi (TADAS)*. Erişim tarihi, 15 Ekim 2023. https://tadas.afad.gov.tr/

[20] PEER Center. PEER NGA-West2 Database. https://ngawest2.berkeley.edu/